NASA CR-72991
HTL TR NO. 102

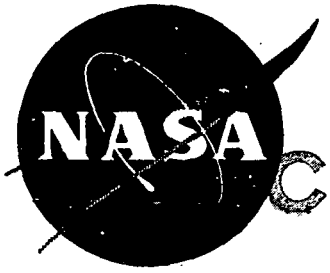

FILM COOLING EFFECTIVENESS AND HEAT TRANSFER WITH INJECTION THROUGH HOLES

V. L. Eriksen

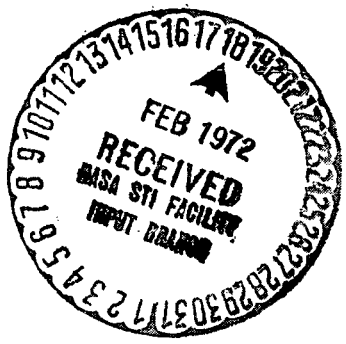

prepared for

NATIONAL AERONAUTICS AND SPACE ADMINISTRATION

NASA CONTRACT NO. NAS 3-13200

HEAT TRANSFER LABORATORY

MECHANICAL ENGINEERING DEPARTMENT

UNIVERSITY OF MINNESOTA

NOTICE

This report was prepared as an account of Government sponsored work. Neither the United States, nor the National Aeronautics and Space Administration (NASA), nor any person acting on behalf of NASA:

A.) Makes any warranty or representation, expressed or implied, with respect to the accuracy, completeness, or usefulness of the information contained in this report, or that the use of any information, apparatus, method, or process disclosed in this report may not infringe privately owned rights; or

B.) Assumes any liabilities with respect to the use of, or for damages resulting from the use of any information, apparatus, method or process disclosed in this report.

As used above, "person acting on behalf of NASA" includes any employee or contractor of NASA, or employee of such contractor, to the extent that such employee or contractor of NASA, or employee of such contractor prepares, disseminates, or provides access to, any information pursuant to his employment or contract with NASA, or his employment with such contractor.

Requests for copies of this report should be referred to:

National Aeronautics and Space Administration
Office of Scientific and Technical Information
P. O. Box 33
College Park, Maryland 20740

NASA CR-72991
HTL TR NO. 102

SUMMARY REPORT
FILM COOLING EFFECTIVENESS AND HEAT TRANSFER WITH INJECTION THROUGH HOLES

by

V.L. Eriksen

prepared for

NATIONAL AERONAUTICS AND SPACE ADMINISTRATION

August, 1971

CONTRACT NAS 3-13200
TECHNICAL MANAGEMENT
NASA Lewis Research Center
Cleveland, Ohio
Lewis Project Manager; Francis S. Stepka

University of Minnesota
Institute of Technology
Department of Mechanical Engineering
Minneapolis, Minnesota 55455

ABSTRACT

An experimental investigation of the local film cooling effectiveness and heat transfer downstream of injection of air through discrete holes into a turbulent boundary layer of air on a flat plate is reported. Secondary air is injected through a single hole normal to the main flow and through both a single hole and a row of holes spaced at three diameter intervals with an injection angle of 35° to the main flow. Two values of the mainstream Reynolds number are used; the blowing rate is varied from 0.1 to 2.0. Photographs of a carbon dioxide-water fog injected into the main flow at an angle of 90° are also presented to show interaction between the jet and mainstream.

FOREWARD

The work described in this report was conducted at the University of Minnesota Heat Transfer Laboratory under NASA Contract No. NAS 3-13200 with Mr. Francis S. Stepka, NASA-Lewis Research Center as Project Manager.

Professors R.J. Goldstein and E.R.G. Eckert of the University of Minnesota Heat Transfer Laboratory have guided this study and their numerous contributions are gratefully acknowledged. The assistance of Mr. P.R. Glamm in the laboratory is deeply appreciated.

TABLE OF CONTENTS

LIST OF FIGURES

LIST OF TABLES

NOMENCLATURE

A	Surface area of heater
b	Total thickness of test plate
b_i	Thickness of component i in test plate
c_p	Specific heat
D	Diameter of injection tube
h	Heat transfer coefficient, see eqn. 1
h_a	Heat transfer coefficient defined using difference between wall and adiabatic wall temperature, see eqn. 2
$\bar{h}_a$	Heat transfer coefficient defined using difference between laterally averaged wall and adiabatic wall temperature, see eqn. 10
$h_{a\ max}$	Maximum value of h_a at a fixed X/D
h_o	Heat transfer coefficient without injection
i	Electric current
I	Momentum flux or dynamic pressure ratio, see eqn. 5
k_e	Equivalent thermal conductivity of test surface
k_i	Thermal conductivity of component i in test plate
M	Blowing rate, see eqn. 4
P_r	Prandtl number
q	Wall heat flux
$\bar{q}$	Laterally averaged wall heat flux
q_{bc}	Heat loss per unit area due to conduction from back of test surface

q_g	Energy generated in a heater per unit area
q_r	Heat loss per unit area due to thermal radiation
R	Electrical resistance of heater
Re_D	Reynolds number using free stream velocity and injection tube diameter ($Re_D=\rho_\infty U_\infty D/\mu_\infty$)
Re_{X_h}	Reynolds number using free stream velocity and length X_h
s	Slot width for two-dimensional film cooling and equivalent slot width for three-dimensional film cooling
St	Stanton number ($St=h/\rho_\infty U_\infty c_p$)
St_o	Stanton number without injection ($St_o=h_o/\rho_\infty U_\infty c_p$)
T_{aw}	Adiabatic wall temperature
$\overline{T_{aw}}$	Laterally averaged adiabatic wall temperature
T_{dat}	Datum temperature
T_{tc}	Temperature indicated by thermocouple output
T_w	Wall temperature
$\overline{T_w}$	Laterally averaged wall temperature
T_2	Injection temperature
T_∞	Mainstream temperature
ΔT_{lw}	Temperature correction for heat loss through thermocouple leads
ΔT_{wc}	Temperature correction for conduction within test wall
U_2	Mean velocity in injection tube
U_∞	Mainstream velocity
X	Distance downstream of downstream edge of injection hole, see Figure 5
X_h	Distance downstream of leading edge of heaters

X_t	Distance downstream of boundary layer trip wire
X_1	Distance downstream of effective starting point for boundary layer growth
Y	Distance normal to test surface, see Figure 5
Z	Lateral distance from center of injection hole, see Figure 5
β	Angle between direction of injection and mainstream direction
δ	Uncertainty
δ_i	Boundary layer momentum thickness
δ^*	Boundary layer displacement thickness
δ_o^*	Boundary layer displacement thickness at the upstream of the injection hole
ϵ	Emittance
η	Film cooling effectiveness, see eqn. 3
$\Delta\eta_{wc}$	Film cooling effectiveness correction due to conduction within wall
μ_∞	Dynamic viscosity of mainstream
ρ_2	Density of injected gas
ρ_∞	Density of mainstream
σ	Stefan-Boltzmann constant

SUMMARY

The film cooling effectiveness and heat transfer coefficient are measured downstream of injection through discrete holes into a turbulent mainstream boundary layer. Air is injected through a single hole at an angle of 90° to the main flow and through both a single hole and a row of holes spaced at three diameter intervals at an angle of 35° to the main flow.

The heat transfer coefficient is determined from wall temperature measurements with a constant heat flux from the test surface. The film cooling effectiveness is calculated from the nearly adiabatic wall temperature that is measured when the test surface is not heated. Heated jets of air are injected to measure the adiabatic wall temperature. The heat transfer coefficient is determined with injection of both heated and unheated air jets.

Comparison of the film cooling effectiveness measured with normal injection with the results of other investigations does not show a significant variation of the film cooling effectiveness with Reynolds number or boundary layer thickness at the point of injection over the limited range of these

parameters for which results are available.

The heat transfer coefficient near the hole for normal injection is observed to be as much as 40-45% larger than the value without injection for a blowing rate of 2.0. At downstream locations, the heat transfer coefficient is observed to be 10-15% greater than the flat plate value for blowing rates greater than 0.2. The increased value of the heat transfer coefficient near the point of injection is due to the high turbulence levels that arise from interaction between the jet and main flow near the point of injection.

Comparison of the film cooling effectiveness measured for 35° injection through a row of holes spaced at three diameter intervals with the results of other investigations indicates that the film cooling effectiveness decreases as the boundary layer thickness at the point of injection is increased.

The heat transfer coefficient following 35° injection through a single hole is much smaller than for normal injection. Since the jet injected at 35° has a velocity component in the direction of main flow, interaction between this jet and the mainstream and thus the heat transfer is less than for normal injection which has no velocity component in the main flow direction.

There is little difference between the heat transfer coefficient for 35° injection through a single hole and 35° injection through a row of holes spaced at three diameter intervals for a blowing rate 0.5. At blowing rates of unity and greater, the heat transfer coefficient for injection through the row of holes is greater than that for a single hole. The heat transfer coefficient for the row of holes is also observed to be greater between holes, where the jets interact with the mainstream and with each other, than on the centerline. The laterally averaged heat transfer coefficient for 35° injection through a row of holes is observed to increase over the first 20 diameters in the downstream direction before decreasing at blowing rates 1.5 and 2. The increasing heat transfer coefficient near injection is attributed to high turbulence levels near the edges of the jets that have penetrated into the free stream and are spreading toward the wall.

Photographs of flow visualization experiments show that very large eddies and vortices are caused by interaction between the normally injected jet and the mainstream. These eddies and vortices qualitatively explain the increased heat transfer that is observed.

I. INTRODUCTION

Film cooling is a method by which a solid surface is protected from the influence of a hot gas stream. A coolant is ejected locally through the wall of the structure to be protected in such a way that it creates a film along the surface for some distance downstream. Although either a gas or a liquid can be used as the injected fluid, only gaseous injection will be considered here.

The coolant can be injected in various ways, some of which are shown on Figure 1. Figures 1(a) and 1(b) show slots with outlets that are flush with the surface to be protected. In Figure 1(a) the coolant leaves the injection channel with a velocity at an angle β with the main flow. The channel in Figure 1(b) turns the injected flow so that it enters the main flow with a velocity parallel to that of the main flow. Figure 1(c) shows a step down slot through which the coolant flows parallel to the main flow. Figure 1(d) shows injection through a porous strip. In this case the direction of the coolant flow is normal to the direction of main flow. These figures are all similar in that the flow and temperature fields above the surfaces are

two-dimensional. If the injected flow does not leave the slot parallel to the main flow, the main flow exerts a force on the coolant flow, causing it to turn and flow along the surface. Interaction between the injected flow and the free stream results in mixing of the two and the influence of the coolant on the wall decreases in the downstream direction. The temperature of the wall varies only in the X direction.

For structural reasons, it is often necessary to eject the coolant through a series of holes or interrupted slots. Injection through a row of holes is shown on Figure 1(e). The coolant enters the main flow with velocity at an angle β with the main flow. Since the coolant flow is interrupted across the span, it is possible for the mainstream to flow around the jets of coolant rather than force them against the wall. The influence of the coolant on the wall is thus less than for the slot geometries. The flow and temperature fields above the wall are not three-dimensional and the wall temperature distribution is two-dimensional. Interaction between the jets and the main flow results in mixing and the temperature of the coolant approaches that of the main flow at downstream locations.

In a typical film cooling application, the problem is to predict or measure the relationship between the wall temperature distribution and heat transfer. The

geometry and mainstream and secondary flows may be fixed or may be permitted to vary. It may be desired to find the wall temperature for a given set of conditions or to optimize the geometry, mainstream or coolant flow while maintaining the wall temperature below some critical value.

For constant property flows, it is convenient to use the concept of heat transfer coefficient h. Thus,

$$q = h(T_w - T_{dat}) \tag{1}$$

where q is the wall heat flux, T_w is the wall temperature, and T_{dat} is a datum temperature. For the case of an adiabatic surface, q=0 and the resulting wall temperature is the adiabatic wall temperature T_{aw}. If this temperature is used as the datum, then the heat flux with film cooling is

$$q = h_a(T_w - T_{aw}). \tag{2}$$

For a constant property flow, the heat transfer coefficient defined by equation (2) is independent of the temperature difference. In the absence of film cooling, the adiabatic wall temperature is equal to the free stream temperature or to the recovery temperature in the case of high speed flow.

To eliminate the dependence of the adiabatic wall temperature on the temperatures of the main flow and injected flow, the adiabatic wall temperature is usually

presented in dimensionless form as the film cooling effectiveness. For low speed, constant property flow the film cooling effectiveness is given by

$$\eta = \frac{T_{aw} - T_\infty}{T_2 - T_\infty} \qquad (3)$$

where T_2 and T_∞ are the respective temperatures of the coolant and main flow. In the case of high speed flows, the main flow temperature is replaced by the recovery temperature.

The heat transfer coefficient as defined by equation (2) is often found to be relatively close to the value without injection. The adiabatic wall temperature can vary considerably and is more difficult to predict. Most film cooling studies are therefore concerned with the determination of the film cooling effectiveness.

From the assumption of a constant property flow, it follows that the dimensionless temperature field and film cooling effectiveness distribution are the same whether the ejected fluid is hotter or colder than the main flow. This fact is utilized in most studies where the experiments are easier to conduct with a heated "coolant."

A large number of parameters are involved in film cooling. Figure 1 shows some of the different geometries that can be used. The shape of the channel through which

the coolant flows and the angle of injection can be altered for both two-dimensional and three-dimensional film cooling. In addition, the spacing between holes and the number of rows of holes can be varied for the three-dimensional case. The film cooling process also depends on the dimensionless parameters describing the main flow as well as the coolant flow. The ratios of the velocities and densities of the flows are especially important. These quantities are often grouped into the parameters known as the blowing rate (mass flux ratio) and momentum flux ratio. The blowing rate is expressed as

$$M = \frac{\rho_2 U_2}{\rho_\infty U_\infty} \tag{4}$$

and the momentum flux ratio is given by

$$I = \frac{\rho_2 U_2^2}{\rho_\infty U_\infty^2} . \tag{5}$$

The subscript 2 denotes the coolant flow; and subscript ∞ represents the main flow. Other important parameters are the Reynolds number of the main flow, the turbulence in the main flow and the thickness of the mainstream boundary layer at the point of injection. If large temperature differences are employed, the variation of properties throughout the flow field is important.

Two-dimensional film cooling has been studied rather extensively. Most of the work that has been done has been concerned with the determination of the

film cooling effectiveness. There are reports of numerous experimental studies and several models for the prediction of film cooling effectiveness in the literature. This work is summarized in reference (1).

The heat transfer coefficient with two-dimensional film cooling has been determined by several investigators. All used air for both the coolant flow and mainstream flow. Hartnett, Birkebak, and Eckert (2,3) used a tangential slot similar to that shown on Figure 1(b). Typical results of their experiments (3) are repeated on Figure 2. The Stanton number using the heat transfer coefficient with film cooling (defined using Equation 2) is normalized by the Stanton number using the heat transfer coefficient without film cooling. The distance downstream of the slot is normalized by the slot width s. The heat transfer coefficient is higher than the value without injection in the region near the slot for the higher values of the blowing rate (M=0.87 and 1.23). At downstream locations it approaches the value without injection. The results at lower blowing rates (M=0.34 and 0.48) are closely approximated by the value without injection at all locations. Similar results are found in the presence of a pressure gradient in the flow direction (3).

Scesa (4) found little difference between the heat

transfer coefficients measured with and without injection using a flush slot with an injection angle of 90° in the range of blowing rates from 0 to 0.95. Seban and co-workers (5,6,7) also found that the heat transfer coefficient was not significantly altered by blowing, although in these studies the heat transfer coefficient was sometimes found to be reduced slightly by blowing. Differences in injection geometry may account for this different trend. A step down slot was used in the range of blowing rates from 0 to 0.70 in (5) and a flush normal slot and a step down slot were used in this same range of blowing rates in (6). In (7), a step down slot is used with blowing rates as high as 2. For blowing rates less than 1, the heat transfer coefficient is found to be less than the value without injection near the slot. When the blowing rate is about equal to one, there is little difference between the results with and without injection. At higher blowing rates, the heat transfer coefficients with injection are higher than those without injection.

Metzger and co-workers (8,9,10) measured the heat transfer coefficient based on average wall and adiabatic wall temperatures for injection through slots at angles of 20 and 60 degrees. For injection at an angle of 20 degrees, there was little difference between results with and without injection. Results for

injection at an angle of 60 degrees from (9) are repeated on Figure 3. These results are higher than those shown on Figure 2. The difference is probably due to the higher injection angle of Figure 3. It could also be due to an increase in the mass flow of the mainstream since the added mass flow due to injection was as high as 25 percent of the total mass flow in the tunnel (11).

Three-dimensional film cooling has not been studied as extensively as two-dimensional film cooling. The bulk of the work that has been done, most of which is reviewed in (1) and (12), has been concerned with adiabatic wall temperature distributions. Wieghardt (13) used both a single and double row of oblong holes across the span at a blowing rate of 0.36. For the double row of holes, he found a relatively uniform film cooling effectiveness distribution across the span, but the magnitude of the effectiveness was less than half that for the same air flow through a slot. He found very low values of the effectiveness for a single row. Papell (14) used both two and four rows of holes spaced at two diameter intervals for injection at an angle of 90 degrees to the main flow. His data correlated using an empirical modification of the relation he used for injection through a continuous slot. In the study by Burggraf, Chin, and Hayes (15), rows of punched crescent

louvers were used to inject the film. The louvers apparently turned the jets so that they did not leave the wall. The data was correlated using the same parameters that were used for injection through a number of continuous slots.

Some of the injection geometries used in a program to study film cooling with injection through holes at the University of Minnesota are shown on Figure 5. Film cooling effectiveness distributions for injection through a single hole at an angle of 35 degrees (a single tube positioned as those on Figure 5(b)) are presented in (16) and (17). Effectiveness distributions for normal injection through a single hole (Figure 5(a)) are also included in (17). The film cooling effectiveness for 35 degree injection through a single smaller diameter tube than that used in (16) and (17) is presented in (18) and (19) along with film cooling effectiveness distributions for 35 degree injection through a row of holes spaced at three diameter intervals (Figure 5(b)) and for lateral injection at angles of 15 and 35 degrees. Velocity and temperature profiles in the flow above the adiabatic wall are presented for injection through a single hole at angles of 35 and 90 degrees in (20) and (21). A model for the prediction of film cooling effectiveness at low values of the blowing rate is

proposed in (20) and (22). This model is modified for use at higher blowing rates in (23).

Typical results for the film cooling effectiveness downstream of injection are presented on Figure 6. The angle of injection is 35 degrees and results for both a single hole and a row of holes are presented. The curves exhibit a maximum in the range M=0.4-0.5. For blowing rates below this value, the effectiveness increases with increasing blowing rate due to the increasing amount of coolant near the wall. At blowing rates above 0.5 the penetration of the jet increases with increasing blowing rate, decreasing the influence of the jet on the wall. The data on Figure 5 are for coolant and main flow of near equal densities ($\rho_2/\rho_\infty=0.85$). If the density of the coolant differs significantly from that of the main flow, the film cooling effectiveness values and the location of the peak could be different from those on Figure 6. There are indications in the literature that the penetration of a jet into a crossflow depends on the momentum flux or dynamic pressure ratio rather than the blowing rate M. Unpublished results from the University of Minnesota, in which air ($\rho_2/\rho_\infty\approx0.85$) and freon ($\rho_2/\rho_\infty\approx4$) are injected into a main flow of air, indicate that the peaks of the curves may be located at the same value of the momentum flux ratio.

Results from (18) and (19) indicate that the individual jets issuing from the row seem to be independent of one another at low blowing rates. The two-dimensional adiabatic wall temperature distribution can then be approximated by superposition of single hole results. At higher blowing rates where the jets penetrate into the main flow, the individual jets tend to block the path for the free stream to flow around the jets. The main flow exerts a greater force on the row of jets secondary flow, turning it towards the wall resulting in decreased penetration. The difference between single hole results and results for injection through a row of holes at high blowing rates on Figure 6 demonstrates this effect.

The path of a jet in a crossflow is also influenced by the thickness of the free stream boundary layer at the point of injection. Film cooling results from (18) and (19) indicate that the mainstream exerts a greater force on the jet when the boundary layer is thin, thus turning the jet faster and increasing its effect on the wall.

Lateral injection tends to spread the jet over a greater lateral width than injection at the same angle with the flow (18,19). Jet penetration decreases as the lateral angle decreases.

Metzger and co-workers (9,10) measured the average

film cooling effectiveness (in lateral and downstream directions) following injection through rows of holes at angles of 20 and 60 degrees to the main flow for lateral hole spacings of 1.55 and 1.71 diameters. The trends for the average film cooling effectiveness are similar to those from (16) and (17). Single hole results from (16) and (17) are averaged using the principle of superposition and compared with the results of (9) in (11). Agreement between the two sets of results is good.

Liess and Carnel (24) measured adiabatic wall temperatures and velocity temperature profiles in the flow downstream of injection through a single row of holes at an angle of 35 degrees. Spacings between holes of 2.22, 3.33 and 4.0 diameters were used with Mach numbers in the range from 0.4 to 0.6. The film cooling effectiveness is highest for the smallest spacing and decreases with increased spacing. At the smallest spacing, the wall temperature does not vary laterally and the flow field is observed to be approximately two-dimensional for downstream distances greater than 14 hole diameters. The flow field is observed to be three-dimensional and the wall temperature varies in the lateral direction for the larger spacings.

With the exception of the region immediately

downstream of injection, the trends in the data are similar to those observed in (18) and (19). For hole spacings of 3.33 and 4.0 diameters and at a blowing rate M=0.85, the results of (24) show the centerline film cooling effectiveness to first increase before decreasing with X/D. This increase is not observed at similar blowing rates in (18) and (19). Comparison of the magnitude of the film cooling effectiveness measured in these two studies is difficult since different hole spacings and blowing rates are used, but the results of (24) seem to be somewhat higher than those of (18) and (19). The difference could be due to differences in the Mach number, Reynolds number or mainstream boundary layer thickness.

Burggraf and Huffmeier (25) measured wall temperatures downstream of injection through single and staggered double rows of holes at an angle of 35 degrees. The spacing between holes was 2.82 diameters and the turbulence in the main flow was high. Single hole results display a peak similar to that shown on Figure 6 but the magnitude of the film cooling effectiveness is less. This difference is attributed to greater mixing between the jets and free stream that would result from the higher turbulence level. The film cooling effectiveness values for the staggered double row of holes increase with blowing rate beyond

M=0.5 and do not show a peak. The first row of jets apparently fills the voids between the second row and jet penetration is reduced.

Information concerning heat exchange between the wall and gas flow in a three-dimensional film cooling environment is sparse. Metzger and co-workers (9,10) measured the average heat transfer for injection through a row of holes at angles of 20 and 60 degrees and hole spacings of 1.55 and 1.71 diameters. Their results do not differ from results without injection for injection at an angle of 20 degrees. Their results for 60 degree injection are repeated on Figure 4. The downstream distance over which the wall temperature is averaged is X; s is the equivalent width of a slot whose area is equal to the area of the holes through which the coolant flows. The average heat transfer coefficient is higher than that without injection in the region immediately downstream of the holes but soon decreases to the same value. Burggraf and Huffmeier (25) measured average heat transfer downstream of injection through single and staggered double rows of holes at an angle of 35 degrees. For blowing rates less than 1.0, they did not find significant differences between results with and without injection. At blowing rates of 1.5 and 2.0 the heat transfer was greater than occurs without

injection. The heat transfer near injection at these higher blowing rates is characterized by the equation for heat transfer without injection when the mass velocity is replaced with the coolant mass velocity.

In the present investigation local values of the heat transfer coefficient are determined for injection of heated and unheated jets of air through holes. Two injection geometries are used--a single tube normal to the direction of main flow (Figure 5(a)) and a row of tubes spaced at three diameter intervals across the span and inclined at an angle of 35 degrees to the main flow (Figure 5(b)). A few measurements are conducted using a single tube from the row. The outlets of the tubes are flush with the surface on which measurements are conducted. A constant heat flux is generated electrically at the test surface and local surface temperatures are measured. Equation 2 is used to calculate the heat transfer coefficient. For injection of unheated jets (equal jet and mainstream temperatures), the mainstream recovery temperature is used as the adiabatic wall temperature. For injection of heated jets, two sets of measurements are conducted. The wall temperature is measured with the wall heated and unheated, the latter values being the adiabatic wall temperature. Experiments with heated jets there-

fore also yield values of the film cooling effectiveness.

The flow through a single tube aligned normal to the mainstream is studied visually. A CO_2-water fog is used for the jet and this is photographed at the two different exposure times. Time exposure photographs show the average path of the jet in the crossflow; very short exposure times are used to show the eddies and vorticies that result from interaction between the jet and main flow.

The inside diameter of the normal injection tube is 2.35cm; that of the inclined tubes is 1.18cm. For injection of heated jets, a temperature difference of approximately 55°C is used, resulting in a density ratio of approximately 0.85. When unheated jets are used, the density ratio is 1.0. The range of variables studied is as follows: free stream velocity U_{∞}=30.5-61.0 m/sec, Reynolds number based on free stream velocity and injection tube diameter Re_D=0.22 x 10^5-0.88 x 10^5, displacement boundary layer thickness at the point of injection δ_o^* =0.14-0.21 cm, blowing rate M=0.1-2.18 and wall heat flux q=0-0.25 W/cm^2, resulting in differences between the wall temperature and adiabatic wall temperature in the range 0-33°C.

II. APPARATUS

A. Wind Tunnel and Secondary Flow System

A photograph and a schematic drawing of the apparatus used in this investigation are shown on Figures 7 and 8 respectively. The air mainstream in the wind tunnel flows from the room through an entrance section, the test section, a diffuser, a blower, and finally through a silencer before being discharged outside the building. Detailed descriptions of all parts but the test section proper are contained in other reports (16,17,20) and will not be repeated here.

The secondary or injected air is supplied by the building air compressor. The flow rate is controlled by a pressure regulator and needle valve and is measured with a thin plate orifice meter. Temperature fluctuations introduced by the compressor are eliminated by passing the air through a long coiled copper tubing submerged in a large tank of water. The air is heated in a stainless steel tube around which heating tapes are wrapped. The heated air flows into a plenum chamber that provides uniform flow to the injection tubes. This system is also described in

greater detail in (16,17,20).

B. Test Section

The test section measures 20.3 cm by 20.3 cm in cross section. Its overall length is different for the different types of injection. For normal injection it is 129.8 cm long; for 35 degree injection it is 153.8 cm long. The bottom wall is constructed of Textolite and the top and side walls are constructed of Plexiglas and Textolite. The test section consists of three segments.

Starting at the downstream end of the contraction and proceeding in the flow direction, the first segment of the test section is 20.3 cm long. It contains an impact probe and wall pressure tap to determine the free stream velocity, a thermocouple probe to measure the temperature of the main flow, and two thermocouple junctions embedded in the bottom wall to determine the free stream recovery temperature. The bottom wall is thin (0.32 cm thick) to allow it to respond quickly to any temperature changes in the main flow. A 0.064 cm diameter boundary layer trip wire is located on the bottom wall approximately 3.8 cm downstream of the contraction section. An additional sandpaper-type trip is located on the bottom surface of the contraction section about 24 cm upstream of its outlet. This

additional trip is included to provide a thicker boundary layer than was used in previous studies (16-21). The diameter of the sand grains lies in the range 700 to 1000 microns. The trip measures 1.1 cm in the flow direction and spans the width of the contraction section.

Proceeding in the flow direction, the next segment is the injection section. Two different segments are used in this portion of the test section. The normal injection segment that corresponds to injection as shown on Figure 5(a) is 6.5 cm long. The tube is approximately one meter long with an inside diameter of 2.35 cm. The segment containing a row of five tubes at an angle of 35 degrees to the direction of main flow as shown on Figure 5(b) is 30.5 cm long. The distance between centers of these 1.18 cm ID tubes is 3.54 cm (3 diameters). They are approximately 73 cm long. The tubes in both segments are cemented into the 0.64 cm thick bottom plates of the segments and ground flush to the tunnel surface. In order to reduce heat conduction from the tube to the plate, the injection plates are thinned from the backside to a thickness of 0.32 cm in the region surrounding the tubes. Thermocouples are soldered on the outside of the normal injection tube and center 35 degree

injection tube at distances of one-half, four and one-half and six diameters from the discharge end. The outer tubes in the row have thermocouples at the location six diameters from their outlet. The inlet ends of the injection tubes join the plenum chamber mentioned above. All tubes are surrounded with fiberglass and styrofoam insulation.

The assembly consisting of the bottom plate of the injection segment, the tubes and the plenum chamber are free to slide in the lateral direction. The hole through which the secondary gas flows can thus be located at any lateral position in the tunnel and a single row of thermocouples is used to measure wall temperature distributions downstream of injection.

The third segment of the test section contains the test plate shown on Figures 9 and 10. Eighteen stainless steel heaters are cemented to the Textolite plate. Electrical current is passed through the heaters that are wired in series and the heat generated within the heaters enters the flow. The test plate is designed to minimize heat losses out the back and conduction within the wall. Heat generated at a point should then enter the flow at that point and the local heat transfer coefficient can be determined from the local wall temperature at the point. In reality, there are heat losses due to conduction out the back and

radiation and there are small errors in the measured local wall temperature due to heat loss through the thermocouple leads and conduction within the wall. Corrections that are applied to the measurements to take these factors into account are discussed in the Appendix.

The segment of the test section containing the test plate is 103 cm long. The plate that the heaters are cemented to is 0.16 cm thick and is supported by two rows of 0.48 cm diameter Textolite pins as shown on Figures 9 and 10. The test plate is not fastened rigidly to the frame along its sides but is free to slide between the frame and tunnel wall as it expands when heated. "O" ring seals are used to prevent leaks. The Styrofoam insulation behind the plate is approximately 5 cm thick. The stainless steel heaters are 0.025 mm thick by 5.04 cm in the flow direction. They span the entire 24.1 cm width of the test plate and are spaced 0.04 mm apart. Silicone rubber cement is used to fasten the heaters to the Textolite plate. By passing under the side walls of the test section, the heaters tend to guard heat against losses out the sides of the test plate. Copper buss bars that measure 0.48 cm by 0.72 cm in cross section by 5.04 cm long are soldered to the ends of the heater strips.

Two sets of heaters were used in this investigation.

The first set, which was used for the experiments with normal injection, started to come loose from the surface midway through the experimental program. Bubbles formed between some of the heaters and the surface on which they were mounted and wrinkles appeared in several other heaters. These effects are probably the result of different rates of expansion between the stainless steel heater material and the Textolite surface. A second set of heaters was installed and operated at lower wall temperatures for experiments with 35 degree injection. These heaters adhered to the surface.

C. Instrumentation

Power for the heaters is provided by two 900 watt direct current power supplies wired in series. The current passes through a shunt and through each of the heaters that are also wired in series. Current flow is determined from the voltage drop across a calibrated shunt and the heat generated is calculated from the current flow and the resistance of the heaters. Wall temperatures are measured by 36 gage iron-constantan thermocouples that are embedded in the test surface. Copper oxide cement holds the thermocouple junction in the 0.89 mm diameter hole in the Textolite plate behind the heater. The thermocouple junction is electrically

insulated from the heater by both a thin (0.063 mm thick) layer of copper oxide cement and a thin (0.063 mm thick) layer of silicone rubber cement. The Appendix contains data analysis details and uncertainty estimates.

Boundary layer profiles are measured with an impact probe and static pressure taps in the tunnel wall. Dimensions of the probe tip are 1.11 mm wide by 0.312 mm high on the outside and 0.762 mm wide by 0.145 mm high on the inside. Static pressure taps are 0.89 mm in diameter. A micrometer head on a sliding carriage is used to position the probe.

D. Flow Visualization System

The heated test plate and tunnel side walls are replaced with different Plexiglas sections for flow visualization experiments. These sections provide a clear view of the jet. They can also be painted, cleaned and covered with adhesive backed sheets of flat black paper and plastic without fear of damaging the heaters or thermocouples.

The secondary flow system is replaced by an apparatus that generates the fog necessary for flow visualization. This apparatus consists of a sealed pressure vessel with a single outlet and the necessary tubing to connect this outlet to the injection tube.

Dry ice and hot water are combined inside the container to produce a carbon dioxide-water fog. Pressure builds up inside the container as the fog is produced, causing it to flow through the injection tube and into the tunnel. The mass flow rate of the fog is determined by the water temperature, the amount of dry ice used and the size of the dry ice pieces.

The mass flow rate is measured by timing the decrease in weight of the mixture of dry ice and hot water as the fog is ejected. Since the mass flow rate of the system is limited, it is necessary to operate the wind tunnel at velocities as low as 15 m/sec to achieve blowing rates as high as 2.0.

The fog that emerges from the flow visualization system is a two-phase mixture of carbon dioxide, water vapor and water droplets. The individual masses of dry ice and water were measured before and after the system was operated to find that the fog mixture contains approximately 88 percent carbon dioxide. In order to calculate the density of the fog, it is necessary to know what fraction of the water droplets are entrained in the fog as a fine mist and what fraction remains on the walls of the tubing of the apparatus. If it is assumed that all of the droplets remain in the tubing and the fog contains only carbon dioxide and saturated water vapor, the density is

approximately 1.47 times that of air. If it is assumed that all of the water droplets are entrained in the fog as mist along with carbon dioxide and saturated water vapor, the density is approximately 1.67 times that of air. Since it is difficult to estimate the fraction of water droplets in the fog, the density is assumed to be the mean of the two limits described above. The ratio of the density of the injected fog to that of the air mainstream is thus $1.57 \pm 6.4\%$.

Photographs are taken with a 35 mm camera. Slide projectors are used to illuminate the jet and photographs are taken at an exposure time of 0.125 sec to determine the average path of the jet. A high intensity strobe light is used as a flash attachment to take additional photographs at an exposure time of 8 μsec. The jet is illuminated with several very intense slide projectors to also record motion pictures at film speeds as high as 3300 frames per second. The lights and flash attachment are positioned to shine through the jet from the side opposite the camera. The angle between the line of sight and direction of the light incident on the jet is typically about 60 degrees.

III. OPERATING CONDITIONS AND PROCEDURES

A. Operating Conditions

This experimental investigation is conducted under the following operating conditions.

1. Steady state conditions exist during the tests.
2. In the absence of secondary flow, there is a fully developed turbulent boundary layer on the test surface.
3. In the absence of secondary flow, the velocity in the mainstream outside of the boundary layer on the test section wall is uniform.
4. The wind tunnel is operated at a mainstream velocity of either 30.5 or 61.0 m/sec.
5. In the absence of primary flow, there is fully developed turbulent pipe flow at the outlet of the injection tubes.
6. In the absence of primary flow, there is a uniform temperature profile at the outlet of the injection tubes.
7. The temperature of the injected fluid is approximately equal to that of the mainstream for studies with unheated injection.

8. The difference between the temperature of the injected fluid and the mainstream is approximately 55°C for studies with heated injection.
9. The wall heat flux is between 0 and 0.25 watts/cm^2, resulting in a difference between the wall temperature and adiabatic wall temperature in the range 0-33°C.

Velocity and temperature profiles at the outlet of the injection tubes in the absence of primary flow are presented in (16,17) and will not be repeated here. The secondary air temperature, T_2, is taken as that measured by thermocouples 6 diameters upstream of the tube outlet. The difference between this temperature and the mainstream temperature varies by approximately one percent across the row of holes, the bulk of this variation being between the outside tubes and those next to them. Variation in excess temperature across the inner three tubes is thus much less than one percent. Velocity at the outlet of the tubes varies by approximately one percent across the row.

The boundary layer on the test surface is thicker than that used in earlier studies with this apparatus (16-21) due to the addition of a sandpaper type trip upstream of the test section. Velocity profiles were therefore measured at locations both on and off the centerline of the test surface and at different

positions along the length of the test section to determine the characteristics of the new boundary layer. The injection plate was replaced by a flat surface that contained no holes for these tests. Boundary layer profiles measured at three different centerline locations along the test surface are presented on Figure 11. These profiles are seen to be in good agreement with each other and with the profile reported by Klebanoff and Diehl (26). Figure 12(a) shows the boundary layer displacement thickness both on and off the centerline of the test surface at three different locations. The variation of boundary layer thickness with lateral position is seen to be small.

Under the assumption that the boundary layer originates as a turbulent one, it is possible to determine from the velocity measurements the effective starting position of the boundary layer and with it to define flow conditions in the test section. If the Blasius equation is used for shear stress at the wall, growth of the boundary layer can be expressed in terms of the displacement thickness (27),

$$\delta^* \propto \left(\frac{\mu_\infty}{\rho_\infty U_\infty}\right)^{0.2} X_1^{0.8} . \qquad (6)$$

This equation is rearranged to be linear in X_1.

$$(\rho_\infty U_\infty)^{0.25} \delta^{*1.25} \propto X_1 \qquad (7)$$

Use of the momentum thickness δ_i to represent the

thickness of the boundary layer results in a similar equation.

$$(\rho_\infty U_\infty)^{.25} \delta_i^{1.25} \propto X_1 \qquad (8)$$

Results of boundary layer profile measurements on the centerline of the test surface are presented in the form of equations 7 and 8 on Figure 13. Straight lines fit to the data are extrapolated to the point of zero boundary layer thickness to yield an effective starting length of 46 cm upstream from the trip wire. The arrows on the abscissa denote the locations where the secondary fluid is injected. The dashed line represents the boundary layer that was present in the studies mentioned above. At the point of injection, the new boundary layer is approximately 80 percent thicker than in the previous normal injection studies and about 45 percent thicker than in the previous 35 degree injection studies.

Boundary layer growth on the walls of the test section causes the main flow to accelerate. The resulting pressure distribution is measured using pressure taps in the wall of the test section. For free stream velocities of both 30.5 and 61.0 m/sec the velocity of the main flow increases by approximately six percent over the length of the test section.

The heat transfer coefficient without secondary

injection is used as a reference for tests with injection. This heat transfer coefficient depends not only on the free stream velocity and position along the heated wall, but also on the hydrodynamic starting length from where the velocity boundary layer starts to grow to the location where heating of the wall begins. If the effect of the hydrodynamic starting length is neglected or if the velocity boundary layer starts to grow at the start of the wall heating, the heat transfer coefficient on a constant heat flux surface with no pressure gradient is given by the following equation (28).

$$St_o\left(\frac{T_w}{T_\infty}\right)^{0.4} = 0.309\, Pr^{-0.4} Re_{x_h}^{-0.2} \qquad (9)$$

This equation is also modified to take the unheated starting length into consideration in (28).

The heat transfer coefficient in the test section without injection is measured at velocities of approximately 30.5 and 61 m/sec using both injection segments. The holes are covered with very thin tape to provide a smooth surface. Typical results are shown on Figure 14. The local free stream velocity in the test section (corrected by the static pressure variation in the flow direction) is used in the Stanton and Reynolds numbers. The distance X_h from the start of heating is used in the Reynolds number. The upper

graph represents the short starting length corresponding to the normal injection segment; the lower graph corresponds to the 35 degree segment. The straight lines on the graphs are given by equation 9 in which the unheated starting length is neglected. The starting point for boundary layer growth from Figure 13 is used to determine starting lengths to use in the modification of equation 9 given by (28). The resulting curves are also shown on Figure 14. At locations near the start of heating experimental results fall between the relationships that neglect and consider the unheated starting length. At downstream locations where the effect of starting length is less important, the experimental results and theories merge together. The difference between experimental results and the theory that considers the effect of unheated starting length indicates that either the theory overcorrects equation 9 or that the starting lengths from Figure 13 used in the theory are too large. A second unheated starting length is therefore determined by fitting the equation in (28) that corrects for starting length to experimental data. Starting lengths determined in this way and the relative standard deviation between the data and the curve fit to the data are given in the table below.

Table I

Unheated Starting Lengths and Relative Standard Deviations for Curves Fit to Heat Transfer Results Without Injection

	90° Injection Section		35° Injection Section	
U (m/sec)	30.5	61	30.5	61
Unheated Starting Lengths (cm)	4.8	7.9	9.4	26.2
From boundary layer growth	71.3	71.3	95.4	95.4
From equation of (28)	4.8	7.9	9.4	26.2
Relative Standard Deviation of Curve Fits (equation from (28))				
Starting length from boundary layer growth	.106	.088	.111	.072
Starting length from equation of (28)	.030	.040	.042	.034
Zero starting length	.076	.107	.102	.154

The wall temperature should not vary across the span when there is no secondary injection. Wall temperatures measured by off-centerline thermocouples at several locations along the length of the test section are presented on Figure 12(b). The difference between the wall temperature and the free stream temperature is normalized by the difference between the temperature measured by the centerline thermocouple at that same longitudinal position in the test section and the free stream temperature. The temperature

distribution is very flat across the center 60 percent of the test section where all measurements are conducted. Temperatures near the side walls of the test section are somewhat high because the heat generated under the walls is conducted into the tunnel.

B. Operating Procedure

The primary flow in the wind tunnel, the secondary flow through the injection tubes and the heat flux from the test surface can be changed to conduct the experiments under a variety of conditions. Adiabatic wall temperatures are determined by operating the tunnel with injection of heated secondary air and no heat flux from the test surface. Heat transfer coefficients can be determined two different ways. One method is to operate the tunnel with heated injection and a heated wall. The heat transfer coefficient is defined using the difference between the heated wall temperature and the adiabatic wall temperature that was measured under the same flow conditions. The second way is to operate the tunnel with unheated injection and a heated wall. Under these conditions, the heat transfer coefficient is defined using the difference between the heated wall temperature and the free stream recovery temperature

since the adiabatic wall temperature and free stream recovery temperature are the same for unheated injection. Two separate sets of measurements are necessary to determine the heat transfer coefficient by the first method whereas only one set is necessary for the second.

In all cases, the primary flow, the secondary flow and the wall heat flux are set at the desired operating conditions and wall temperatures are measured after thermal steady state has been attained. The lateral position of the injection hole relative to the row of thermocouples is changed and wall temperatures are again measured after steady state has been reached. This procedure is repeated until the desired mapping of wall temperatures is obtained. Small adjustments in the primary flow rate, secondary flow rate or wall heat flux are made during the run when necessary to set the desired M, U_{∞} and q.

Details of data reduction techniques and uncertainty estimates are contained in Appendix A.

IV. RESULTS

A. Flow Visualization

Results of the flow visualization study are presented on Figure 15. Carbon dioxide-water fog is injected through a single tube at an angle of 90 degrees to the main flow. The free stream velocity varies from 30.5 m/sec at the low blowing rates to 15 m/sec at the high blowing rates. The two columns on the left contain photographs of the jet as viewed from the side; the columns on the right contain photographs of the jet from above. A white line denotes the centerline of the test section. The three lines crossing this line are located at distances of one, five and ten diameters downstream of the hole. They are approximately three diameters long.

The photographs at an exposure time of 0.125 sec show the outline of the jet in an average sense. As the blowing rate is increased, the jet penetrates farther into the main flow. Lateral spreading of the jet also increases with blowing rate. Photographs at an exposure time of 8 μsec indicate that the true outline of the jet is very irregular and varies with time. Interaction between the jet and mainstream creates very

large eddies and vorticies. The jet does not fill the entire outline indicated by the time averaged photographs at any given instant, but fluctuates within this outline. The short exposure time photograph at M=2.0 clearly shows the jet away from the wall whereas the time averaged photograph indicates that the jet clings to the wall. The outline of the jet at the long and short exposure times is similar to that on photographs in (20) and (21) where the blowing rate is M=0.9.

To show that the large eddies and vortices observed on the "instantaneous" photographs on Figure 15 are a result of the interaction between the jet and mainstream, photographs of the jet without a crossflow are shown on Figure 16. The eddies along the edge of the jet in still air are much smaller than those observed in the presence of a crossflow.

In order to observe the formation of eddies and vortices in the jet, high speed motion pictures were taken. The film speed is about 3300 pictures per second; the exposure time of each picture on the film is approximately 0.0001 sec (100 μsec). When viewed from the side, the jet appears to be pulsing as it leaves the hole, thus forming the large eddies that are seen along the upper edge of the jet. The eddies formed by these pulses rotate as they are accelerated

and turned by the mainstream. After turning the initial sharp curve in the jet trajectory, they proceed downstream without rotation. The high speed motion pictures viewing the jet from above show vorticies leaving both sides of the jet.

Reilly (29) has also conducted a flow visualization study for jets injected normal to a crossflow also. Most of the blowing rates in his investigation are higher than those used here, but some comparisons can be made. The interaction between the jet and crossflow that he observes is similar to that described above. Photographs of the jet trajectory that he presents for M=0.98 and 1.84 show the jet penetrating further into the mainstream than the jets at similar blowing rates on Figure 15. This difference could be due to the difference in density of the injected fluids. Reilly's secondary gas is a smoke in air mixture of which the density is probably about that of air. The carbon dioxide-water droplet mixture used as the secondary fluid in the present study has a density approximately 1.57 times that of air. Since many correlations of jet trajectories in crossflows use the momentum flux ratio I rather than the blowing rate M, a comparison between the two studies at similar values of I might be more reasonable. Blowing rates M=0.98 and 1.84 in Reilly's study then correspond to M=1.22

and 2.31 in the present investigation. Agreement between photographs is somewhat better when compared on this basis although the results of (29) still indicate slightly greater penetration. This difference could be due to differences in Reynolds number or free stream boundary layer thickness at the point of injection. Since the free stream velocity (approximately 3.2 m/sec) in (29) is much smaller than those used in the present study, the boundary layer at the point of injection in (29) could even possibly be laminar which would permit greater penetration.

Temperature profiles measured in the flow for normal injection (20,21) show that the heated air jet penetrates into the main flow for M=0.5 with the penetration increasing with blowing rate. Taking the density ratio for heated air jets (ρ_2/ρ_∞ =0.85) into consideration as is done above, this blowing rate corresponds to a blowing rate of M=0.68 with the CO_2 fog on Figure 15. The photographs on Figure 15 show the jet appears to remain near the wall at M=1.0 and starts to penetrate into the free stream at M=1.5. This discrepancy could be due to comparison of the experiments on the basis of momentum flux ratio. Most relations that correlate jet trajectory with momentum flux ratio I are for high blowing rates where the presence of the wall and the boundary layer growing on

the wall can be neglected. Comparison between experiments on the basis of I may therefore not be valid near a wall.

B. Normal Injection

1. Film Cooling Effectiveness

Results of adiabatic wall temperature measurements with the single normal injection tube are presented for different blowing rates and Reynolds numbers on Figures 17-25. The data on Figures 17-21 were measured at a higher free stream velocity than the data on Figures 22-25 to see if the Reynolds number Re_D or the boundary layer thickness at the point of injection influence the film cooling effectiveness. The film cooling effectiveness is plotted against the distance downstream of injection X/D at fixed values of the lateral position. The small inset on these figures contains a cross-plot of the film cooling effectiveness against lateral position at fixed values of the distance downstream.

The trends observed on these plots are similar to those observed in other investigations for injection through a single hole (16-19). Along the centerline (Z/D=0), the film cooling effectiveness decreases in the downstream direction as the jet temperature decreases due to spreading and mixing with the main

flow. At lateral locations beyond the initial width of the jet, the film cooling effectiveness first increases with distance downstream due to spreading of the jet before then decreasing as the jet mixes with the main flow.

The centerline film cooling effectiveness is plotted against the blowing rate M at four downstream locations on Figure 26. The effectiveness first increases with blowing rate, reaches maximum in the range M=0.4-0.5 and then decreases as the blowing rate is further increased. The behavior of these curves is controlled by two effects. As the blowing rate is increased, the amount of enthalpy contained in the jet is increased. When the jet remains near the wall, the effectiveness therefore increases as Figure 26 shows for small values of M. At blowing rates greater than 0.5, an increase in the blowing rate increases the penetration of the jet into the main flow, resulting in a decrease in the film cooling effectiveness.

Results from (17) are included on Figures 22 and 26 along with results from the present investigation. Agreement is quite good with both sets of data varying with X/D, Z/D and M in the same way. However, the results of (17) fall a few percent below those of the present study. It is unlikely that the difference is due to the wall conduction correction that is applied

to the present data or to differences in the boundary layer thickness at the point of injection, since the wall conduction correction is smaller than the difference between the two sets of results and the thicker boundary layer in the present investigation is expected to give a value of the film cooling effectiveness that is lower than that found in (17) rather than the higher value that is observed.

2. Heat Transfer Coefficient

The heat transfer coefficient downstream of injection of heated ($T_2-T_\infty \approx 55^\circ C$) and unheated ($T_2=T_\infty$) air jets is presented on Figures 27-48 for different values of the blowing rate. The large number of figures are a result of varying injection temperature, Reynolds number and wall heat flux at most blowing rates. The heat transfer coefficient h_a is defined using the difference between the wall temperature and adiabatic wall temperature as in equation 2 for heated injection. For unheated injection the adiabatic wall temperature equals the free stream temperature T_∞ and the temperature difference used to calculate h_a is T_w-T_∞. The heat transfer coefficient h_a is normalized by the heat transfer coefficient h_o measured at the same location in the test section and with the same free stream

velocity, but without secondary injection. h_a is a function of both X and Z; h_o varies with X only. The ratio h_a/h_o is plotted against the distance downstream of injection X/D at fixed values of the lateral position Z/D. The small inset on each figure presents a crossplot of h_a/h_o against Z/D at fixed values of X/D.

Data at a blowing rate M=0.1 are presented on Figures 27 and 28. Injection at this low blowing rate has little effect on the heat transfer coefficient near the hole. Further downstream, (X/D>10), the heat transfer coefficient in the region Z/D=0.25-0.75 increases to approximately 10% higher than the flat plate value. The heat transfer coefficient on the centerline is slightly lower than near the edge of the jet where a great deal of interaction occurs between the jet and the mainstream. For Z/D>1.0, injection has little effect on the heat transfer coefficient. There is good agreement between data for heated injection (Figure 27) and for unheated injection (Figure 28).

Data at a blowing rate M=0.2 are presented on Figures 29-32 for heated and unheated injection at different values of q and Re_D. All figures show the same basic trends, however, the magnitude of the heat transfer coefficient varies somewhat from figure to

figure. The heat transfer coefficient is observed to be a maximum near the edge of the jet where large eddies were observed in the flow visualization experiments and is slightly lower on the centerline as it was for M=0.1. Maximum values are approximately 12% higher than the flat plate value for Re_D=0.45 x 10^5 (Figures 29,30 and 32) and 14-16% higher for Re_D= 0.87 x 10^5 (Figure 31). The influence of the jet on the heat transfer coefficient is spread over a slightly wider area for M=0.2 than for M=0.1 and the heat transfer coefficient is slightly lower than the flat plate value for Z/D > 1.25. Figure 30 shows the heat transfer coefficient determined at a heat flux of 0.246 W/cm^2 to be 1-2% higher than that on Figure 29 where the wall heat flux is lower. The difference is probably due to experimental uncertainty as the Appendix shows that uncertainties are less at higher heat fluxes where the difference between the wall temperature and adiabatic wall temperature is greater and errors due to conduction within the wall are smaller when compared to this temperature difference. The run with unheated injection (Figure 32) and the run with heated injection at the same wall heat flux (Figure 29) agree within 1-2% with neither run being consistently higher or lower than the other. Trends observed in the run with a higher free stream velocity and thus at a

higher Reynolds number (Figure 31) are similar to those at the lower Reynolds number but the magnitude of the heat transfer coefficient is slightly higher.

Data at a blowing rate M=0.5 are presented on Figures 33-36. The maximum heat transfer coefficient is seen to be 24-26% higher than the value without injection near the hole (X/D=2.74). This maximum occurs near the edge of the jet (Z/D$\approx$0.5) with the centerline value being 2-4% lower. Near the hole, the heat transfer coefficient in the region $0 < Z/D < 0.75$ decreases quite rapidly in the downstream direction; its value lies in the range 12-15% greater than flat plate values at X/D=10 and then decreases slowly with X/D. At downstream locations the heat transfer coefficient is approximately 10-12% higher than the value without injection for Z/D in the range 0-1.0. Injection has little effect on the heat transfer coefficient at this blowing rate for $Z/D > 2.0$. Heat transfer coefficients determined at the higher heat flux (Figure 34) are seen to be 2-3% higher than those at the low heat flux (Figure 33). The run at the higher Reynolds number (Figure 35) is not significantly different from Figures 33 and 34. The run with unheated injection (Figure 36) is similar to those with heated injection (Figures 33 and 34).

Since the ratio of the density of the injected gas

to the mainstream density is different for heated injection (ρ_2/ρ_∞=0.85) and unheated injection (ρ_2/ρ_∞=1), the momentum flux ratio I is different and the jet path may also be somewhat different. A run with unheated injection that corresponds to the same value of I as heated injection at M=0.5 is therefore included on Figure 37. The blowing rate for this run is 0.54. Since this blowing rate is not much different from that on Figures 33,34 and 36 (ρ_2/ρ_∞ is still close to unity for heated injection), the results are similar and it is not possible to tell if the comparison between heated and unheated injection is better if conducted at like values of M or I.

Data at a blowing rate M=1.0 are presented on Figures 38-41. The maximum heat transfer coefficient is now located at the centerline rather than at the edge of the jet as was observed at lower blowing rates. Its magnitude is as much as 35% greater than the value without injection for Re_D=0.45 x 10^5. This maximum decreases to approximately 17% by X/D=10 and 14% by X/D=18, remaining approximately constant at greater downstream distances. At downstream locations ($18 < X/D < 35$) the heat transfer coefficient is seen to be nearly constant for $Z/D < 1.5$. It decreases to a value 4-6% higher than the value without injection at Z/D=2.5. Results on Figure 39 with a higher heat flux

are approximately 2% higher than those at a lower heat flux (Figure 38) as in earlier tests. Near the hole, results at a higher Reynolds number (Figure 40, Re_D=0.87 x 10^5) are 2-3% higher than those at Re_D=0.45 x 10^5 on the centerline and lower for Z/D>1.0. Results at the two different Reynolds numbers are similar at downstream locations. The heat transfer coefficient determined with unheated injection at M=1.0 (Figure 41) is similar to that found on Figures 38 and 39 for heated injection at the same blowing rate. The heat transfer coefficient for unheated injection at the same value of I as heated injection for M=1.0 is shown on Figure 42. Results on this figure do not differ from those on Figures 38,39 or 41 by an amount significant enough to draw any conclusions as to whether comparison between heated and unheated injection is better at similar values of M or I.

Results for heated and unheated injection at M=1.5 are shown on Figures 43 and 44 respectively. Trends on both figures are similar to those observed at M=1.0. The maximum (centerline at this M) heat transfer coefficient is approximately 40% higher than the value without injection near the hole, decreasing rapidly with X/D to X/D$\approx$18 and then remaining approximately 10% above the flat plate value. Results

for unheated injection are slightly higher than those for heated injection.

Figures 45-47 contain measurements with heated and unheated jets at M=2.0. Data on these plots behave in the same way as at M=1.0 and 1.5 except that the maximum (centerline at this M) heat transfer coefficient is approximately 42-44% higher than the value without injection near the hole. Results from the run with the higher heat flux (Figure 46) are approximately 2% higher than those with a lower heat flux (Figure 45). Data for heated and unheated injection at M=2.0 are similar. Since the jets penetrate into the free stream at this blowing rate, there are no steep temperature gradients within the test surface for heated injection and the uncertainties associated with these gradients disappear. Uncertainties for heated and unheated injection are now approximately the same and agreement between the two sets of results is good. Results on Figure 48 for unheated injection at the same value of I as heated injection at M=2.0 are not significantly different from those observed for both heated and unheated injection at M=2.0.

The heat transfer results are summarized on Figure 49. The maximum (not always at the centerline as mentioned above) heat transfer coefficient at a

fixed value of X/D is plotted against the blowing rate at three different downstream locations. Near the hole, injection has little effect on the heat transfer coefficient at low values of M. A strong effect appears as M is increased, the maximum heat transfer coefficient near the hole (X/D=2.74) being approximately 35% higher than the value without injection at M=1.0 and 40-45% above the value without injection at M=2.0. These high values of the heat transfer coefficient are probably due to the high turbulence level that arises from the interaction between the jet and main flow near the point of injection. It was observed earlier (Figure 15) that very large eddies result from this interaction. References (20) and (21) report the turbulence intensity to be as high as 60% in this region for blowing rates greater than 1.0.

The maximum heat transfer coefficient decreases quite rapidly in the downstream direction. At X/D=7.33, the maximum heat transfer coefficient is in the range 15-20% greater than the value without injection for $M \geq 1.0$. Turbulence intensities have decreased to 15-20% at this location (20,21). The maximum heat transfer coefficient decreases slowly in the downstream direction from this point on. For all but the lowest blowing rate at which tests were conducted (M=0.1), its magnitude lies in the range

10-15% above flat plate values at X/D=35.44. References (20) and (21) show the turbulence intensity to be slightly less than 10% at X/D=26.24 for M=1 and 2.

Near the point of injection, values of the heat transfer coefficient with injection that are higher than those without injection are due to the large eddies and high turbulence levels that result from interaction between the jet and mainstream. The 10-15% increase in the heat transfer coefficient with injection over that without injection that is observed at downstream locations is not easily explained. Secondary injection increases the mass flow through the test section by approximately 1.1% for M=1 and 2.2% for M=2. Resulting increases in the heat transfer coefficient due to these increased mass flows are only approximately 0.8% and 1.7% respectively. If it is assumed that injection destroys the boundary layer approaching the heaters and a new one starts to grow at the start of heating, the increase in the heat transfer coefficient is approximately 1-2% at X/D=20 and less than 1% at X/D=40. Attempts to find an effective starting point for turbulent boundary layer growth downstream of the start of heating yield a heat transfer coefficient with injection that varies from approximately

15% above the value without injection at X/D=10 to 2% greater than the value without injection at X/D=40 rather than the nearly constant value that is observed in this range of X/D. Mean velocity profiles in (21) and (22) show the boundary layer with injection at M=1 to be thinner than that without injection as far downstream as X/D=26.24. The higher wall shear stress in the thinner boundary layer is in agreement with the increased heat transfer coefficient that is observed with injection at downstream locations. However, this higher heat transfer coefficient at downstream locations can not be calculated on the basis of a new turbulent flat plate boundary layer that starts to grow at or downstream of injection.

For $M \leq 0.5$, the maximum heat transfer coefficient is at the edge of the jet rather than at the centerline (Z/D=0) as at higher blowing rates. The jet remains near the wall at these low blowing rates and the main flow interacts with the jet at its sides and above it. The high turbulence resulting from interaction between the main flow and sides of the jet causes the maximum heat transfer coefficient to be at the sides of the jet. At higher blowing rates, the jet penetrates into the main flow permitting the mainstream to flow around and under the jet. Interaction between the jet and mainstream now also occurs between the jet and the wall

and the heat transfer coefficient on the centerline is no longer lower than at lateral positions.

At a given value of the blowing rate M, the heat transfer coefficient measured with heated injection and a higher value of the wall heat flux is usually observed to be approximately 2% higher than that determined with heated injection at a lower wall heat flux. This difference is within the uncertainty in the heat transfer coefficient as shown in the Appendix. With the exception of M=2.0, the heat transfer coefficient determined with unheated injection at the lower wall heat flux is usually 1-2% higher than that measured with heated injection at the same heat flux. This difference is also less than the uncertainty given in the Appendix.

Uncertainty in the heat transfer coefficient for unheated injection is less than that for heated injection since temperature gradients within the test surface are not as great as for heated injection. Uncertainty in the heat transfer coefficient is also less for measurements at the higher heat flux. The measurements with heated injection and a low wall heat flux are therefore probably not quite as accurate as those with unheated injection or heated injection and a higher wall heat flux.

Density ratios for heated (ρ_2/ρ_∞=0.85) and

unheated ($\rho_2 / \rho_\infty = 1$) injection are similar enough to give practically the same results when heated and unheated injection are compared at the same value of either M or I. It is therefore not possible to say from these results whether the results should be applied at like values of M or I when density ratios significantly different from 1 are used.

C. 35 Degree Injection

In the previous section it is shown that the heat transfer coefficient with heated and unheated injection are almost identical. Since it is easier (and also more accurate as shown in the Appendix) to determine the heat transfer coefficient with unheated injection where it is not necessary to measure the adiabatic wall temperature, this mode of operation is used for the bulk of the measurements with 35 degree injection. Adiabatic wall temperatures corresponding to these measurements are included in (18) and (19). Heated injection is used only for measurements at $Re_D = 0.44 \times 10^5$ where the adiabatic wall temperature has not been previously measured for a row of holes.

1. Film Cooling Effectiveness

Figures 50-52 contain film cooling effectiveness distributions at $Re_D = 0.44 \times 10^5$ for M=0.2, 0.5 and 1. The trends on these figures are similar to those

observed in (18) and (19) and for normal injection. The dashed line on each figure shows the centerline film cooling effectiveness before the correction for conduction within the wall that is described in the Appendix is applied. This correction is largest on the centerline. The correction is significant for injection through this diameter tube (D=1.18cm) and should be taken into consideration in the region near the hole. The correction is not important for the larger diameter tube used for normal injection because the thickness of the wall relative to the tube diameter is smaller for the larger tube.

The centerline film cooling effectiveness is plotted against the blowing rate M on Figure 53. Data from (18) and (19) to which the wall conduction correction similar to and of the same order of magnitude as that described in the Appendix is applied are also included. Trends in the two sets of data are similar, each displaying a peak between M=0.4 and 0.5, but the magnitudes differ. The film cooling effectiveness for injection at 35 degrees thus seems to be influenced by the Reynolds number and/or boundary layer thickness at the point of injection. Such an effect was not observed for normal injection (Figure 26) where the centerline film cooling effectiveness is seen to vary only with M and not with Re_D or δ_o^*/D in

the limited range of Re_D and δ_o^*/D that was studied.

Variation of the film cooling effectiveness with Reynolds number and boundary layer thickness at the point of injection for injection through a single tube at 35 degrees is explained on the basis of the boundary layer thickness at the point of injection in (18) and (19). When the boundary layer at the point of injection is thin, the jet encounters a greater force upon leaving the injection tube than for a thicker boundary layer and is turned faster, remaining closer to the wall and increasing the film cooling effectiveness. The film cooling effectiveness therefore decreases as the boundary layer thickness at the point of injection increases. The centerline film cooling effectiveness is plotted against the displacement boundary layer thickness at the point of injection normalized by the hole diameter on Figure 54. Since no difference was found between centerline values of the film cooling effectiveness for injection through a single hole and through a row of holes spaced at three diameter intervals for $M \leq 1.0$ in (18) and (19), both single hole results and results for a row of holes are included on this figure. Data from the present investigation ($\delta_o^*/D \approx 0.15$) does not follow the trend described earlier but is greater than some of the results in which δ_o^*/D is smaller. This is because of

Reynolds number variations within the data on the figure. The dimensionless boundary layer thickness in (16-19) is varied by changing the free stream velocity or the hole diameter and is thus not independent of the Reynolds number. Since an additional boundary layer trip is used in the wind tunnel for the present investigation, the boundary layer is thicker than that used in (16-19) at similar values of the free stream velocity. When the variation of the centerline film cooling effectiveness with δ_o^*/D is observed at a single value of the Reynolds number, data from this investigation and results from (16-19) agree, showing the film cooling effectiveness to decrease as δ_o^*/D is increased. The decrease is not as great at the larger values of δ_o^*/D as for the smaller values of δ_o^*/D in (18) and (19). Figure 54 also indicates that the film cooling effectiveness seems to increase with Reynolds number Re_D but it is difficult to determine the amount of the increase with the limited amount of data on the figure. If anything, one might expect the opposite effect because of greater mixing at higher Reynolds numbers. An investigation which permits independent variation of the Reynolds number and boundary layer thickness over a wider range than is done here is necessary to better determine the influence of these parameters on the film cooling process.

2. Heat Transfer Coefficient

The heat transfer coefficient downstream of injection through a row of holes at an angle of 35 degrees to the main flow is presented on Figures 55-66 for different values of the blowing rate and Reynolds number. The holes are spaced at three diameter intervals across the span.

Results for blowing rates M=0.1 and 0.2 are presented on Figures 55-58. Figure 55 shows that injection has little effect on the heat transfer coefficient for M=0.1. The local heat transfer coefficient never differs from the value without injection by more than 5%. Figure 56 shows the heat transfer coefficient for M=0.2 to be less than the flat plate value at $Re_D=0.23 \times 10^5$. The heat transfer coefficient does not vary much across the span. At $Re_D=0.44 \times 10^5$, the centerline heat transfer coefficient is somewhat less than between holes near the point of injection. At downstream locations, it does not vary much across the span. In general, the heat transfer coefficient at $Re_D=0.44 \times 10^5$ (Figures 57 and 58) is approximately 3% higher than at the lower Reynolds number (Figure 56). Results for heated (Figure 56) injection give similar values of the heat transfer coefficient as unheated (Figure 57) injection. The effect of injection on heat transfer at M=0.1 and 0.2

is seen to be less for injection through a row of holes at 35° than for normal injection through a single tube where the heat transfer coefficient was observed to be as much as 10-15% greater than the flat plate value at these blowing rates.

Figures 59 and 60 show the heat transfer coefficient with unheated injection at M=0.5 to be lower on the centerline (Z/D=0) than between holes where the jets interact with the main flow. For Re_D=0.44 x 10^5, the heat transfer coefficient varies from approximately 10% lower to about 3% above the value without injection. For Re_D=0.44 x 10^5, results are about 3% higher than those at the lower Reynolds number. Results for heated injection (Figure 61) are similar to those for unheated injection at M=0.5 except for the region immediately downstream of the hole (Figure 60) where centerline results for heated injection are higher.

Results for M=0.99 are presented on Figures 62-64. For unheated injection at Re_D=0.44 x 10^5 (Figure 63), the heat transfer coefficient on the centerline decreases from a value that is approximately 10% greater than the flat plate value and nearly constant across the span to a value approximately 4-5% below the value without injection for X/D>30. At downstream locations, the heat transfer coefficient between holes where the jets interact with each other and with the

main flow is approximately 15-20% greater than the centerline value. The heat transfer coefficient at a lower Reynolds number (Figure 62, $Re_D=0.22 \times 10^5$) is approximately 4% lower than the heat transfer coefficient for $Re_D=0.44 \times 10^5$ (Figure 63). Results for heated injection (Figure 64) are greater than those for unheated injection (Figure 63). The difference varies from approximately 6% near the hole to approximately 2% at downstream locations.

Figures 65 and 66 contain results at blowing rates M=1.45 and 1.94 respectively. The centerline heat transfer coefficient behaves in the same way as for M=0.99, decreasing from a value that is nearly constant across the span. The heat transfer coefficient between holes increases rapidly in the downstream direction, reaching a maximum at X/D=20-25 and then decreasing. At M=1.45, the heat transfer coefficient achieves a maximum value (occurring at $Z/D \approx 1$) about 22% higher than without injection. For M=1.94, this maximum (also occurring at $Z/D \approx 1$) is approximately 37% greater than the flat plate value.

In film cooling applications where the surface to be cooled is a good heat conductor, conduction within the wall decreases lateral variations in the wall temperature and the film cooling effectiveness and heat transfer coefficient depend primarily on X/D. A heat

transfer coefficient $\bar{h}_a$ that can be used in these applications is calculated by averaging the wall temperatures that are used to determine local heat transfer coefficients

$$\bar{h}_a(X/D) = \frac{\bar{q}}{\bar{T}_w(X/D) - \bar{T}_{aw}(X/D)} \tag{10}$$

The bar denotes an average in the lateral direction only.

$$\bar{T}_w(X/D) = \frac{1}{3}\int_{-1.5}^{+1.5} T_w(X/D, Z/D)\, d(Z/D) \tag{11}$$

The adiabatic wall temperature and approximately constant (variation is due to change of resistance of heaters with temperature) wall heat flux are averaged in this same way.

The heat transfer coefficient defined using laterally averaged wall temperatures is presented on Figures 67 and 68 for $Re_D = 0.44 \times 10^5$ and $Re_D = 0.22 \times 10^5$ respectively. Figure 69 contains a cross plot of this heat transfer coefficient against the blowing rate M. Numerical results are included in Table II. Figure 67 shows that results for $M \leq 0.5$ do not differ from values without injection by more than 3% for $Re_D = 0.44 \times 10^5$. The heat transfer coefficient at the lower Reynolds number (Figure 68) varies from approximately 6% below the flat plate value near injection to approximately 3-5% below the value without injection at downstream

locations for M=0.2 and 0.5. Differences between results for heated and unheated injection are not as large as the expanded scale on Figure 67 makes them appear. The heat transfer coefficient for heated injection is smaller than for unheated injection by approximately 1% for M=0.2 and 1.5% for M=0.5. These differences are similar to those that are observed for normal injection through a single tube and are probably due the higher uncertainties that are associated with heated injection.

At M=0.99, the heat transfer coefficient decreases from approximately 10-12% above the value without injection near the hole to 5-6% above flat plate values at downstream locations for $Re_D=0.44 \times 10^5$. Figure 69 shows results for $Re_D=0.22 \times 10^5$ to be approximately 5% lower than those at the higher Reynolds number for M=0.99. The higher heat transfer coefficient at the higher Reynolds number is perhaps due to increased mixing of the secondary flow at the higher Reynolds number. The heat transfer coefficient determined with heated injection ($\rho_2/\rho_\infty=0.85$) is approximately 2% higher than that found with unheated injection ($\rho_2/\rho_\infty=1$) at this blowing rate. For M=0.2 and 0.5 the heat transfer coefficient with heated injection was observed to be less than for unheated injection. This difference was similar to that found for normal

injection and was attributed to greater uncertainties in the measurements with heated injection. Since the jet is penetrating into the mainstream for M=1, the increased heat transfer coefficient for heated injection at this blowing rate could be due to the difference in the momentum flux ratio I between heated and unheated injection.

Results at M=1.45 and M=1.94 show that injection has a significant effect on the heat transfer coefficient at these larger blowing rates. The heat transfer coefficient increases in the downstream direction, reaches a peak at $X/D \approx 20$ and then decreases as X/D is further increased. The peak value is about 14% greater than the value without injection for M=1.45 and about 27% higher for M=1.94. References (18) and (19) show the film cooling effectiveness increasing with X/D for 35° injection through a row of holes at M=1.5 and 2. The jets penetrate into the main flow at these blowing rates and the increase in effectiveness is explained as being the result of spreading of the jets. The increase in the heat transfer coefficient can be explained in the same way. The heat transfer coefficient increases because of the high turbulence level near the edges of the jets that are spreading toward the wall.

The heat transfer coefficient based on the average (in both the lateral and downstream directions) wall

temperature is determed by Metzger and co-workers (9,10) for injection through a row of holes at an angle of 60° with the main flow. These results are shown on Figure 4. Hole spacings of 1.55 and 1.71 diameters are used at blowing rates M=0.25, 0.50, and 0.75. Although the wall temperatures used to calculate $\bar{h}_a$ in the present work are averaged only in the lateral direction, $\bar{h}_a$ can be compared with the results of (9) and (10) at low blowing rates where h_a does not vary much in the downstream direction. The results of (9) and (10) are a few percent above flat plate values at M=0.25, results on Figures 67 and 68 for M=0.2 are 3-5% below flat plate values at $Re_D=0.22 \times 10^5$ and approximately equal to the value without injection for $Re_D=0.44 \times 10^5$. The small difference between the results could be due to the difference in blowing rates, different Reynolds numbers or the different injection geometries. For M=0.5, the heat transfer coefficients of (9) and (10) decrease from approximately 25% above the flat plate value near the hole to approximately 10% above the value without injection at $X/s \approx 65$ (X/s =65 corresponds to X/D=29.8 for 1.71 diameter spacing and X/D=33 for 1.55 diameter spacing). The large difference between these results and results on Figures 67 and 68 which fall a few percent below the value without injection may be due to differences in geometry

or increased mass flow in the mainstream due to secondary injection. The larger injection angle would increase interaction between the jet and mainstream and the smaller hole spacings should increase interaction between neighboring jets. Both of these effects would tend to increase the heat transfer coefficient. For M=0.5, secondary injection apparently increases the mainstream flow rate in (9) and (10) by 5-10%. This additional mass flow could increase the heat transfer coefficient by 4-8%.

3. Single Hole

The heat transfer coefficient downstream of 35° injection through a single hole is presented on Figures 70-73 for M=0.5, 0.97, 1.46, and 1.95. At a blowing rate M=0.5, there is little difference between results for a single hole (Figure 70) and for a row of holes with 3 diameter spacings (Figure 59). At M=1.0, centerline results are similar for the single hole (Figure 71) and the row (Figure 62), but heat transfer coefficients between holes are higher for the row than those at the same lateral distance from the single jet. At blowing rates M-1.5 and 2.0, results for the row of holes (Figures 65 and 66) are much greater than those for injection through a single hole (Figures 72 and 73). Interaction between adjacent jets thus causes

larger heat transfer coefficients even near the hole at blowing rates above M=0.5.

Comparison of Figures 36 and 70 for M≈0.5, Figures 41 and 71 for M≈1, Figures 44 and 72 for M≈1.5 and Figures 47 and 73 for M≈2 shows the heat transfer coefficient for 35° injection through a single hole to be smaller than for normal injection through a single hole. Figure 49 which summarizes heat transfer results for normal injection shows the heat transfer coefficient to be 15-20% greater than the value without injection at X/D=7.33 and 10-15% greater than the flat plate value at X/D=35.44 for M>0.5. The heat transfer coefficient for 35 degree injection through a single tube is less than 13% greater than the value without injection for X/D≈7 and less than 4% greater than the flat plate value for X/D≈35. For blowing rates M=1.45 and 1.95, the heat transfer coefficient at X/D≈80 for 35° injection through a single tube is less than the value at this location without injection. These large differences in the heat transfer results between 90° and 35° injection through a single hole, especially at the higher blowing rates, are probably due to the different ways in which the jets interact with the mainstream. The jet injected at 35° has a velocity component in the direction of the main flow; the jet injected

normal to the mainstream has no initial velocity component in the direction of main flow. There is therefore more interaction between the normally injected jet and the mainstream, resulting in higher turbulence levels and a higher heat transfer coefficient than for 35° injection. This effect is in agreement with film cooling effectiveness results of (17) where lower effectiveness values and increased spreading of the jet for normal injection when compared to 35° injection are attributed to greater interaction between the jet and mainstream for normal injection.

V. CONCLUSIONS

Normal Injection

The centerline (Z/D=0) film cooling effectiveness for normal injection decreases in the downstream direction because the jet temperature decreases due to spreading and mixing with the main flow. At lateral locations beyond the initial width of the jet, the film cooling effectiveness first increases with distance downstream due to spreading of the jet before then decreasing as the jet mixes with the main flow. Variation of the centerline film cooling effectiveness with blowing rate M at four downstream locations is shown on Figure 26. The effectiveness first increases with blowing rate, reaches a maximum in the range M=0.4-0.5 and then decreases as the blowing rate is further increased. For $M < 0.4\text{-}0.5$, the jet remains near the wall and the film cooling effectiveness increases as the relative enthalpy contained within the jet increases with M. At blowing rates greater than 0.5, an increase in the blowing rate increases the penetration of the jet into the main flow, resulting in a decrease in the film cooling effectiveness. The increasing jet penetration with blowing

rate is shown on the photographs on Figure 15. Agreement between the film cooling effectiveness measured in this investigation and the results of (17) is good. Comparison of the results of (17) with those of the present investigation (Figure 26) does not show a significant variation of the film cooling effectiveness with Reynolds number Re_D or dimensionless boundary layer thickness at the point of injection δ_s^*/D over the limited range of these parameters for which results are available.

Heat transfer results for normal injection are summarized on Figure 49 where the maximum heat transfer coefficient (not at the centerline for $M \leq 0.5$ but near the edge of the jet), at three fixed downstream locations is plotted against the blowing rate. Near the hole, injection has little effect on heat transfer for M=0.1. At blowing rates 0.1 and 0.2, the heat transfer coefficient is observed to be less than the value without injection at times. A strong effect appears as M is increased, the maximum heat transfer coefficient near the hole (X/D=2.74) being approximately 35% higher than the value without injection at M=1.0 and 40-45% above the value without injection at M=2.0. These high values of the heat transfer coefficient are probably due to the high turbulence level that arises from interaction between the jet and main flow near the

point of injection. Results of flow visualization (Figure 15) show that very large eddies and vortices are caused by this interaction. References (20) and (21) report the turbulence intensity to be as high as 60% in this region for blowing rates greater than M=1.0.

The maximum heat transfer coefficient decreases quite rapidly with downstream position (cf. Figure 47) and then levels off. At X/D=7.33 the maximum heat transfer coefficient is in the range 15-20% greater than the value without injection for $M \geq 1.0$. At X/D= 35.44, the maximum heat transfer coefficient lies in the range 10-15% above the flat plate value for $M \geq 0.2$. This 10-15% increase in the heat transfer coefficient over that without injection is not as easily explained as the increased values near the hole. Turbulence intensities (20,21) have decreased to 15-20% at $X/D \approx 7$ and to approximately 10% at $X/D \approx 26$ for M=1 and 2. Increased heat transfer due to the increased mass flow in the test section caused by injection is calculated to be less than 1.7%. Mean velocity profiles in (21) and (22) show the boundary layer with injection at M=1 to be thinner than that without injection as far downstream as X/D=26.24. The higher wall shear stress in the thinner boundary layer is in agreement with the increased heat transfer coefficient that is observed at

downstream locations. However, this higher heat transfer coefficient at downstream locations cannot be calculated on the basis of a new turbulent flat plate boundary layer that starts at or downstream of injection.

For $M \leq 0.5$, the maximum heat transfer coefficient is at the edge of the jet rather than at the centerline ($Z/D=0$) as at higher blowing rates (cf. Figure 32). The jet remains near the wall at these low blowing rates and the main flow interacts with the jet at its sides and above it. The high turbulence resulting from interaction between the main flow and sides of the jet causes the maximum heat transfer coefficient to be at the sides of the jet. At higher blowing rates, the jet penetrates into the main flow permitting the mainstream to flow around and under the jet. Interaction between the jet and mainstream now also occurs between the jet and the wall and the heat transfer coefficient on the centerline is no longer lower than at lateral positions (cf. Figure 41).

Variations of the heat transfer coefficient with Reynolds number, wall heat flux and injection temperature for normal injection are within the uncertainty of the experiment. Density ratios for heated ($\rho_2/\rho_\infty = 0.85$) and unheated ($\rho_2/\rho_\infty = 1$) injection are similar

enough to give practically the same results when heated and unheated injection are compared at the same value of either M or I. It is therefore not possible to say from these results whether the results should be applied at like values of M or I or some combination of these parameters when density ratios significantly different from 1 are used.

35 Degree Injection

The film cooling effectiveness for 35° injection through a row of holes varies with X/D, Z/D and M in a similar manner as for normal injection through a single tube for $M<1$. Comparison of effectiveness values with results from (18) and (19) indicate that the film cooling effectiveness also varies with Reynolds number and boundary layer thickness at the point of injection (unlike the normal injection results cited above). Figure 54 shows that the centerline film cooling effectiveness decreases as the boundary layer thickness at the point of injection is increased. When the boundary layer at the point of injection is thin, the jet encounters a greater force upon leaving the injection tube than for a thicker boundary layer and is turned faster, remaining closer to the wall and increasing the film cooling effectiveness. This effect, as would be expected, seems most important at $M\approx0.5$

which is the blowing rate where penetration of the jet begins to be important.

The film cooling effectiveness seems to increase with Reynolds number Re_D (cf. Figure 54). If anything, one might expect the opposite effect because of greater mixing at higher Reynolds numbers.

The heat transfer coefficient for 35 degree injection through a single hole is observed to be smaller than for normal injection. Whereas the heat transfer coefficient for normal injection (cf. Figure 49) is observed to be 15-20% greater than the value without injection at $X/D \approx 7$ and 10-15% greater than the flat plate value at $X/D \approx 35$ for $M > 0.5$, the heat transfer coefficient for injection through a single 35° tube (cf. Figure 73) is less than 13% greater than the value without injection at $X/D \approx 7$ and less than 4% greater than the flat plate value for $X/D \approx 35$. The jet injected at 35° has a velocity component in the direction of main flow; the jet injected normal to the mainstream has no initial velocity component in the direction of main flow. There is therefore more interaction between the normally injected jet and the mainstream, resulting in higher turbulence levels and a higher heat transfer coefficient than for 35 degree injection. This effect is in agreement with film cooling results of (17) where lower effectiveness

values and increased spreading of the jet for normal injection when compared to 35 degree injection are attributed to greater interaction between the jet and mainstream for normal injection.

There is little difference between the heat transfer coefficient for 35° injection through a single hole and 35° injection through a row of holes spaced at three diameter intervals across the span for M=0.5 (Figures 59 and 70). At M=1.0, centerline heat transfer results are similar for the single hole and row, but heat transfer for the row is higher between holes than at the same lateral distance from the single jet (Figures 62 and 71). At M=1.5 and 2, heat transfer results for the row of holes are much higher than those for injection through a single hole at all lateral positions (e.g. Figures 66 and 73). Interaction between adjacent jets and between the jets and the mainstream thus increases heat transfer at blowing rates above M=0.5. A similar effect was observed in (18) and (19) where interaction between jets increased the film cooling effectiveness at blowing rates greater than 1.

The influence of injection on heat transfer for 35° injection through a row of holes is much smaller than for normal injection through a single hole at blowing rates $M \leq 0.5$. The local heat transfer

coefficient for normal injection is observed to be as much as 10-15% greater than the value without injection for M=C.1 and C.2 and as much as 25% greater than the value without injection for M=C.5 (cf. Figure 49). The local heat transfer coefficient for 35° injection through a row of holes does not exceed the flat plate value by more than 5% at these blowing rates (cf. Figure 60); the heat transfer coefficient based on the laterally averaged temperature difference ranges from approximately 5% below to approximately 2% above the value without injection at these blowing rates (cf. Figures 67 and 68). At downstream locations (X/D> 35), the heat transfer coefficient for 35° injection through a row of holes varies by less than 7% across the span for M=C.1 and C.2. The heat transfer coefficient is observed to vary by as much as 13% across the span for M=C.5, the values being higher between holes than on the centerline.

At blowing rates M=1, 1.5 and 2, the heat transfer coefficient is observed to vary by as much as 20% in the lateral direction for 35° injection through the row of holes (eg. Figures 63,65, and 66). The heat transfer coefficient is greatest between holes where the jets interact with the mainstream and with each other. At blowing rates M=1.5 and 2, the heat transfer coefficient based on laterally averaged wall temperatures

first increased in the downstream direction, reaches a maximum value at $X/D \approx 20$ and then decreases with X/D (cf. Figures 67 and 68). The jets penetrate into the free stream at these blowing rates and then spread toward the wall. The heat transfer coefficient increases with X/D for $X/D \leq 20$ because of the high turbulence level near the edges of the jets that are spreading toward the wall.

The heat transfer coefficient for 35° injection through the row of holes at $Re_D = 0.44 \times 10^5$ is approximately 3-5% higher than at $Re_D = 0.22 \times 10^5$. The higher heat transfer coefficient at the higher Reynolds number is perhaps due to increased mixing of the secondary flow at the higher Reynolds number.

REFERENCES

1. R.J. Goldstein, "Film Cooling," Advances in Heat Transfer, vol. 7, Academic Press, New York and London, 1971, pp 321-379.

2. J.P. Hartnett, R.C. Birkebak and E.R.G. Eckert, "Velocity Distributions, Temperature Distributions, Effectiveness and Heat Transfer for Air Injected Through a Tangential Slot into a Turbulent Boundary Layer," Journal of Heat Transfer, Trans. ASME, Series C, vol. 83, 1961, pp 293-306.

3. J.P. Hartnett, R.C. Birkebak and E.R.G. Eckert, "Velocity Distributions, Temperature Distributions, Effectiveness and Heat Transfer in Cooling of a Surface with a Pressure Gradient," International Developments in Heat Transfer, Part IV, ASME, New York, 1961, pp 682-689.

4. S. Scesa, "Effect of Local Normal Injection on Flat Plate Heat Transfer," Ph.D. Thesis, University of California, 1954.

5. R.A. Seban and L.H. Back, "Effectiveness and Heat Transfer for Turbulent Boundary Layer With Tangential Injection and Variable Free-Stream Velocity," Journal of Heat Transfer, Trans. ASME, Series C, vol. 84, 1962, pp 235-244.

6. R.A. Seban, H.W. Chan and S. Scesa, "Heat Transfer to a Turbulent Boundary Layer Downstream of an Injection Slot," ASME Paper No. 57-A-36, 1957.

7. R.A. Seban, "Heat Transfer and Effectiveness for Turbulent Boundary Layer with Tangential Fluid Injection," Journal of Heat Transfer, Trans. ASME, Series C, vol. 82, 1960, pp 303-312.

8. D.E. Metzger, H.J. Carper and L.R. Swank, "Heat Transfer With Film Cooling Near Nontangential Injection Slots," Journal of Engineering for Power, Trans. ASME, Series A, vol. 90, 1968, pp 157-163.

9. D.E. Metzger and D.D. Fletcher, "Surface Heat Transfer Immediately Downstream of Flush, Non-Tangential Injection Holes and Slots," AIAA Paper No. 69-523, 1969.

10. D.E. Metzger, J.R. Biddle and J.M. Warren, "Evaluation of Film Cooling Performance on Gas Turbine Surfaces," High Temperature Turbines, AGARD-CP-73-71, 1971, pp 24-1-24-7.

11. E.R.G. Eckert, R.J. Goldstein and D.R. Pedersen, "Comment on 'Evaluation of Heat Transfer for Film-Cooled Turbine Blades,'" Journal of Aircraft, vol. 8, no. 1, 1971, pp 63-64.

12. E.R.G. Eckert, "Film Cooling With Injection Through Holes," High Temperature Turbines, AGARD-CP-73-71, 1971, pp 17-1-17-17.

13. K. Wieghardt, "Hot-Air Discharge for De-Icing," AAF Translation, Report No. F-TS-919-Re, Wright Field, 1946.

14. S.J. Papell, "Effect on Gaseous Film Cooling of Coolant Injection Through Angled Slots and Normal Holes," NASA Technical Note D-299, 1960.

15. J.H. Chin, S.C. Skirvin, L.E. Hayes and F. Burggraf, "Film Cooling with Multiple Slots and Louvers," Journal of Heat Transfer, Trans. ASME, Series C, vol. 83, 1961, pp 281-292.

16. R.J. Goldstein, E.R.G. Eckert and J.W. Ramsey, "Film Cooling with Injection Through Holes: Adiabatic Wall Temperatures Downstream of a Circular Hole," Journal of Engineering for Power, Trans. ASME, Series A, vol. 90, 1968, pp 384-395.

17. R.J. Goldstein, E.R.G. Eckert and J.W. Ramsey, "Film Cooling with Injection Through a Circular Hole," NASA CR-54604, May 1968 (also University of Minnesota Heat Transfer Laboratory TR No. 82).

18. R.J. Goldstein, E.R.G. Eckert, V.L. Eriksen and J.W. Ramsey, "Film Cooling Following Injection Through Inclined Circular Tubes," NASA CR-72612, November 1969 (also University of Minnesota Heat Transfer Laboratory TR No. 91).

19. R.J. Goldstein, E.R.G. Eckert, V.L. Eriksen and J.W. Ramsey, "Film Cooling Following Injection Through Inclined Circular Tubes," Israel Journal of Technology, vol. 8, no. 1-2, 1970, pp 145-154.

20. J.W. Ramsey, "The Interaction of a Heated Air Jet with a Deflecting Flow, Ph.D. Thesis, University of Minnesota, 1969.

21. J.W. Ramsey and R.J. Goldstein, "Interaction of a Heated Jet with a Deflecting Flow," NASA CR-72613, April 1970 (also University of Minnesota Heat Transfer Laboratory TR No. 92, cf ASME Paper No. 71-HT-2, to appear in Journal of Heat Transfer).

22. J.W. Ramsey, R.J. Goldstein and E.R.G. Eckert, "A Model for Analysis of the Temperature Distribution With Injection of a Heated Jet Into an Isothermal Flow," presented at the 4th International Heat Transfer Conference, Versailles, 1970.

23. V.L. Eriksen, E.R.G. Eckert and R.J. Goldstein, "A Model For Analysis of the Temperature Field Downstream of a Heated Jet Injected into an Isothermal Crossflow at an Angle of 90°," University of Minnesota Heat Transfer Laboratory TR No. 101.

24. C. Liess and J. Carnel, "Application of Film Cooling to Gas-Turbine Blades," High Temperature Turbines, AGARD-CP-73-71, 1971, pp 23-1-23-9.

25. F. Burggraf and R.W. Huffmeier, "Film Effectiveness and Heat Transfer Coefficients for Injection from One and Two Rows of Holes at 35° to the Surface," AEG-Technical Information Series Report No. R70AEG351, General Electric Co., Lynn, Mass., Cincinnati, Ohio, August 1970.

26. P.S. Klebanoff and Z.W. Diehl, "Some Features of Artificially Thickened Fully Developed Turbulent Boundary Layers With Zero Pressure Gradient," NACA Report 111C, 1952.

27. E.R.G. Eckert and R.M. Drake, Heat and Mass Transfer, McGraw-Hill, New York, 1959, pp 142-144.

28. W.C. Reynolds, W.M. Kays and S.J. Kline, "Heat Transfer in the Turbulent Incompressible Boundary Layer, III-Arbitrary Wall Temperature and Heat Flux," NASA Memorandum 12-3-58W, 1958.

29. R.S. Reilly, "Investigation of the Deformation and Penetration of a Turbulent, Subsonic Jet Issuing Transversely into a Uniform, Subsonic Main Stream," Ph.D. Thesis, University of Maryland, 1968.

30. S.J. Kline and F.A. McClintock, "Describing Uncertainties in Single-Sample Experiments," Mechanical Engineering, vol. 75, no. 1, 1953, pp 3-8.

31. P.J. Schneider, Conduction Heat Transfer, Addison-Wesley, Reading, Mass., 1955, pp 172-181.

APPENDIX

Data Analysis and Uncertainty Estimates

Equation 2 in the Introduction is used to determine the heat transfer coefficient.

$$h_a = \frac{q}{T_w - T_{aw}} \qquad (A.1)$$

The local heat flux from the wall to the flow q is calculated from the electrical power input to the wall; temperatures T_w and T_{aw} are measured with a thermocouple as shown on Figure 10. Corrections are applied to consider errors in q, T_w and T_{aw} that arise due to heat fluxes within the system. Uncertainties are evaluated by the method of Kline and McLintock (30) in which the uncertainty in an expression is calculated from the square root of the sum of the squares of the uncertainties of the separate terms within the expression.

The local wall heat flux is considered to be the average heat generated within a heater minus heat flux corrections for radiation from the surface of the heater and conduction out the back of the test surface. Thus,

$$q = q_g - q_r - q_{bc}. \qquad (A.2)$$

The heat generation term is calculated from the electrical current i to the heater and the resistance R and the surface area A of the heater.

$$q_g = \frac{i^2 R}{A} \qquad (A.3)$$

i is measured by a shunt that is calibrated to 0.5%. Since i appears in equation A.3 to the second power, the uncertainty in q_g due to i is twice the uncertainty in i or 1%. A is known within 0.25%. Changes in resistance of the heaters with temperature are considered by correcting the average resistance of the 18 heaters at 20°C to the measured temperature at each thermocouple to get R at that point. The variation of R due to temperature variations within the test surface is less than 2%. This variation is not considered to be an uncertainty since R is calculated at each thermocouple, however, the heat generated within the test surface and thus the wall heat flux varies from being constant by less than 2%. The standard deviation of the resistance of the individual heaters at 20°C is approximately 1% for both sets of heaters that are used. The uniformity of the heater material is checked by a small probe that measures the voltage drop between the two points approximately 1 cm apart when a current is passed through the heater. With the exception of the area where the buss bars are

soldered to the heater, these measurements indicate that the local resistance of the material is also uniform within 1%. Resistance of the heaters at 20°C and thus R is therefore assumed to be known within 1%.

The term for heat loss due to radiation from the surface is calculated using the following equation.

$$q_r = \epsilon \sigma (T_w^4 - T_\infty^4) \qquad (A.4)$$

The emittance of the stainless steel surface is assumed to be 0.12. This term is typically about 1% of the heat generation term.

One-dimensional heat flow through a composite slab is assumed to calculate the heat loss due to conduction from the back of the heater. The largest value that this term assumes is 0.4% of the heat generation term.

The lateral temperature distribution in the test surface without injection is shown on Figure 12(b). Since this distribution is very flat across the center portion of the surface where measurements are conducted, heat losses out the sides of the test section are neglected. Lateral and axial conduction within the test surface are considered when correcting the wall temperature measurement rather than the local heat flux.

It is difficult to estimate how accurate the

corrections described above are. For example, different sources list values of the emittance of stainless steel that vary by as much as 50%. It is also difficult to tell how accurate the one-dimensional heat flow model predicts heat loss by conduction. The correction terms, which are always applied to the heat flux, are therefore assumed to be accurate to 50%. The uncertainty in the wall heat flux term due to the radiation correction is then 0.5% and that due to conduction from the back of the test surface is 0.2%.

The individual uncertainties within the wall heat flux term are listed on Table A.I. Their combined effect is a 1.5% uncertainty in the wall heat flux.

Corrections are applied to the measured wall temperature to take heat loss through thermocouple leads and heat flux within the test surface into account. The wall temperature is thus

$$T_w - T_\infty = T_{tc} - T_\infty + \Delta T_{lw} + \Delta T_{wc} \qquad (A.5)$$

where T_{tc} is the temperature calculated from the thermocouple output, ΔT_{lw} is the correction for conduction through the thermocouple leads and ΔT_{wc} is the correction for heat conduction within the test surface.

The thermocouple junction and heater are separated by a thin layer of cement. The temperature drop across this layer is calculated to be approximately 0.01% of

Table A.I

Relative Uncertainty Estimates

Wall Heat Flux	
Electric current $2\delta i/i$	.010
Heater resistance $\delta R/R$	.010
Heater area $\delta A/A$	.0025
Radiation heat loss correction $\delta q_r/q=0.5\,\Delta q_r/q$	.005
Conduction heat loss correction $\delta q_{bc}/q=0.5\,\Delta q_{bc}/q$	.002
Combined effect $\delta q/q$	.015
Wall Temperature	
Calibration and instrumentation $\delta(T_{tc}-T_\infty)/(T_{tc}-T_\infty)$	.0045
Thermocouple lead wire correction $0.5\,\Delta T_{lw}/(T_{tc}-T_\infty)$	.0010
Heat flux within test surface $0.5\,\Delta T_{wc}/(T_{tc}-T_\infty)$	

Unheated injection

Normal injection	35° injection
.0075	.010

Heated injection

Normal injection		35° injection	
X/D	Uncertainty	X/D	Uncertainty
2.74	.0125	6.65	.050
18.14	.0075	37.36	.0075
35.44	.0050	71.84	.0075

the difference between the wall temperature and free stream temperature and is therefore neglected. The temperature drop across the Textolite sheet in which the thermocouple is embedded is calculated to be approximately 0.1% of the temperature difference. Since the thermocouple is located at the top of this sheet, this temperature drop is also neglected.

The thermocouple calibration curve is accurate to 0.07% of the difference between the measured

temperature and the ice junction. T_{∞} (approximately 25°C) is therefore accurate to approximately 0.18°C and wall temperatures (approximately 42°C) are accurate to 0.030°C. The instrument that records the thermocouple output is read to 0.02°C. The temperature difference $T_{tc}-T_{\infty}$ is therefore accurate to approximately 0.45%.

The temperature output by the thermocouple is slightly low due to heat loss through the thermocouple lead wires. The model described by Schneider (31) is therefore used to correct the data by the amount ΔT_{lw}. This correction is approximately 0.2% of the temperature difference $T_{tc}-T_{\infty}$.

In regions where the temperature gradient within the wall is changing very fast (e.g. near the point of injection) the wall temperature is influenced by the heat flux distribution within the wall. If it is assumed that the temperature does not change in the Y direction within the test surface (the portion of the wall above the insulation on Figure 10) an energy balance on an element within this wall yields the following expression for the temperature error due to heat conduction within the wall.

$$\Delta T_{wc} = -\frac{k_e b}{h D^2}\left[\frac{\partial^2(T_{tc}-T_{\infty})}{\partial(X/D)^2} + \frac{\partial^2(T_{tc}-T_{\infty})}{\partial(Z/D)^2}\right] \qquad (A.6)$$

The thickness of the test surface is b (b=1.69 mm); h

is the heat transfer coefficient on the test surface ($h=0.07-0.2$ W/cm^2-$^\circ$C). The diameter of the injection tubes are 2.35 cm for normal injection and 1.18 cm for 35° injection. Assuming that heat flows in the test surface as it would for parallel heat flow through a multilayered slab, k_e denotes the equivalent thermal conductivity for such a wall.

$$k_e = \frac{1}{b}\sum_{i=1}^{3} k_i b_i = 0.0055 \quad W/cm-{}^\circ C \tag{A.7}$$

The subscript i varies to include the three materials in the test surface. For adiabatic wall temperature measurements, this correction can be applied to the film cooling effectiveness.

$$\Delta\eta_{wc} = -\frac{k_e b}{h D^2}\left[\frac{\partial^2 \eta_{tc}}{\partial (X/D)^2} + \frac{\partial^2 \eta_{tc}}{\partial (Z/D)^2}\right] \tag{A.8}$$

The second derivatives in equations A.6 and A.8 are evaluated by differentiating least squares second degree polynomials that are fit to sets of five points in which the point in question is centered. Note that these corrections depend rather strongly on the diameter of the injection tube since the second derivatives in equations A.6 and A.8 should be relatively independent of D. The magnitude of the correction relative to $T_w - T_\infty$ can be as high as 2.5% for normal injection (D=2.35 cm) and as high as 10% for

35 degree injection (D=1.18cm) near the point of injection. The corrections become small at downstream locations.

The corrections for heat loss through thermocouple leads and heat flow within the wall are assumed to be accurate to 50%. Uncertainties associated with these corrections along with the uncertainty due to calibration and instrumentation are listed on Table A.I.

The uncertainty estimates described above and listed on Table A.I are now used to determine the uncertainty in the film cooling effectiveness and heat transfer coefficient. The method of (30) is used to combine these uncertainties. Uncertainties that vary with position are evaluated at centerline locations (Z/D=0.0) only.

The uncertainty in the film cooling effectiveness is given by

$$\frac{\Delta\eta}{\eta} = \left[\left(\frac{\Delta T_{aw}}{T_{aw}-T_\infty}\right)^2 + \left(\frac{\Delta T_2}{T_2-T_\infty}\right)^2 + \left(\frac{\Delta T_\infty}{T_2-T_\infty}\right)^2\left(1-\frac{1}{\eta}\right)^2\right]^{\frac{1}{2}}. \quad \text{(A.9)}$$

Results of this calculation for normal and 35 degree injection are presented in Table A.II. For normal injection (D=2.35cm) the uncertainty varies from approximately 1.4% near the hole to approximately 0.8% at downstream locations. For 35 degree injection (D=1.18cm) it varies from approximately 5% near the hole to 1% at downstream locations. Uncertainties are

greater for 35 degree injection due to the larger heat flux correction that is necessary for the smaller diameter tube.

Table A.II

Film Cooling Effectiveness Uncertainty
(after corrections are applied to data)

Normal Injection		35° Injection	
X/D	Uncertainty	X/D	Uncertainty
2.74	.014	6.65	.050
18.14	.010	37.36	.010
35.44	.008	71.84	.010

Uncertainty in the heat transfer coefficient is given by

$$\frac{\Delta h_a}{h_a} = \left[\left(\frac{\Delta q}{q}\right)^2 + \left(\frac{\Delta T_w}{T_w - T_{aw}}\right)^2 + \left(\frac{\Delta T_{aw}}{T_w - T_{aw}}\right)^2\right]^{\frac{1}{2}}. \qquad (A.10)$$

With no secondary injection, the only rapidly changing temperature gradients in the test surface are very near the leading edge of the first heater. Measurements are not conducted in this area so uncertainty due to heat flow within the test surface is neglected. The adiabatic wall temperature is set equal to the free stream temperature in equation A.10 and the uncertainty in the heat transfer coefficient without secondary injection is found to be approximately 1.6%.

When the secondary flow is not heated, the difference between the injection temperature and the free stream temperature is small enough so that the

difference between the adiabatic wall temperature and free stream temperature is less than 0.5% of the difference between the heated wall temperature and the free stream temperature. T_{∞} is therefore used for T_{aw} in equation A.10 and the uncertainty in the heat transfer coefficient is found to be 1.9% for normal injection and 2.0% for 35 degree injection.

Uncertainty estimates for heated injection are presented in Table A.III. The uncertainties are high near the injection holes because of the rapidly changing temperature gradients in the wall in this region. At downstream locations the uncertainties are similar to those for no injection and unheated injection. For normal injection, the high heat flux causes a larger temperature difference $T_w - T_{aw}$ than the low heat flux, resulting in greater accuracies near the injection holes. Uncertainties for 35 degree injection are greater than those for normal injection because of the steeper temperature gradients that the jets impart in the test surface with the smaller diameter tubes that are used for 35 degree injection. At higher blowing rates, the heated jets penetrate into the free stream temperature gradients in the wall are smaller and uncertainties are similar to those observed for no injection and unheated injection.

Table A.III

Heat Transfer Coefficient Uncertainty
(after corrections are applied to data)

No Secondary Injection			0.016
Unheated Secondary Injection			
Normal Injection			0.019
35° Injection			0.020
Heated Secondary Injection			
X/D	M=0.2	M=0.5	M=1.0
	Normal Injection		
	Low Wall Heat Flux		
2.74	.048	.052	.035
18.14	.019	.019	.019
35.44	.017	.017	.017
	Normal Injection		
	High Wall Heat Flux		
2.74	.036	.038	.028
18.14	.019	.019	.019
35.44	.017	.017	.017
	35 Degree Injection		
6.65	.122	.156	.119
37.36	.018	.020	.019
71.84	.018	.018	.019

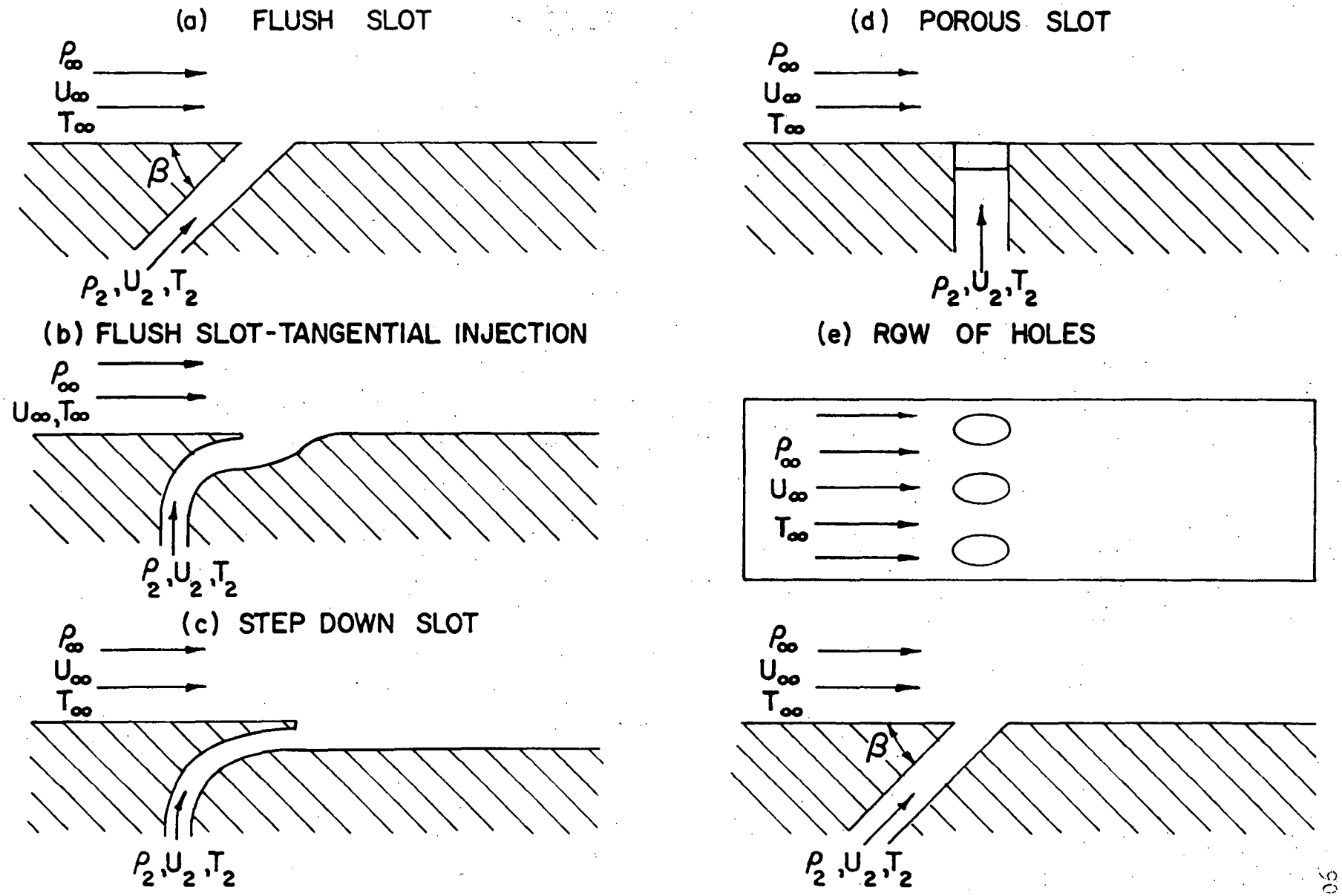

Figure 1 Film cooling geometries

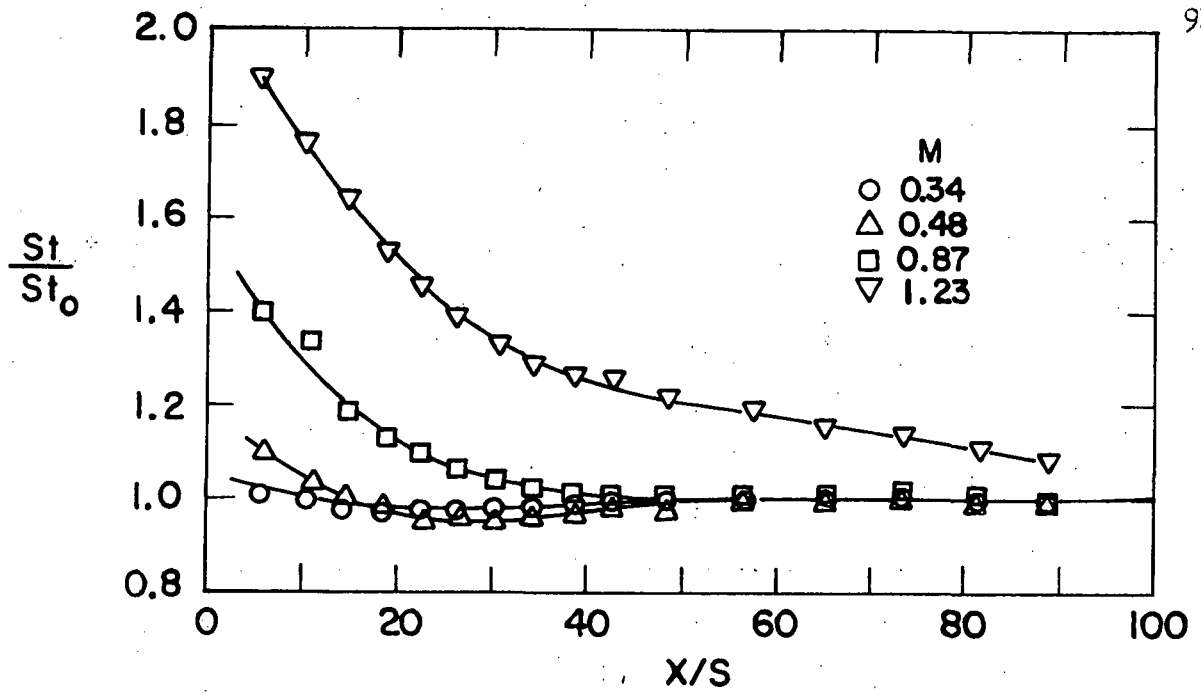

Figure 2 Heat transfer coefficient downstream of injection through a tangential slot (Hartnett, Birkbak and Eckert (3))

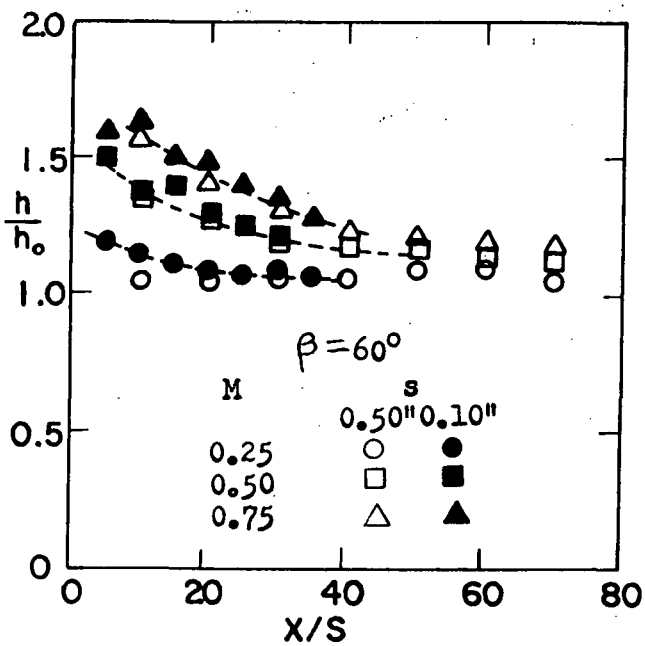

Figure 3 Heat transfer coefficient downstream of injection through a slot at 60° (Metzger and Fletcher (9))

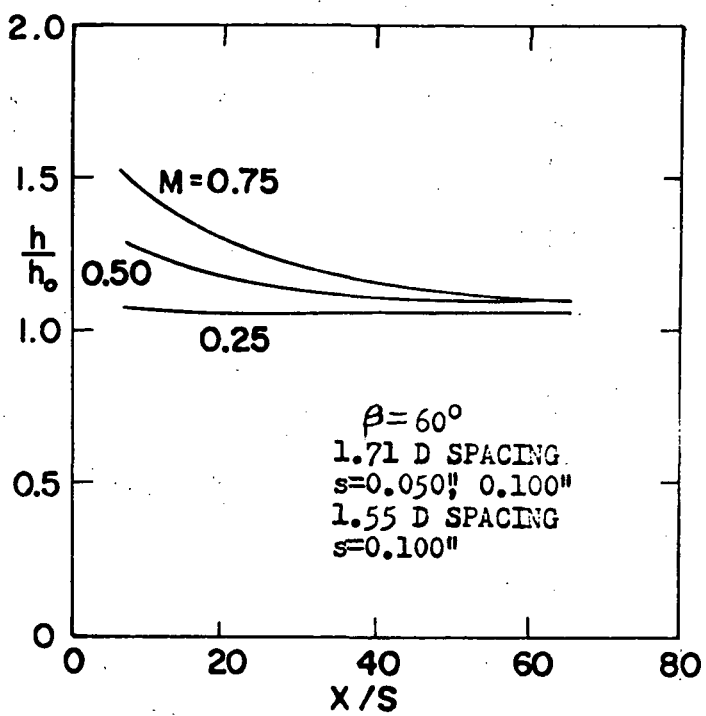

Figure 4 Heat transfer coefficient downstream of injection through holes at 60° (Metzger and Fletcher (9))

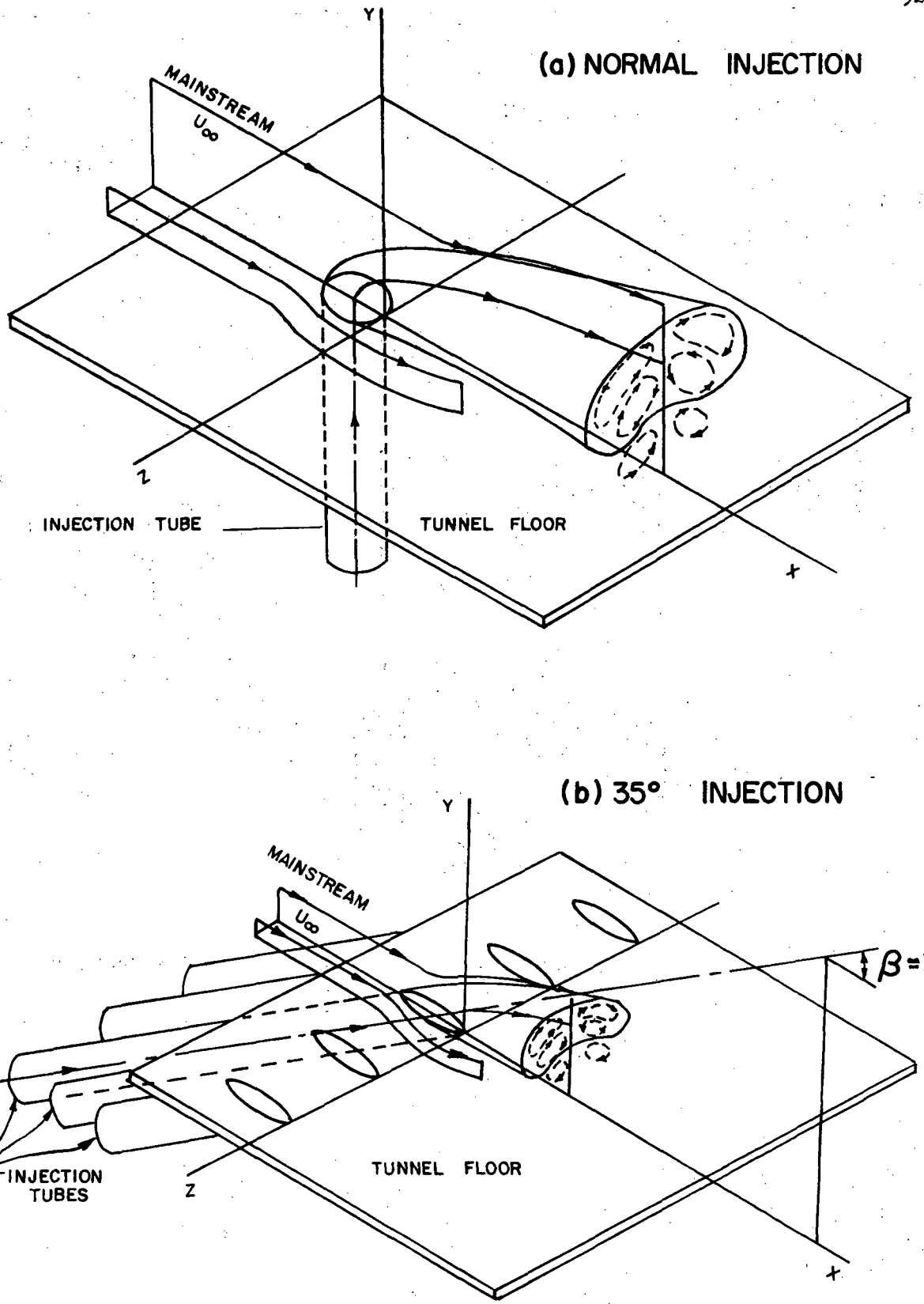

Figure 5 Three-dimensional film cooling geometries

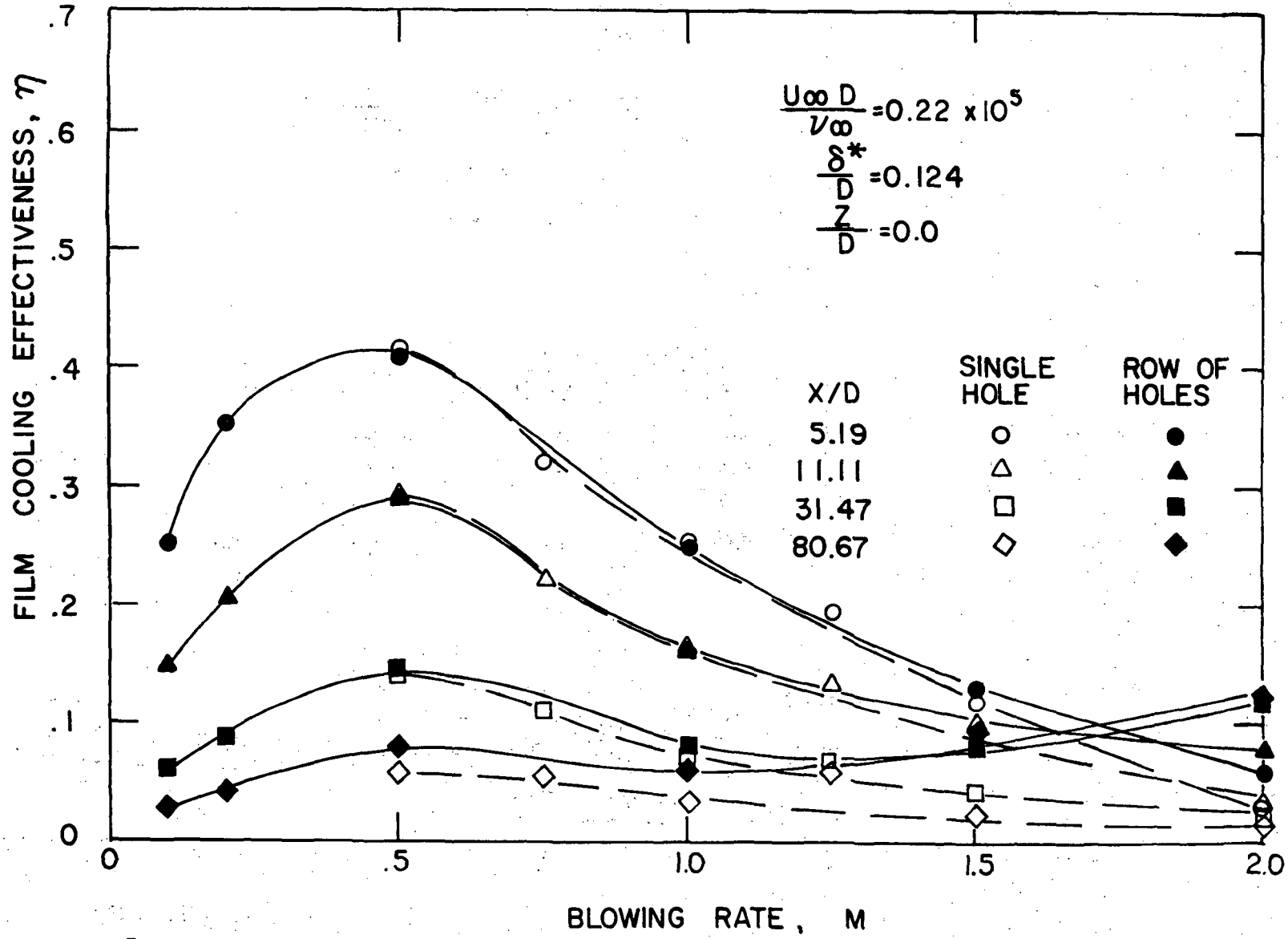

Figure 6 Variation of centerline film cooling effectiveness with blowing rate for injection through holes at 35° ((18) and (19))

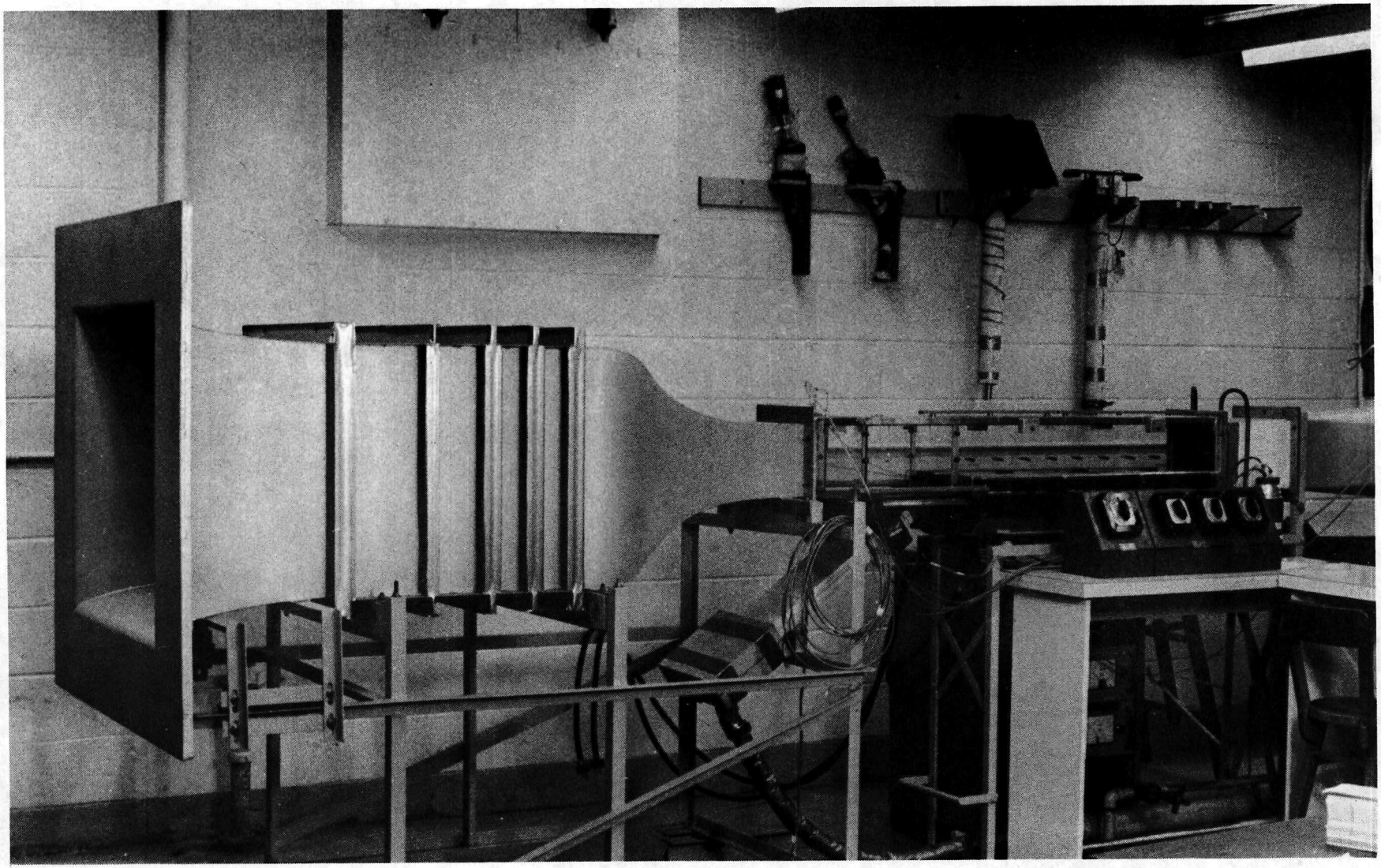

Figure 7 Photograph of wind tunnel

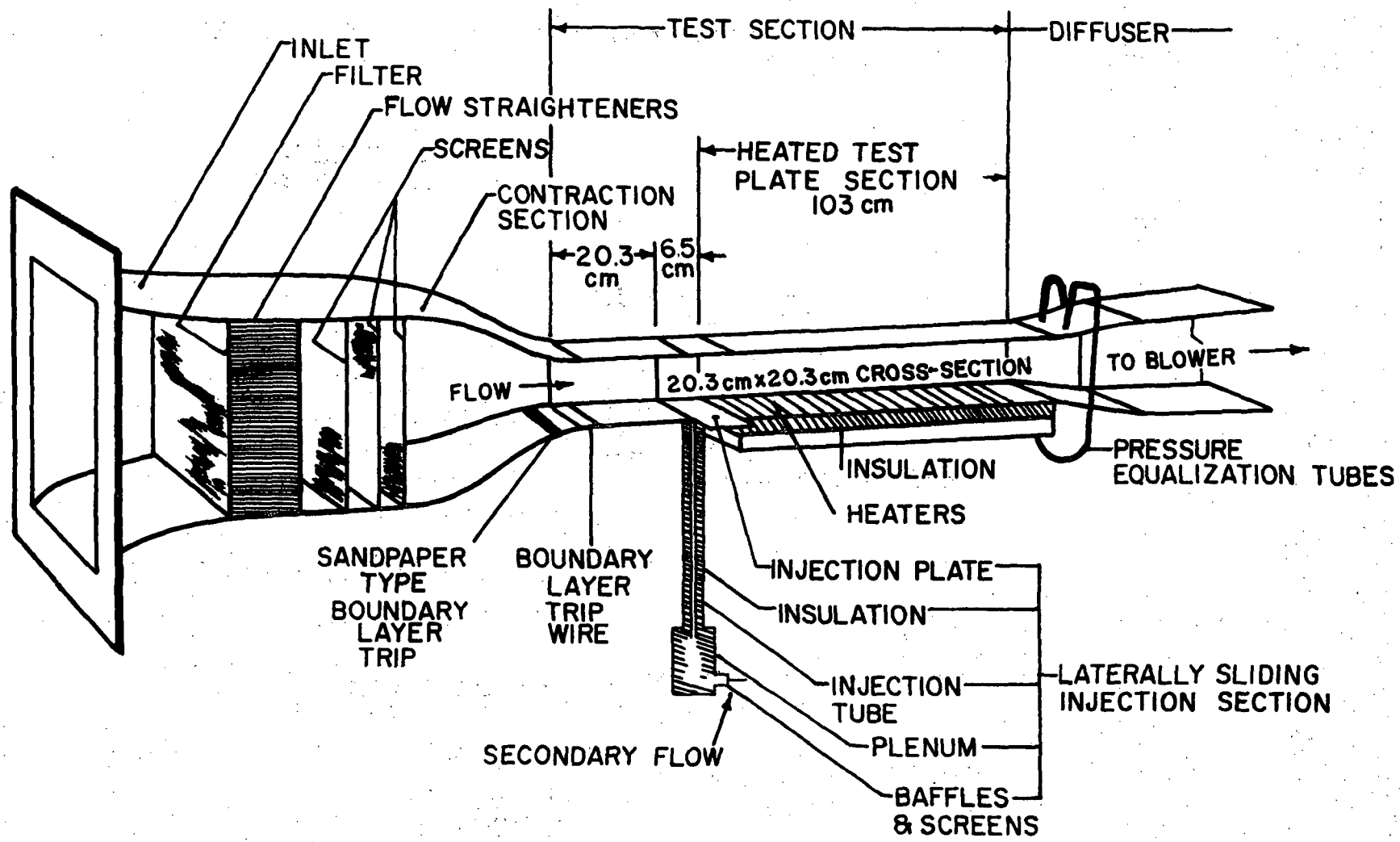

Figure 8 Schematic of wind tunnel

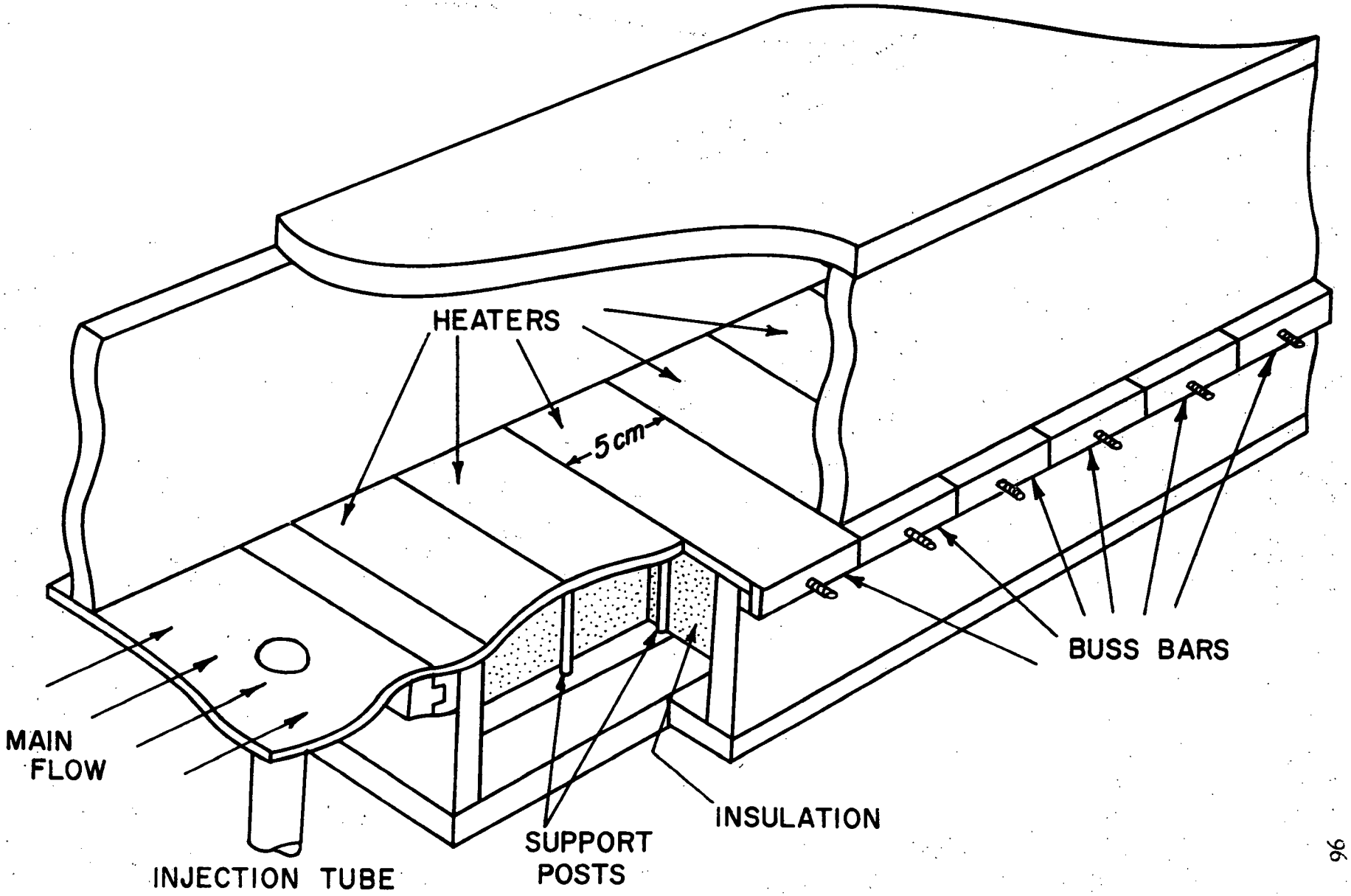

Figure 9 Drawing of test plate

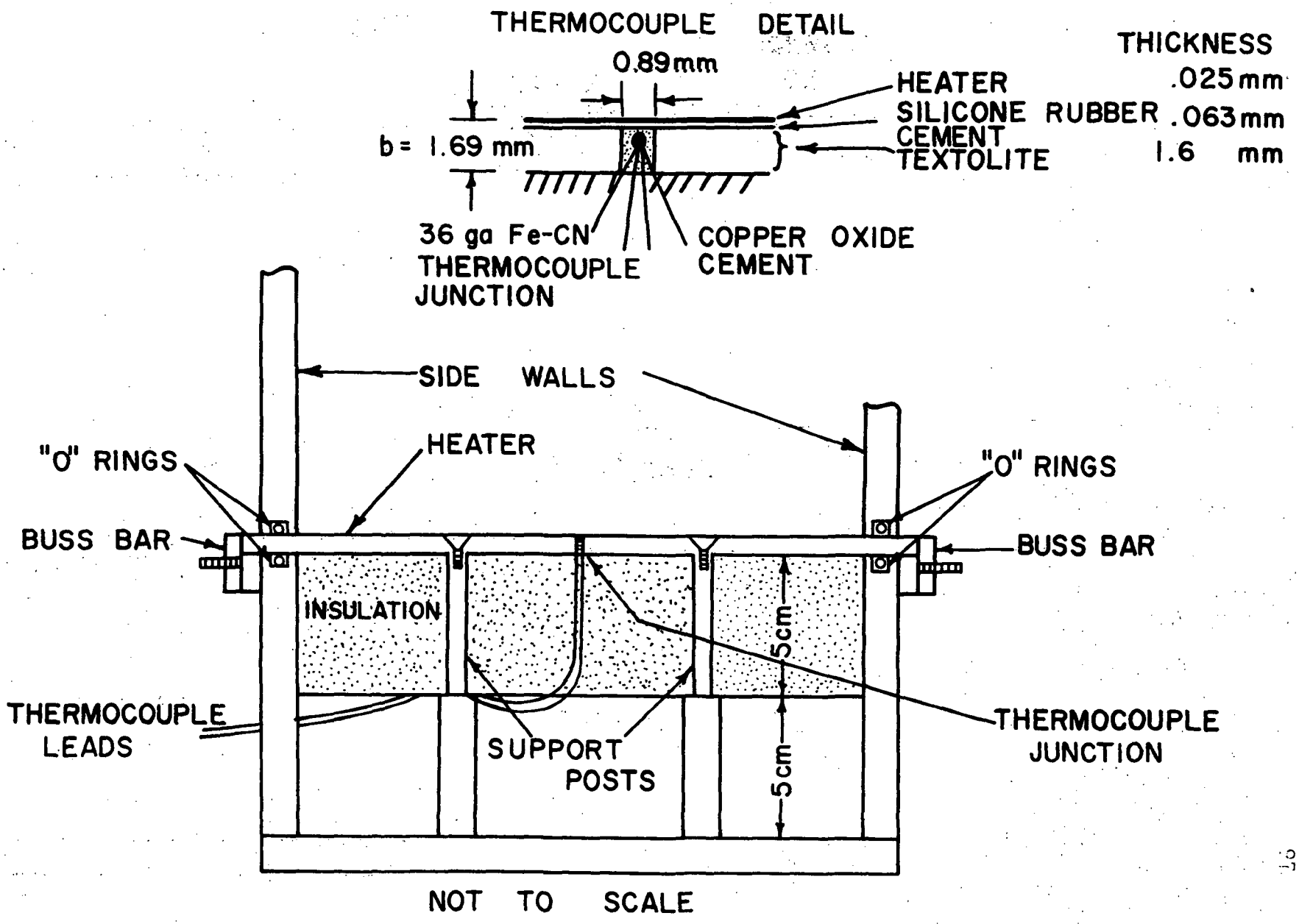

Figure 10 Cross-section of test plate

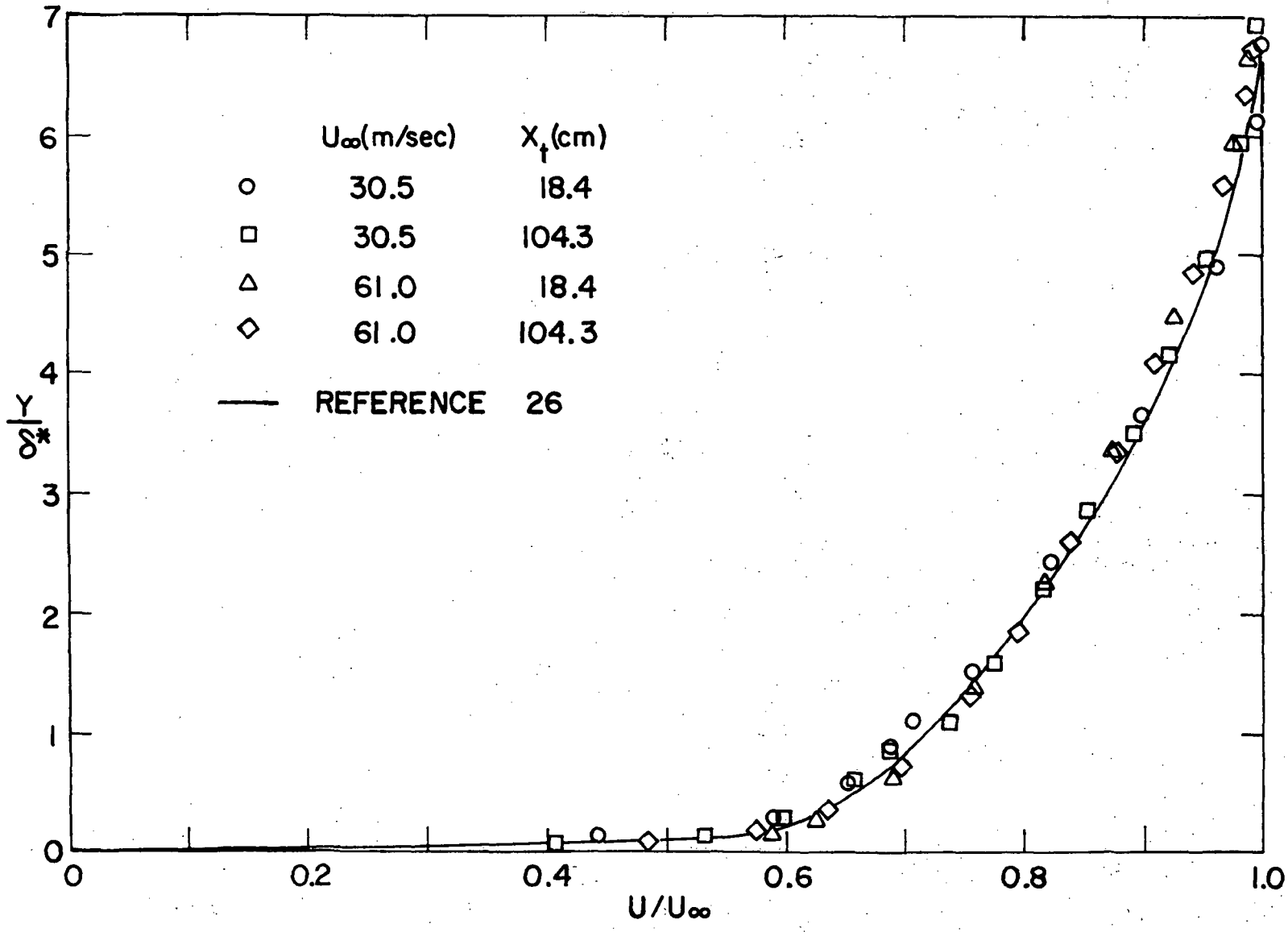

Figure 11 Boundary layer profile on the test surface with no injection

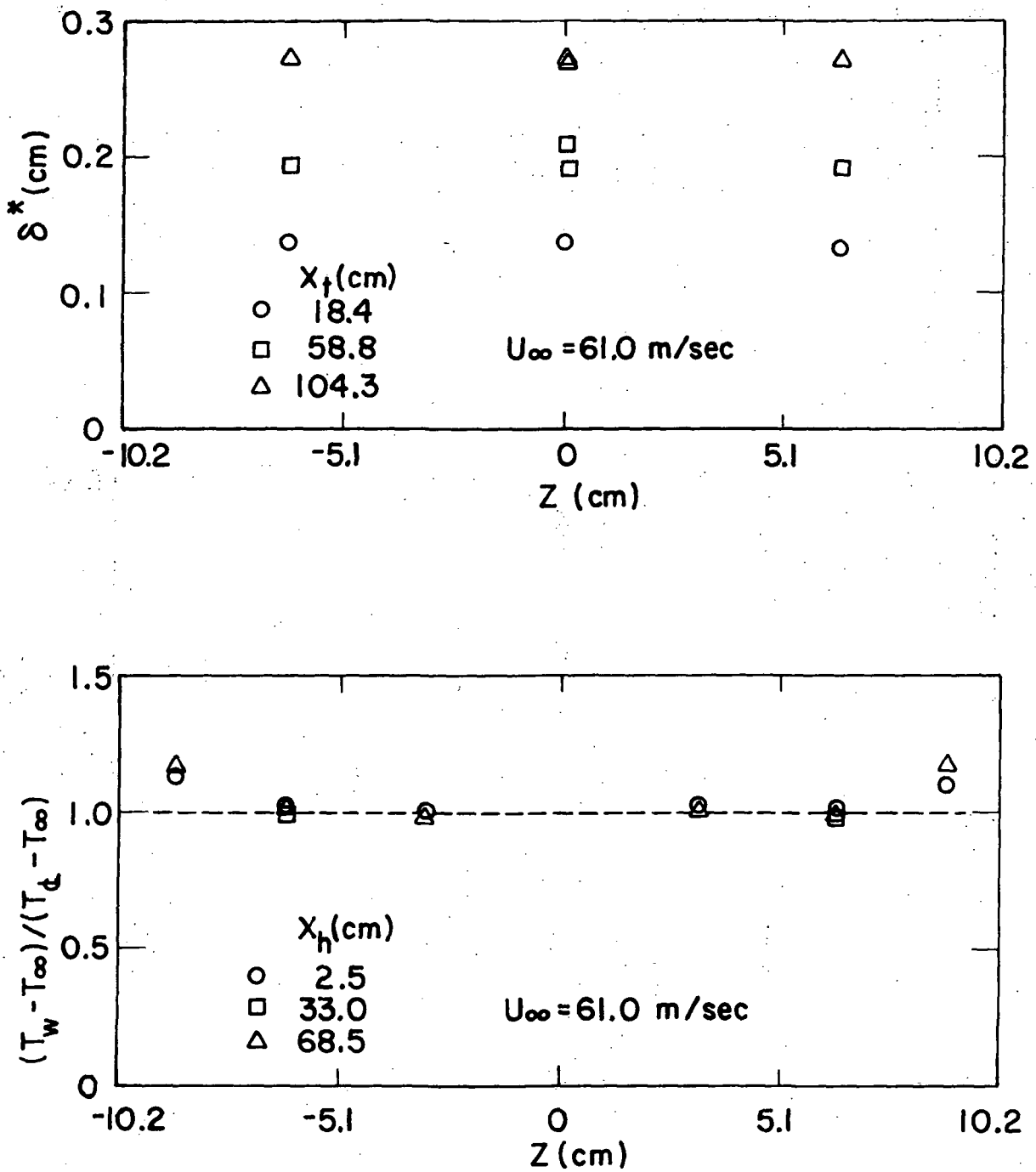

Figure 12 Uniformity of boundary layer thickness and temperature across the span of the test plate with no injection

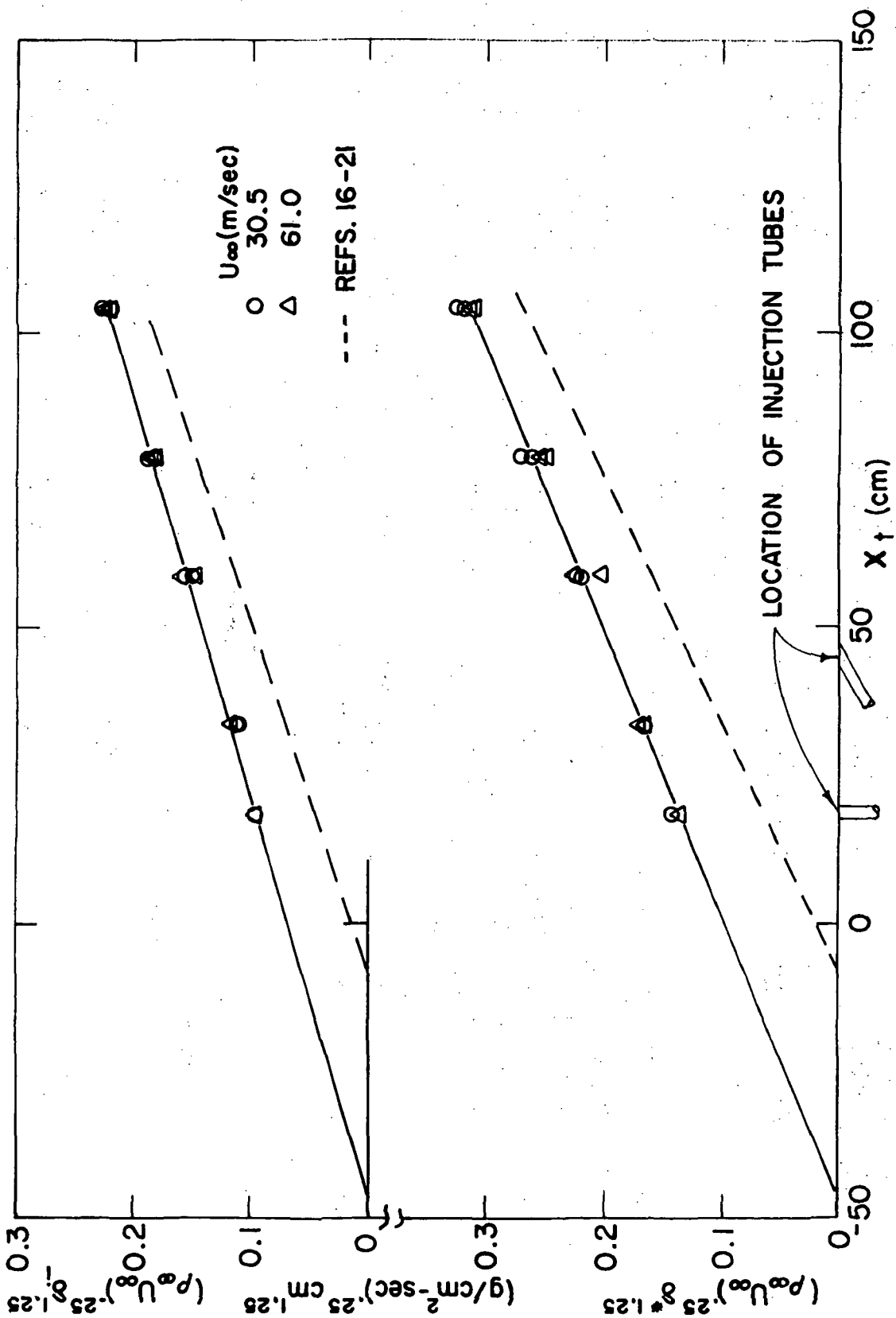

Figure 13 Boundary layer growth on the test surface with no injection

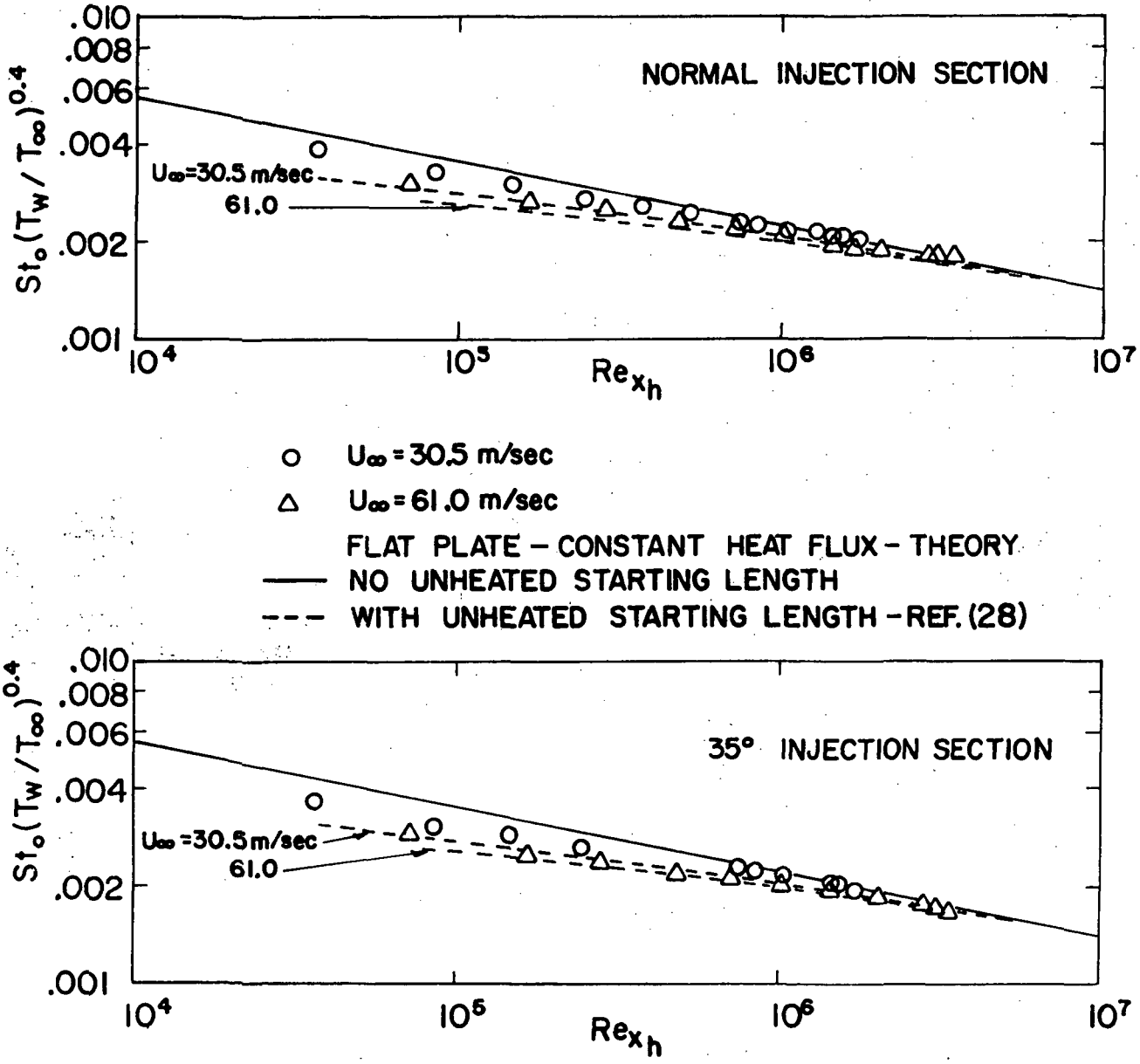

Figure 14 Heat transfer from the test surface with no injection

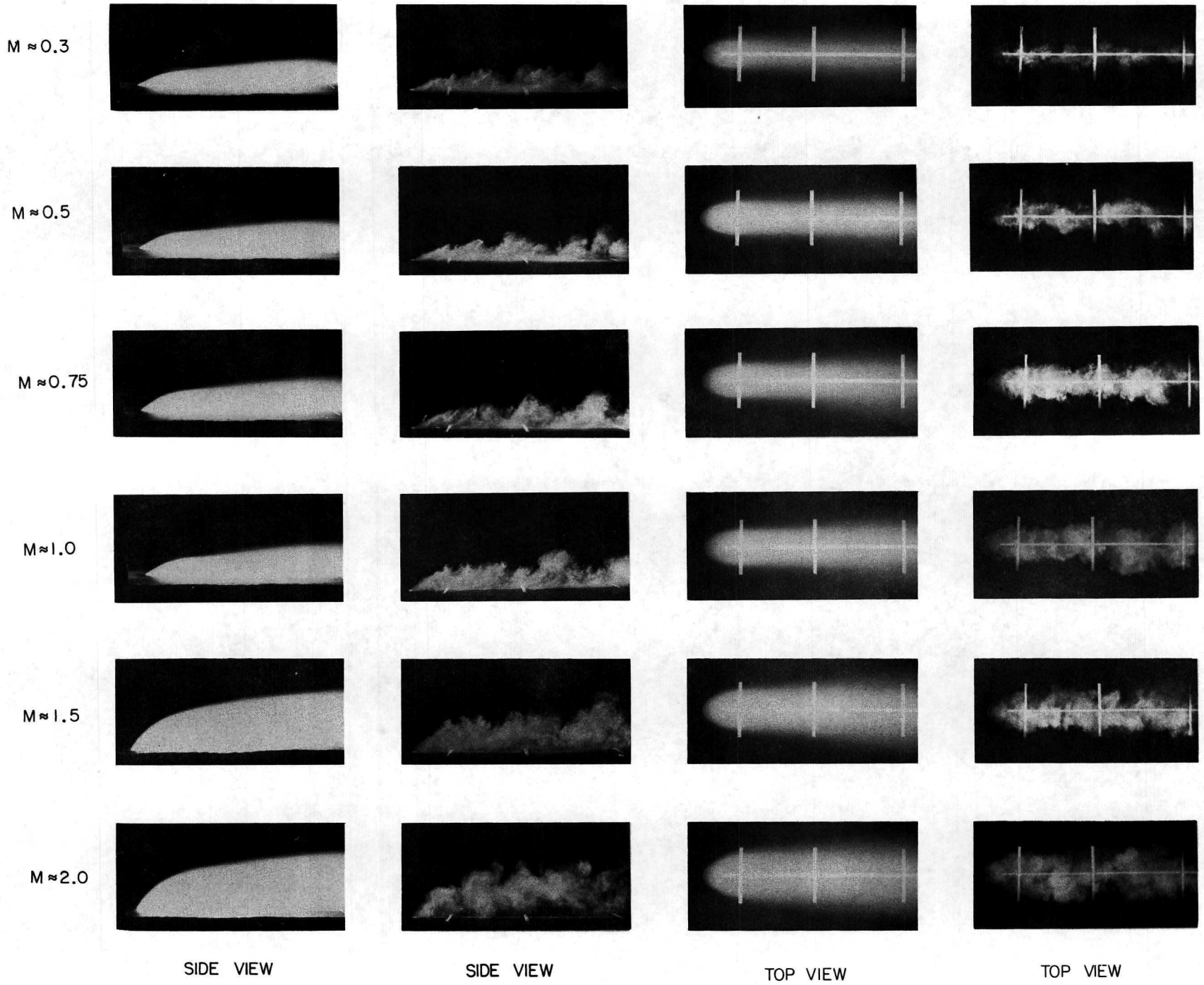

FIGURE 15 PHOTOGRAPHS OF JET IN CROSSFLOW WITH NORMAL INJECTION

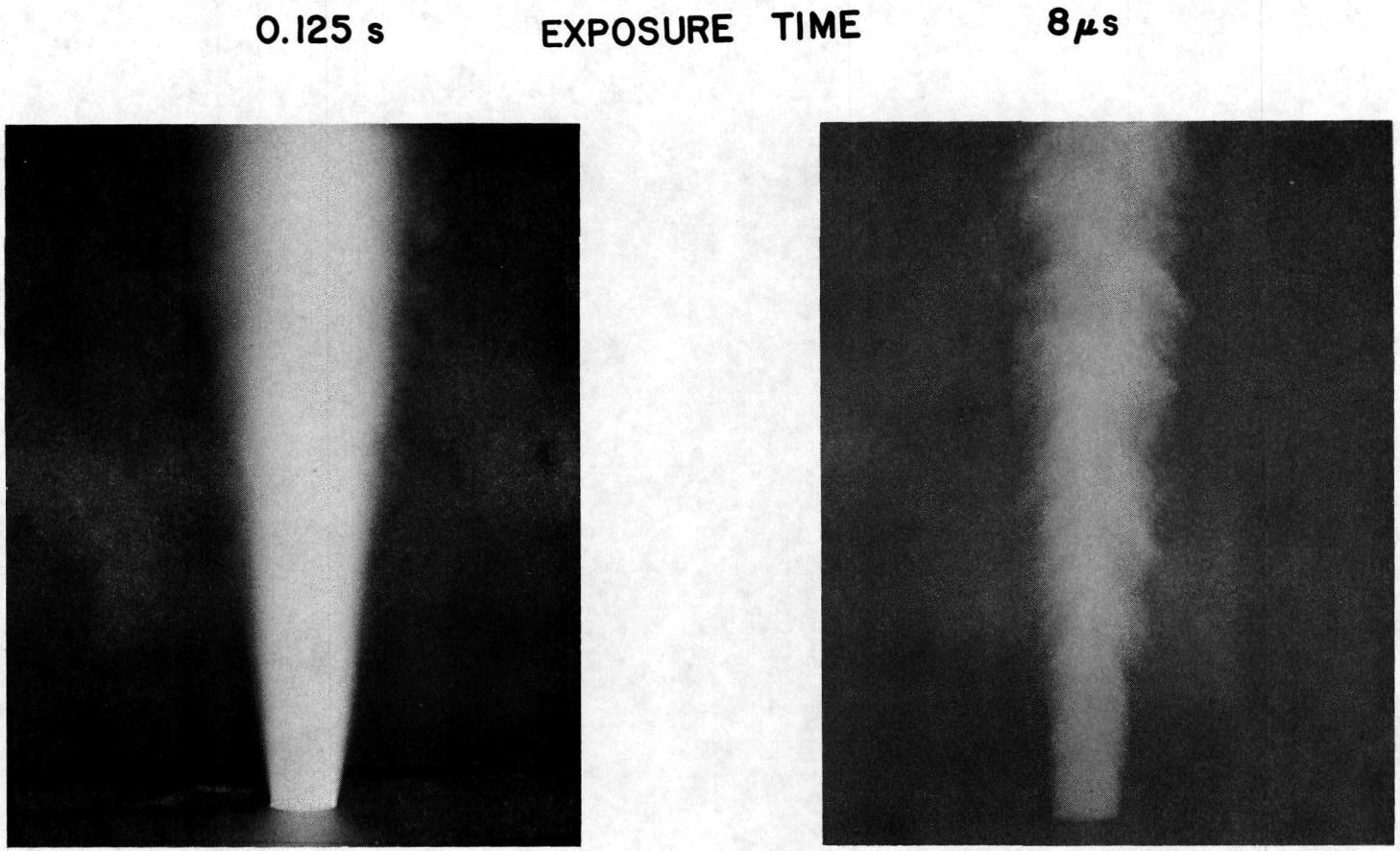

Figure 16 Photographs of jet in still air

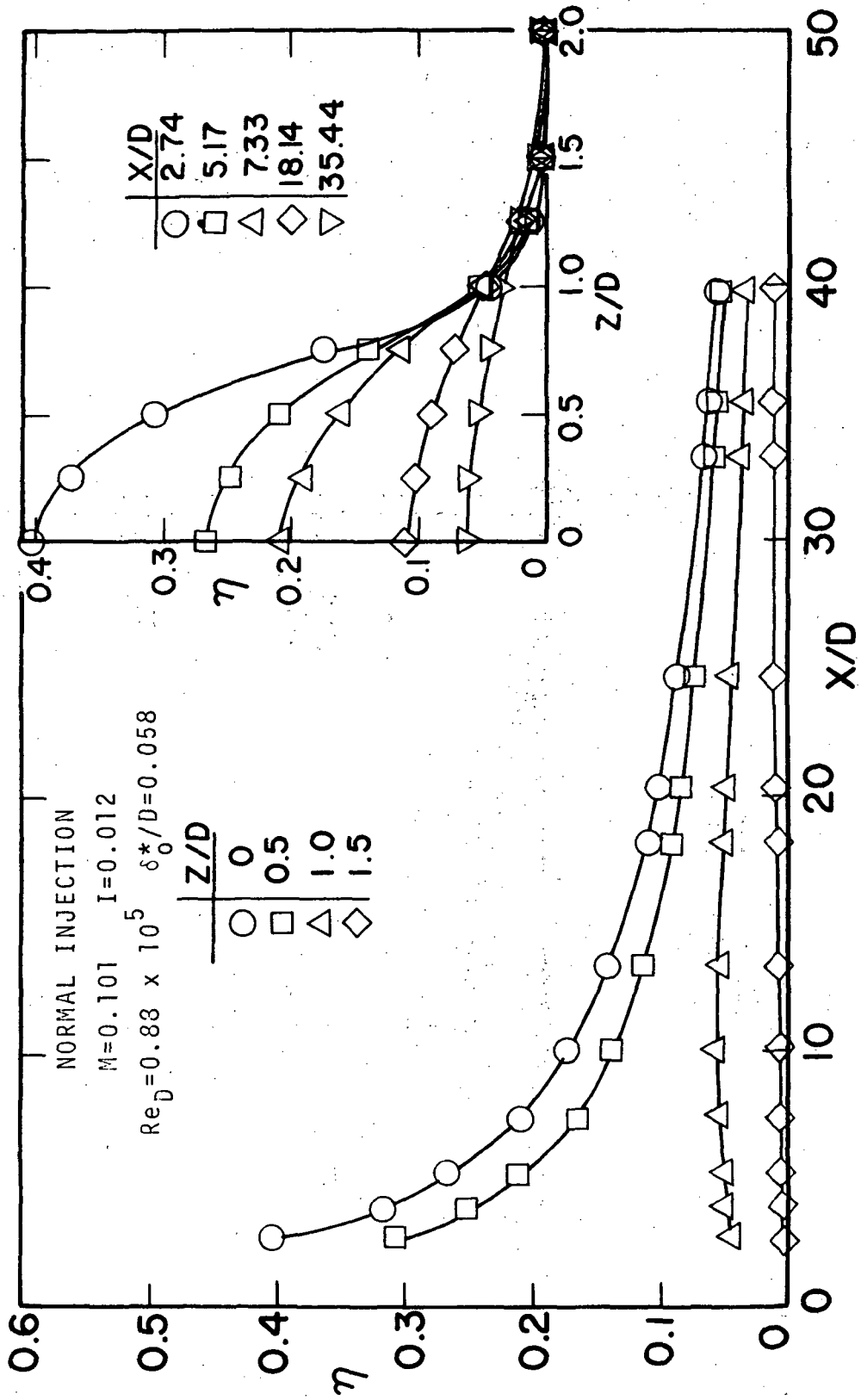

Figure 17 Film cooling effectiveness for normal injection through a single hole, M=0.1, Re_D=0.88 x 10^5

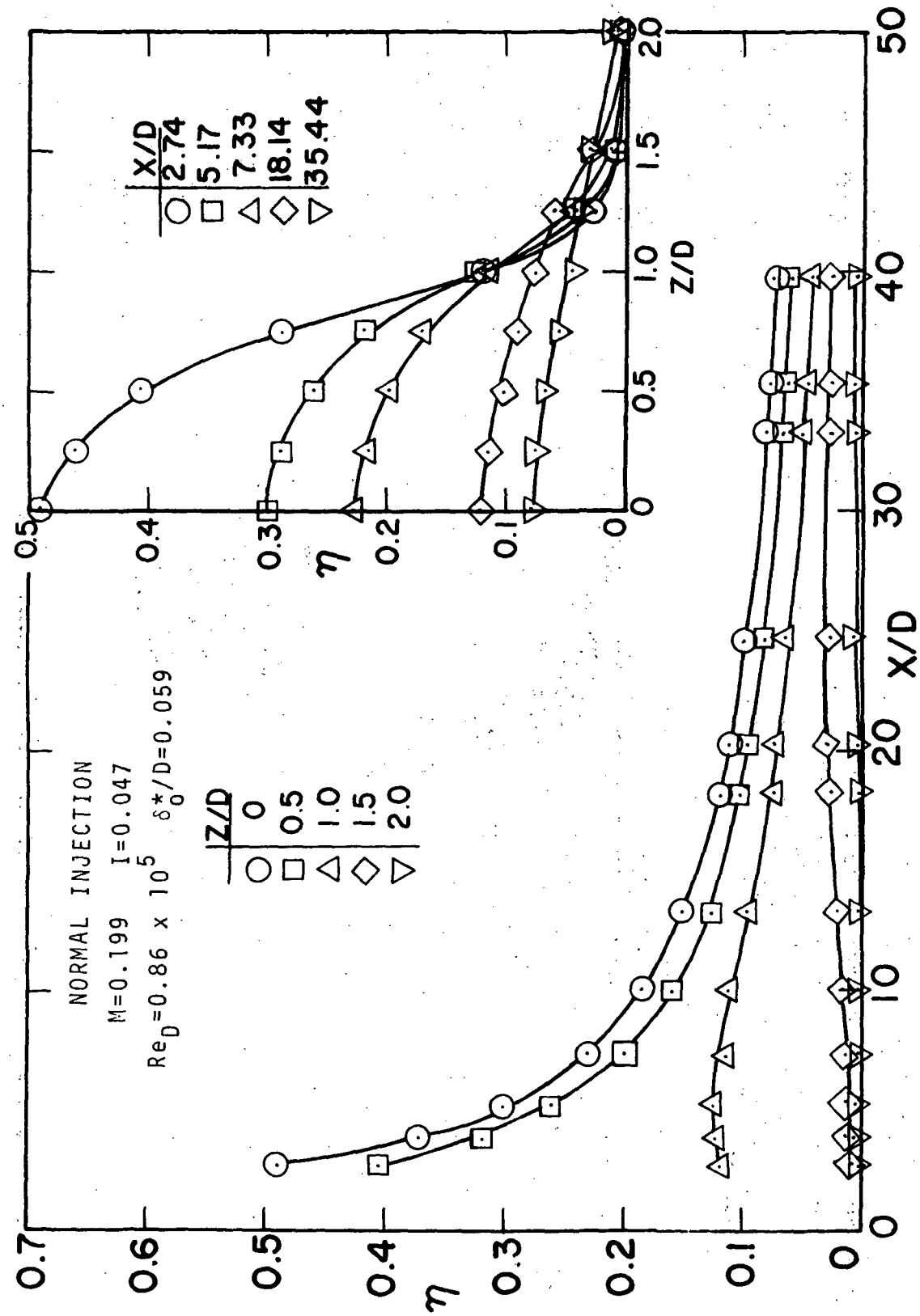

Figure 18 Film cooling effectiveness for normal injection through a single hole, M=0.2, Re_D=0.86 x 10^5

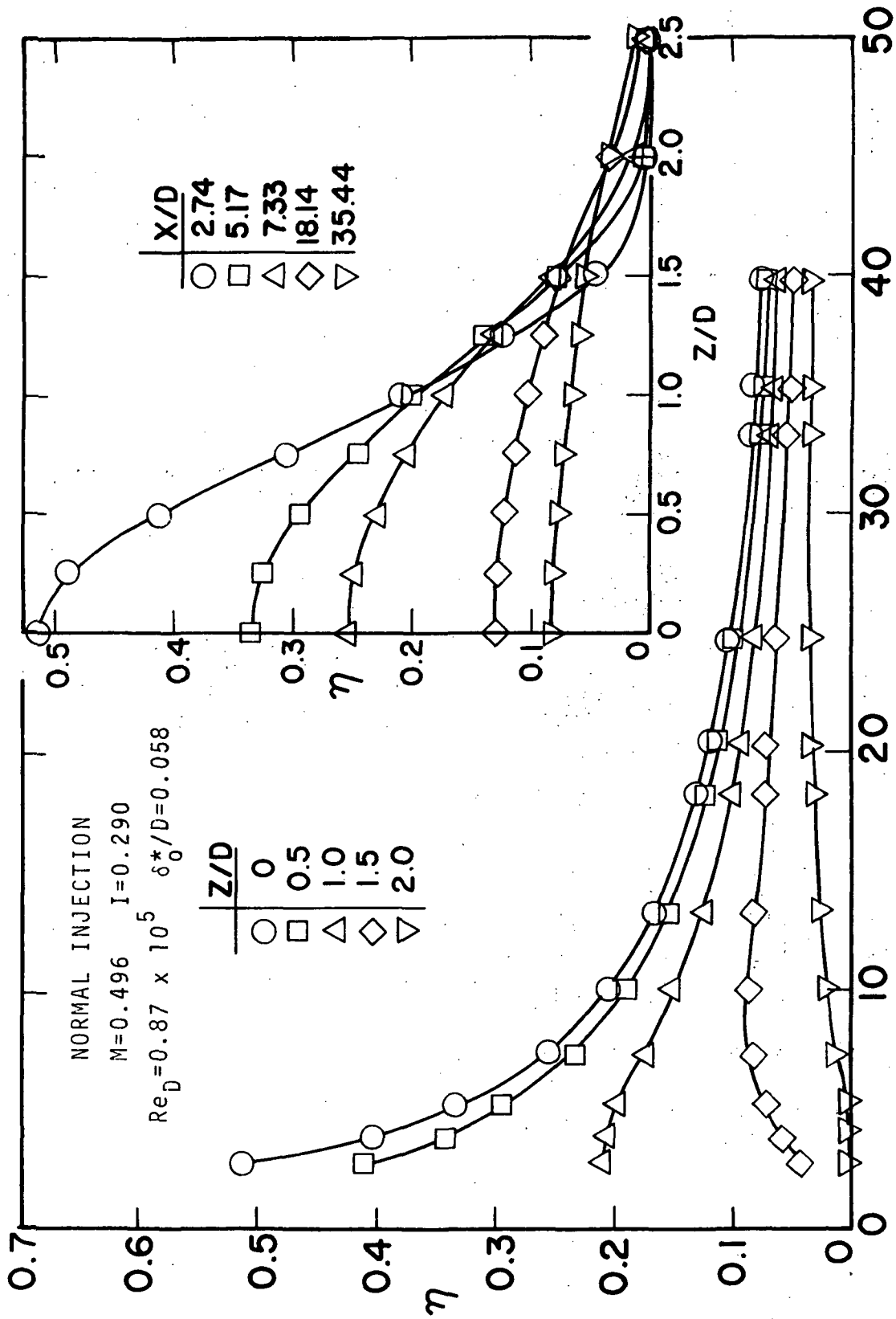

Figure 19 Film cooling effectiveness for normal injection through a single hole, M=0.5, Re_D=0.87 x 10^5

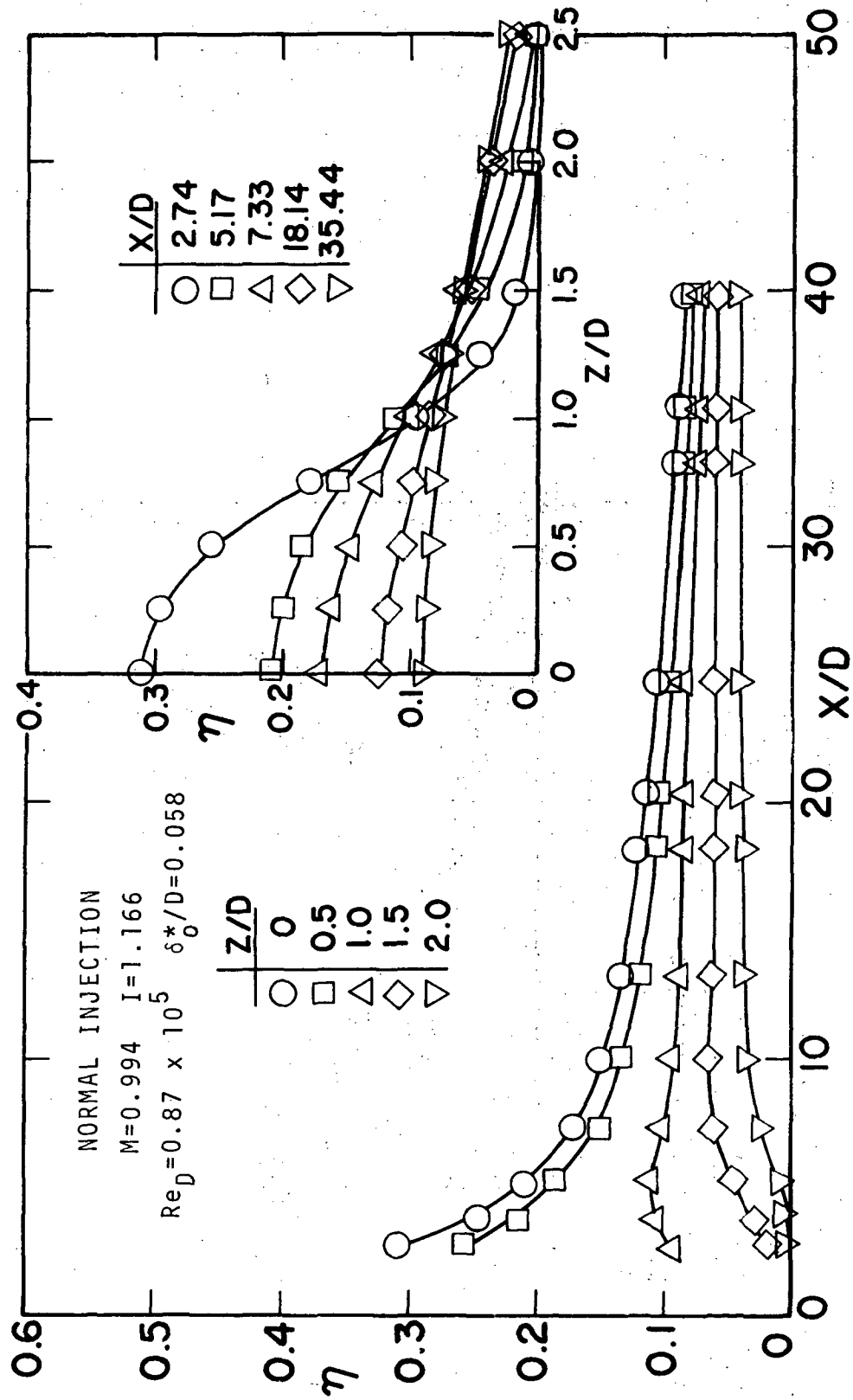

Figure 20 Film cooling effectiveness for normal injection through a single hole, M=1.0, Re_D=0.87 x 10^5

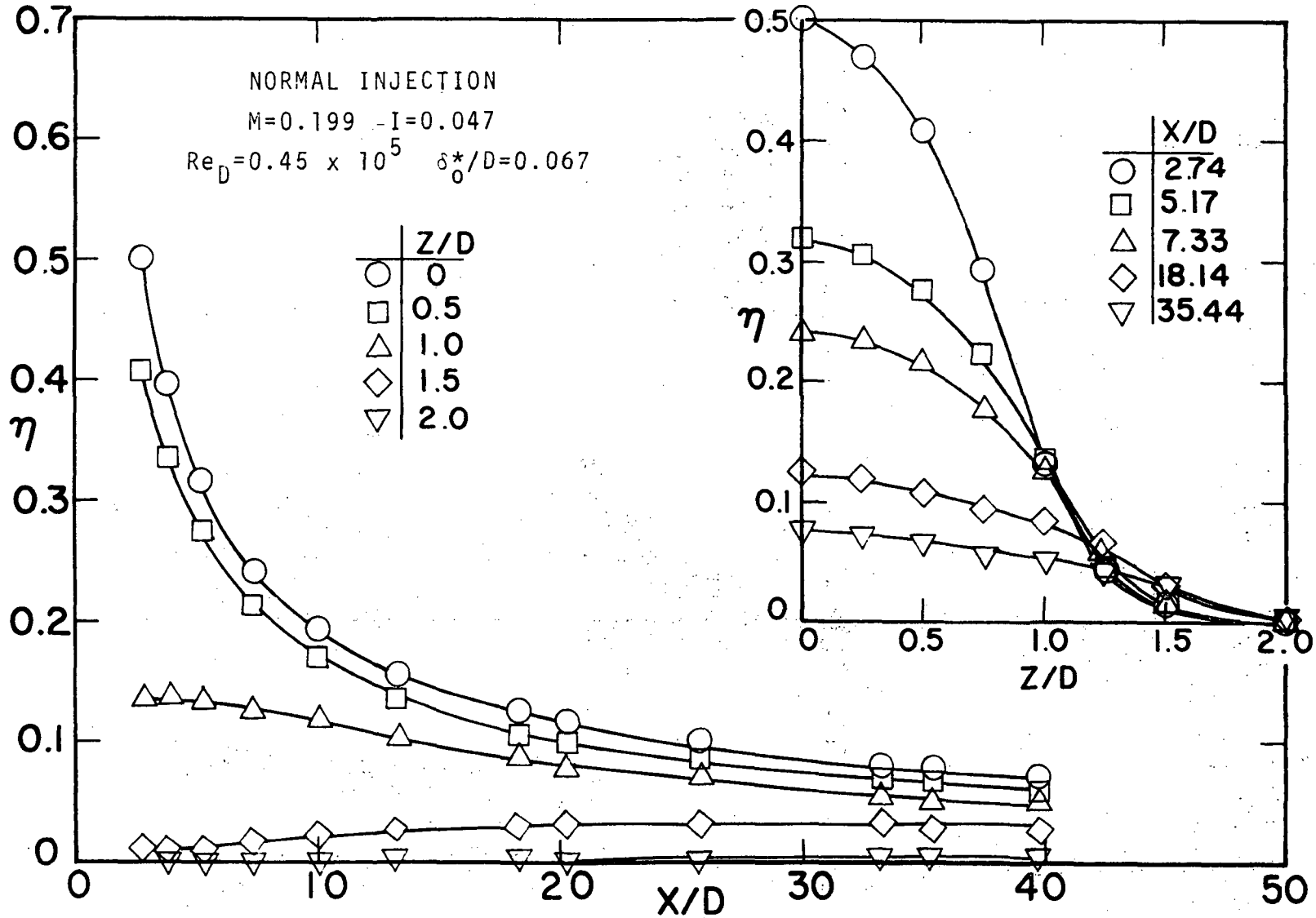

Figure 21 Film cooling effectiveness for normal injection through a single hole, M=0.2, $Re_D=0.45 \times 10^5$

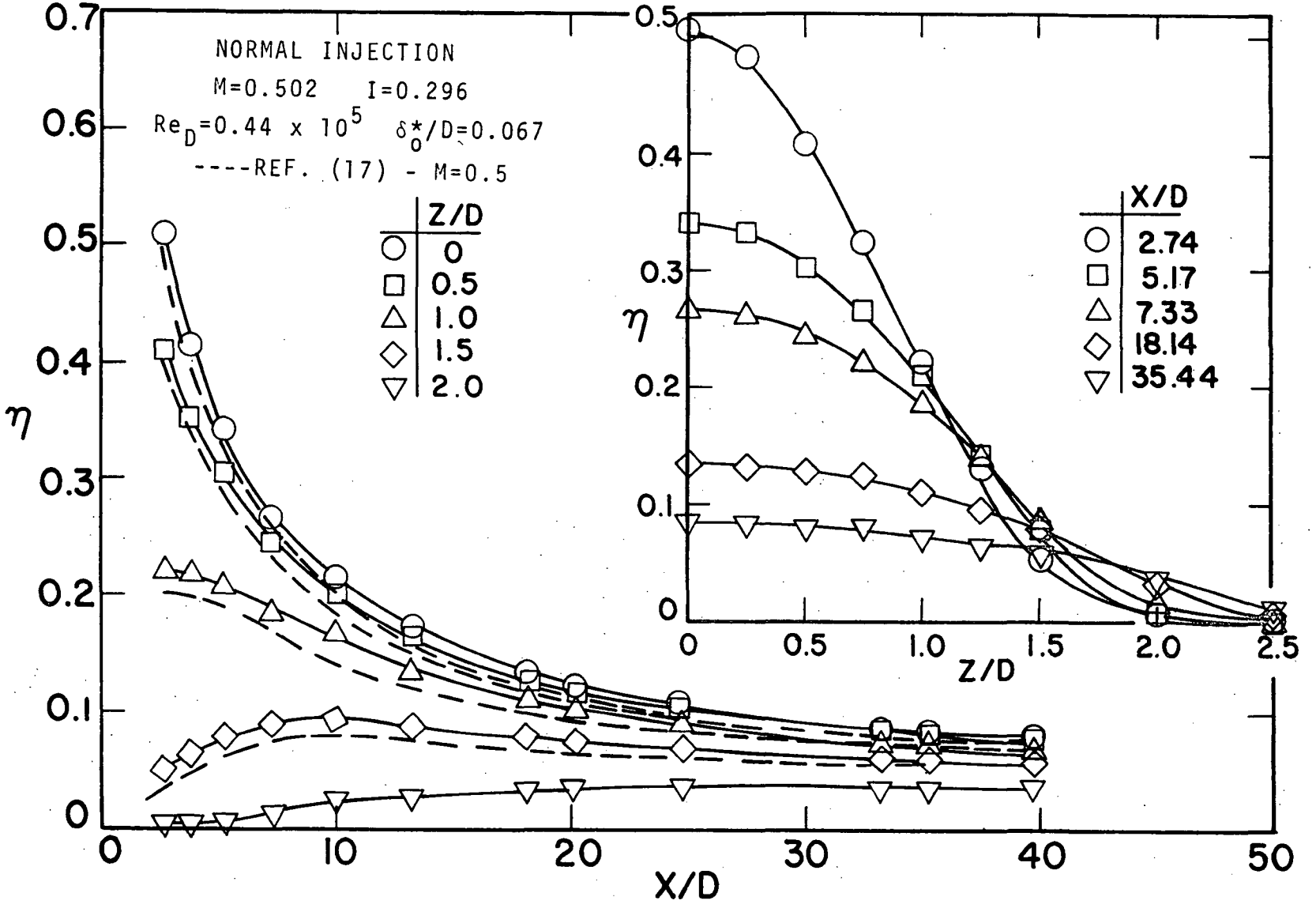

Figure 22 Film cooling effectiveness for normal injection through a single hole, M=0.5, $Re_D=0.44 \times 10^5$

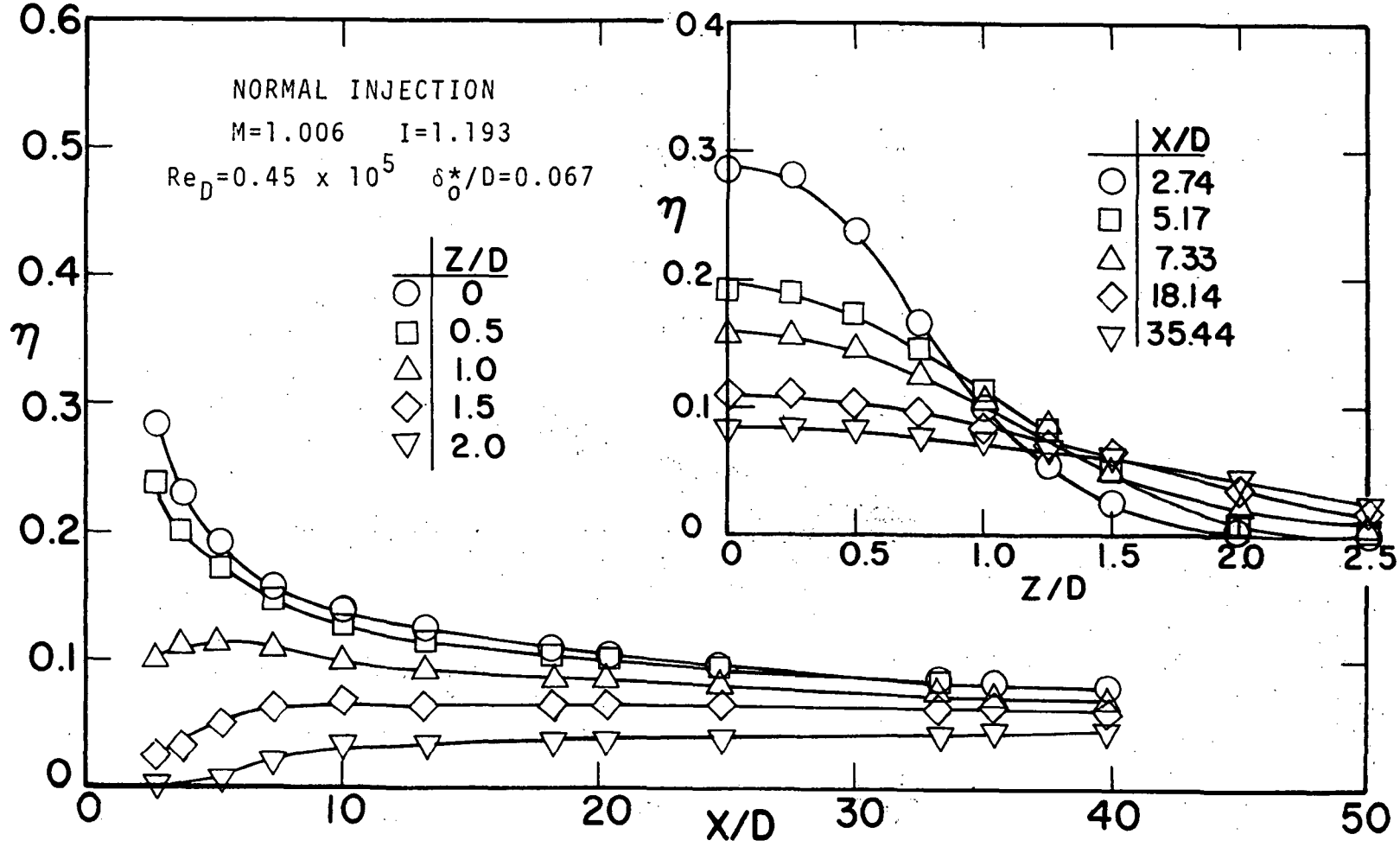

Figure 23 Film cooling effectiveness for normal injection through a single hole, M=1.0, $Re_D=0.45 \times 10^5$

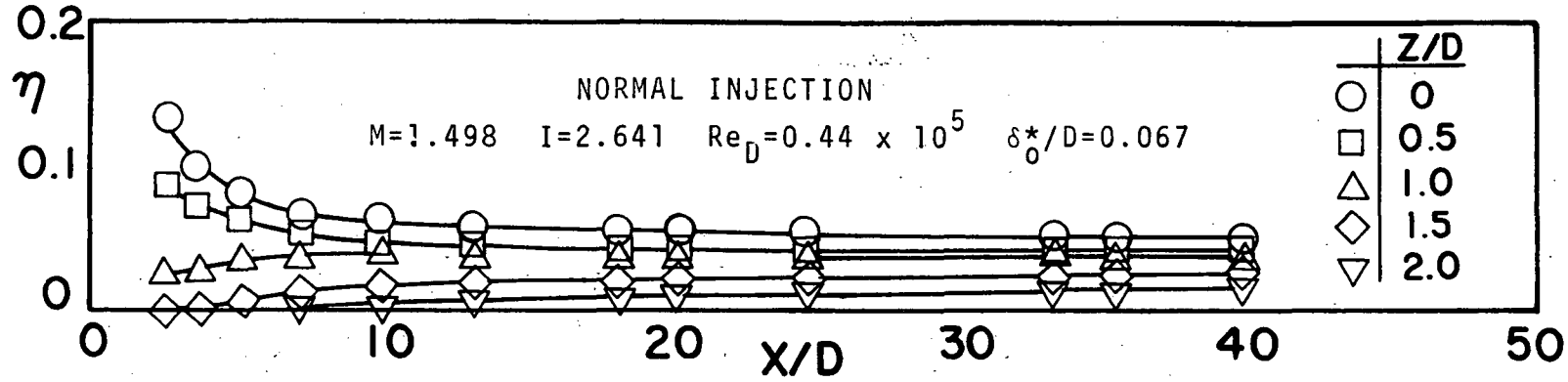

Figure 24 Film cooling effectiveness for normal injection through a single hole, M=1.5, Re_D=0.44 x 10^5

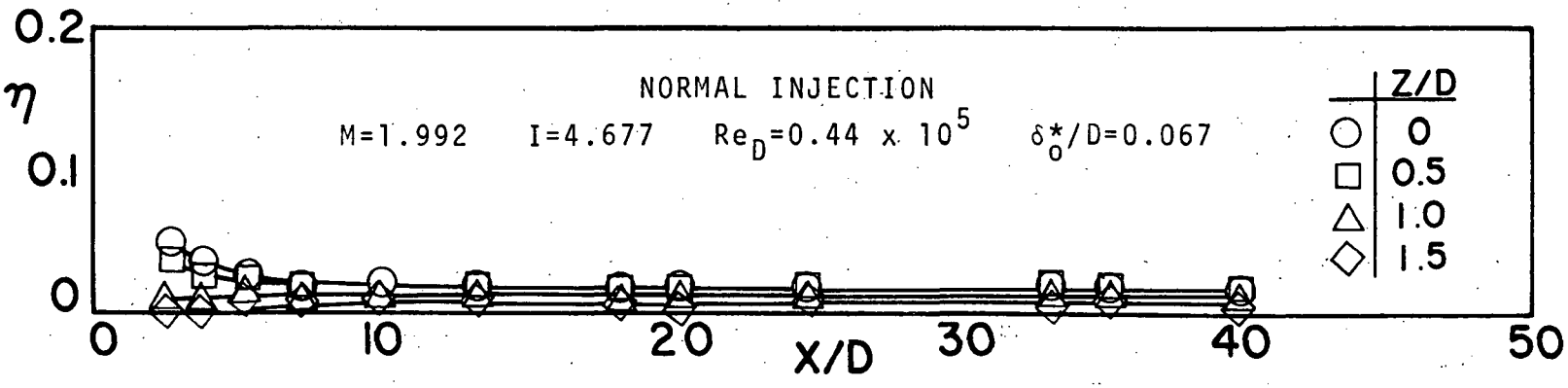

Figure 25 Film cooling effectiveness for normal injection through a single hole, M=2.0, Re_D=0.44 x 10^5

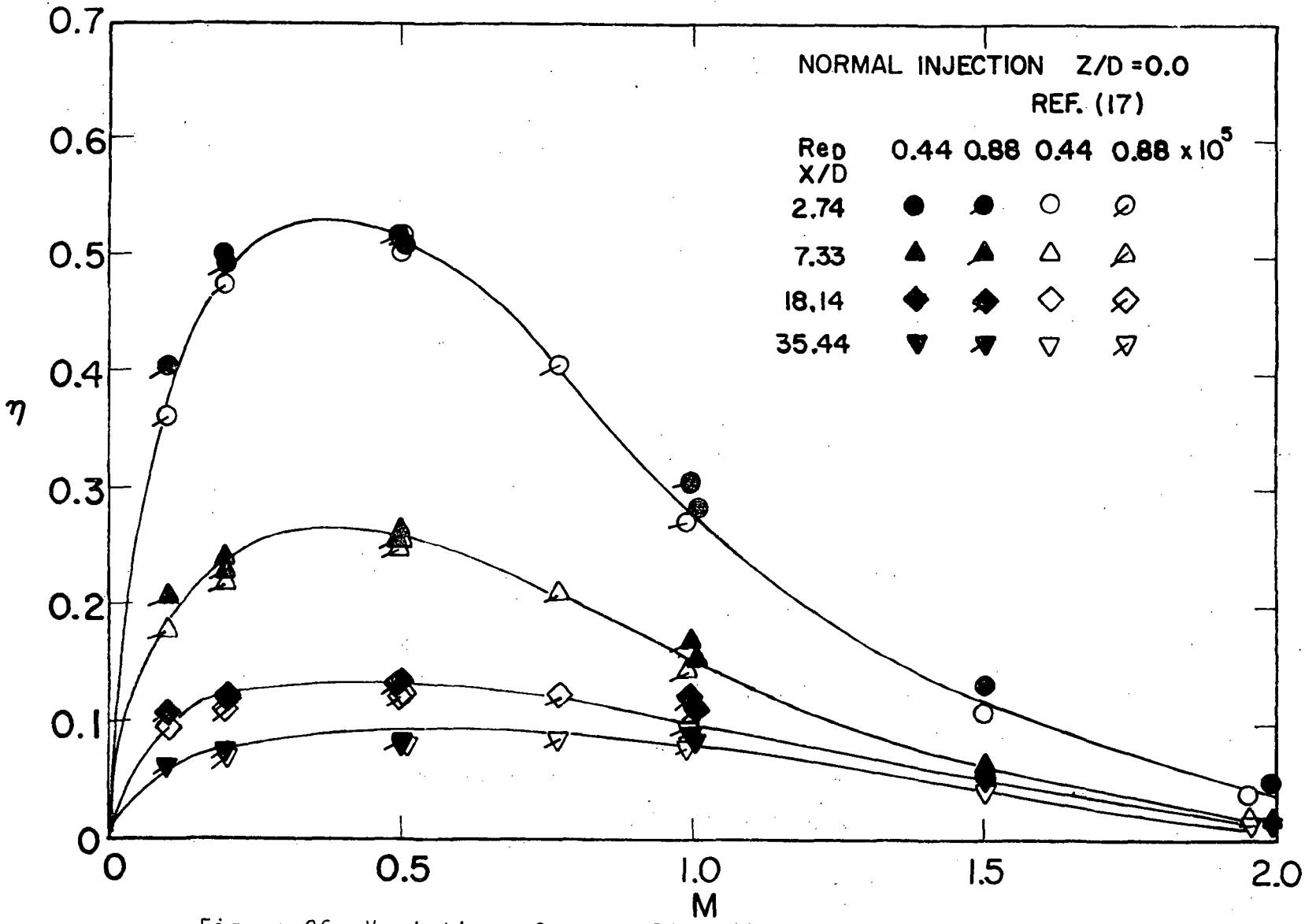

Figure 26 Variation of centerline film cooling effectiveness with blowing rate for normal injection

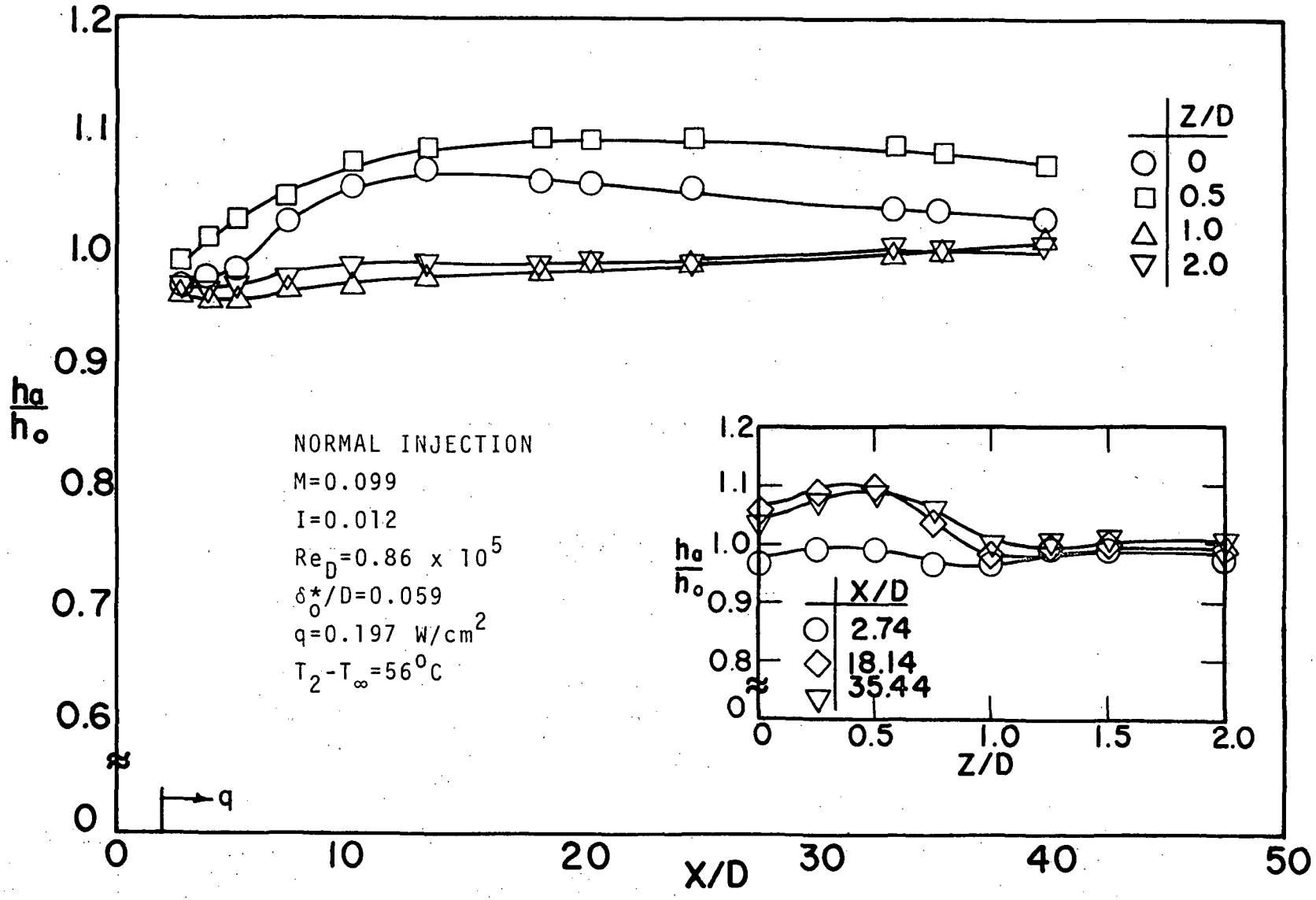

Figure 27 Heat transfer coefficient for heated normal injection through a single hole, M=0.1, Re_D=0.86 x 10^5

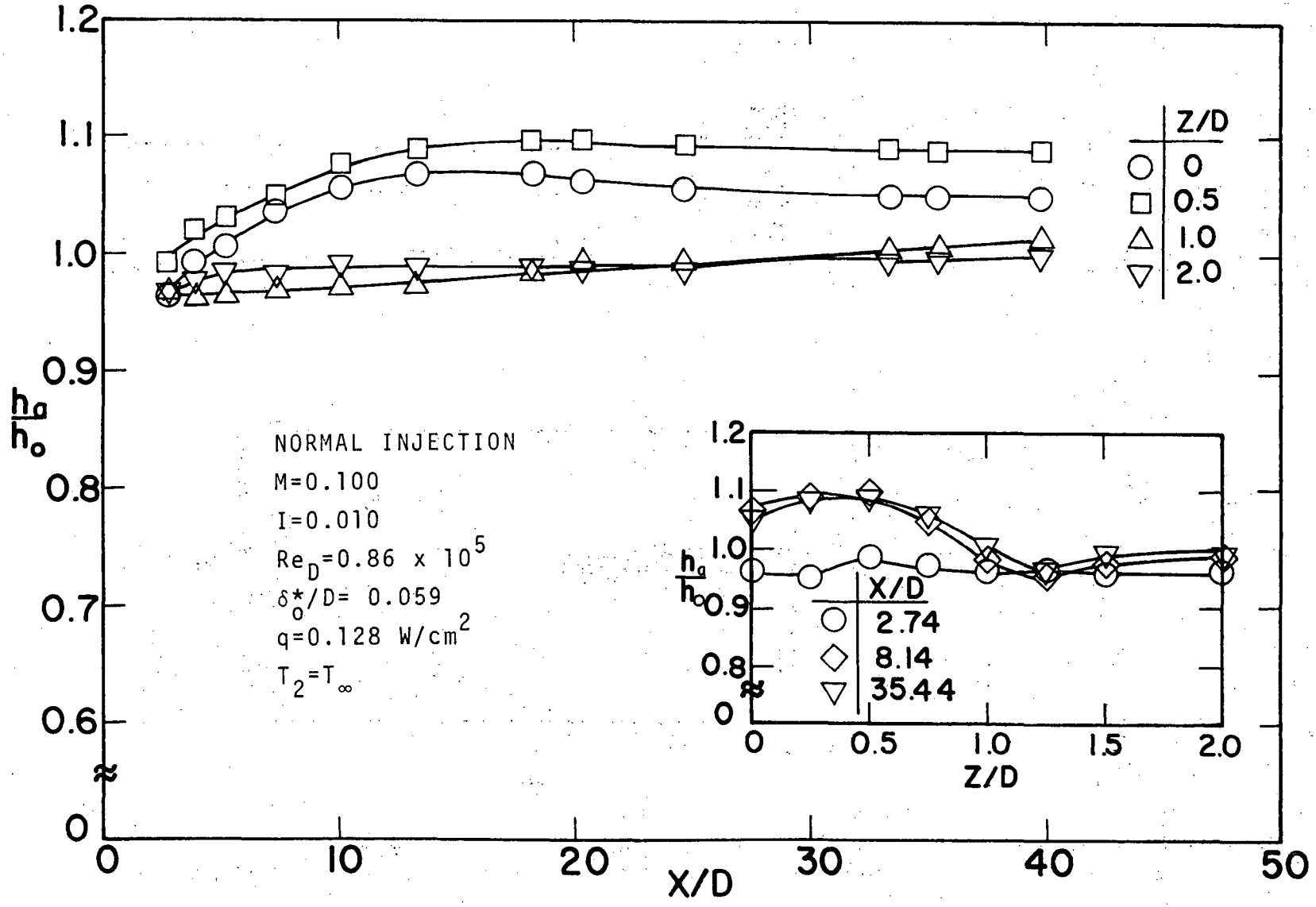

Figure 28 Heat transfer coefficient for unheated normal injection through a single hole, M=0.1, Re_D=0.86 x 10^5

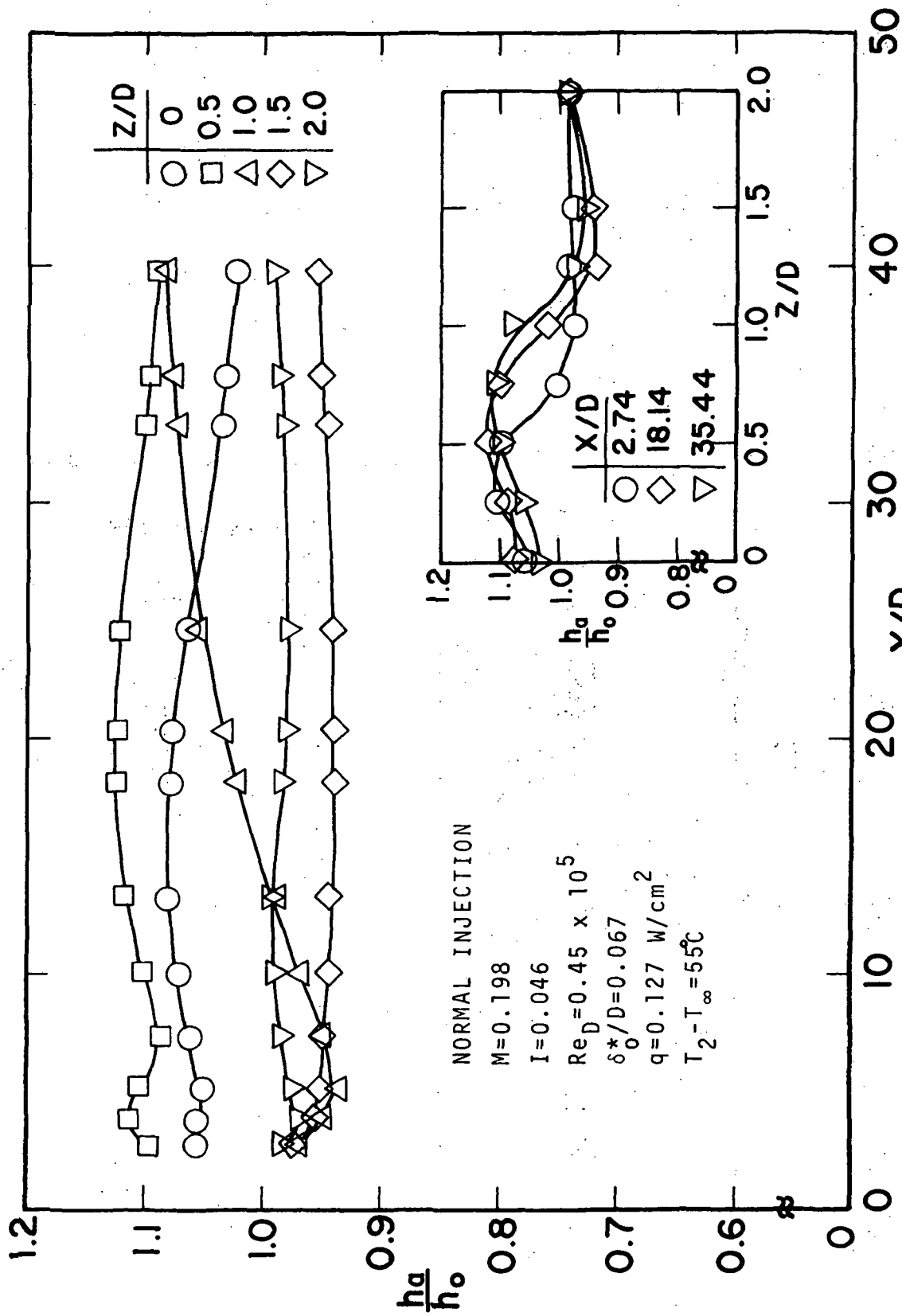

Figure 29 Heat transfer coefficient for heated normal injection through a single hole, M=0.2, Re_D=0.45 x 10^5

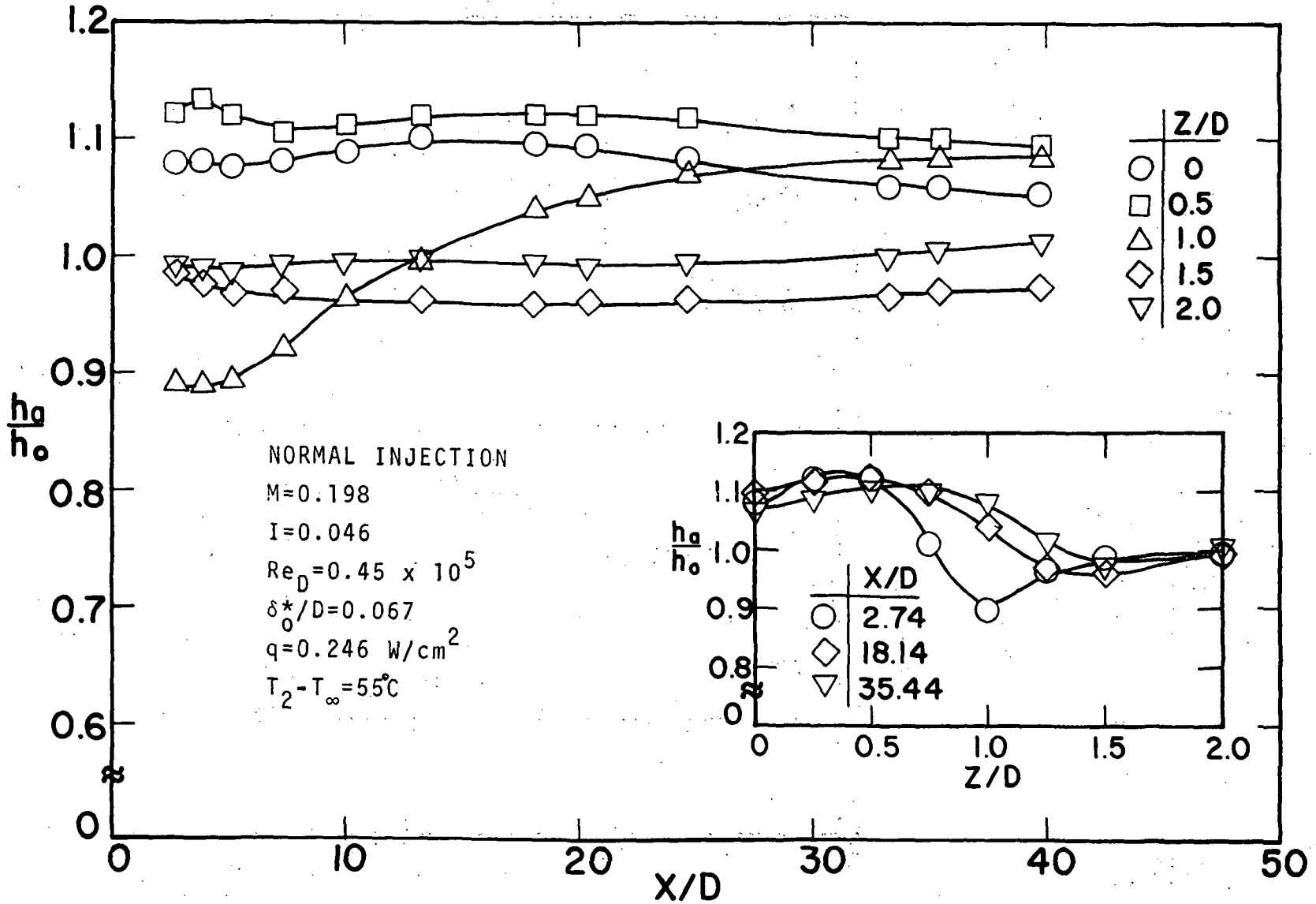

Figure 30 Heat transfer coefficient for heated normal injection through a single hole, M=0.2, Re_D=0.45 x 10^5

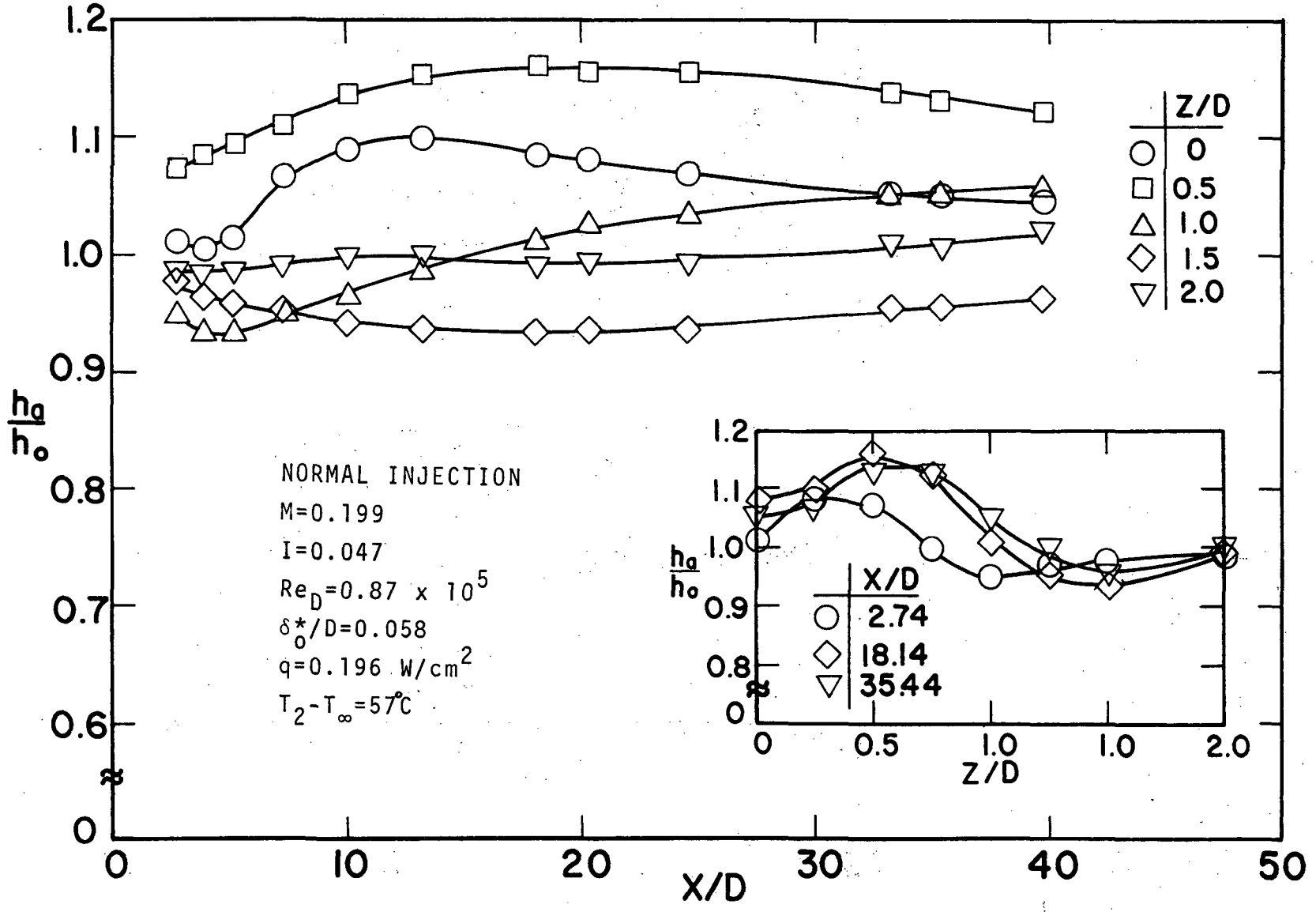

Figure 31 Heat transfer coefficient for heated normal injection through a single hole, M=0.2, Re_D=0.87 x 10^5

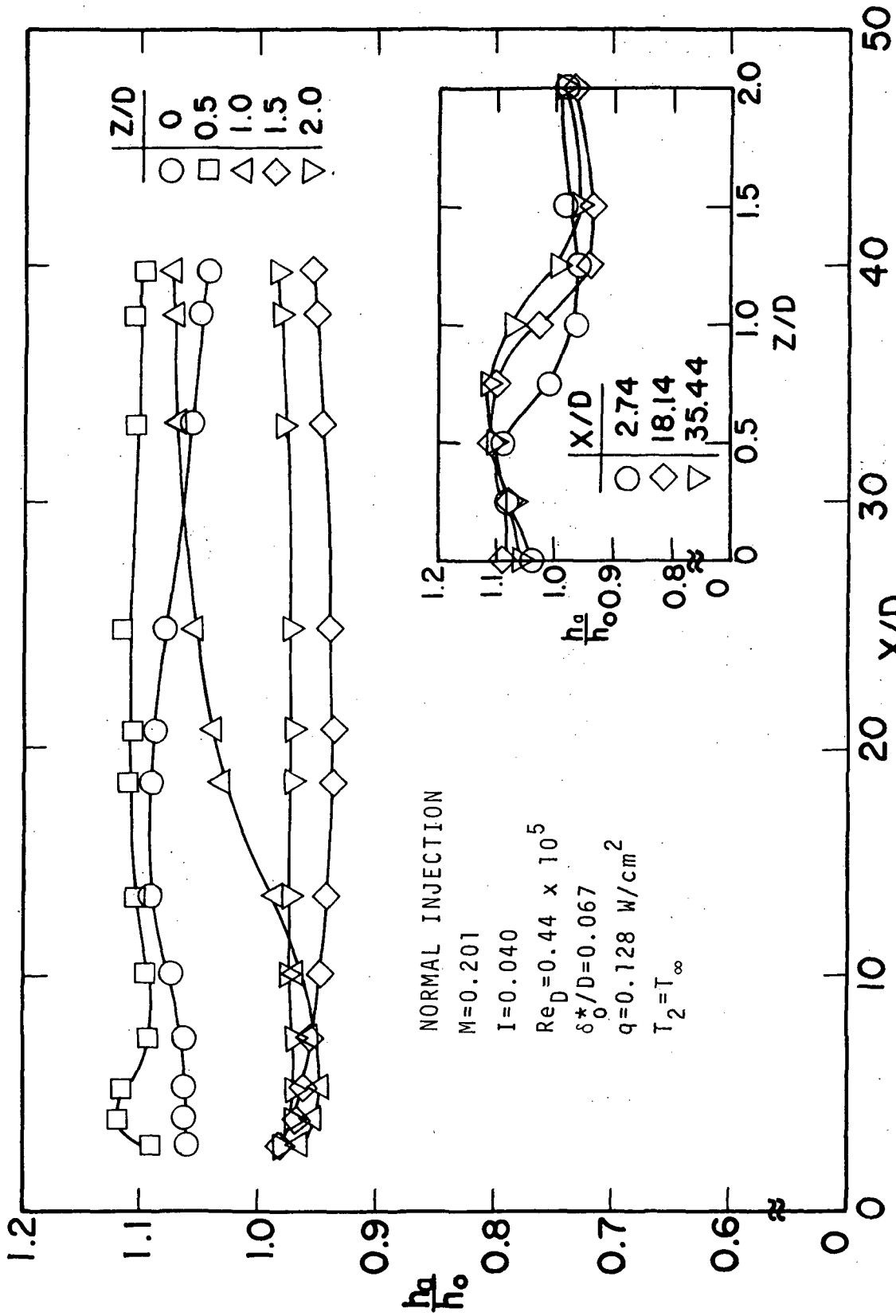

Figure 32 Heat transfer coefficient for unheated normal injection through a single hole, M=0.2, Re_D=0.44 x 10^5

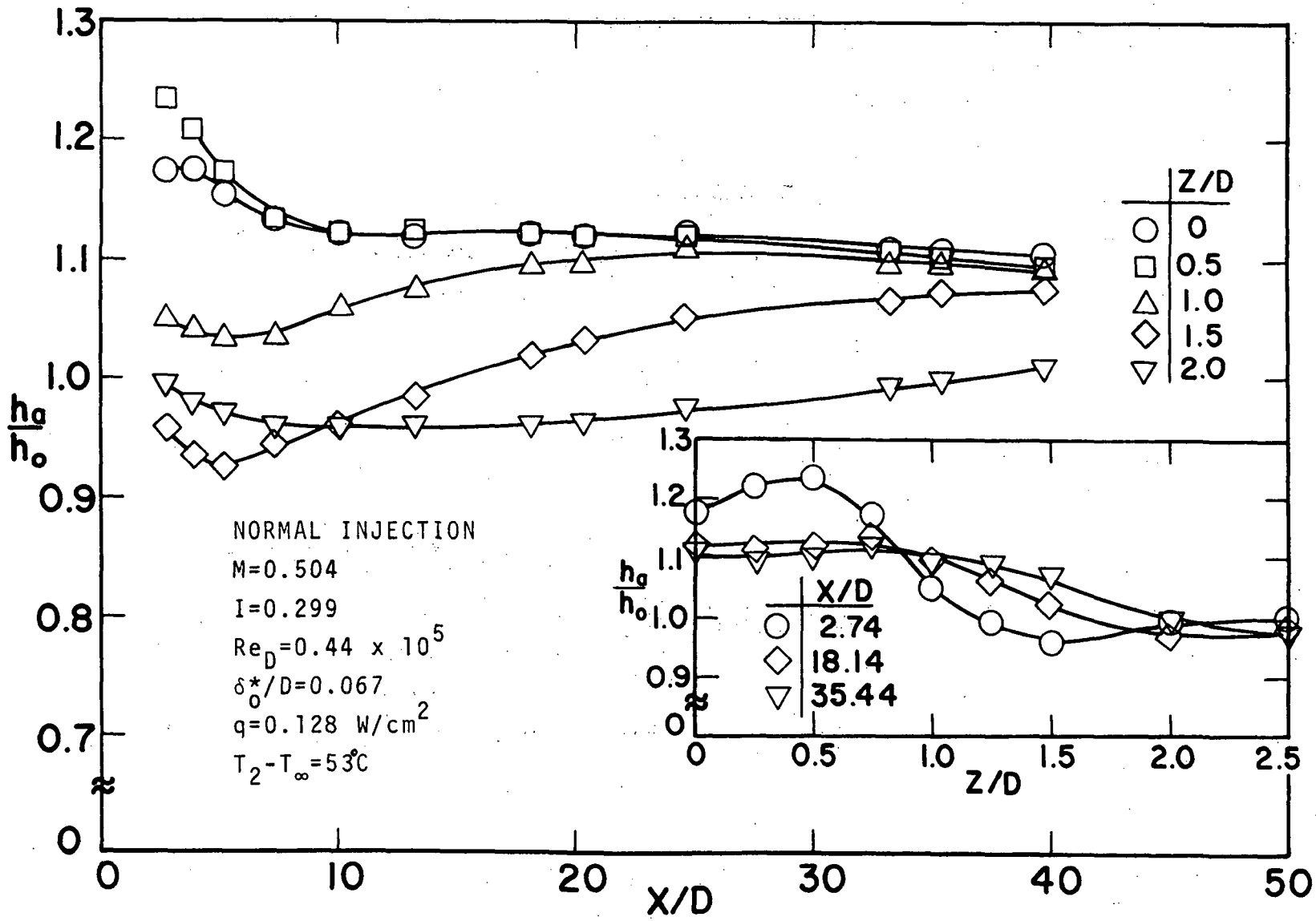

Figure 33 Heat transfer coefficient for heated normal injection through a single hole, M=0.5, Re_D=0.44 x 10^5

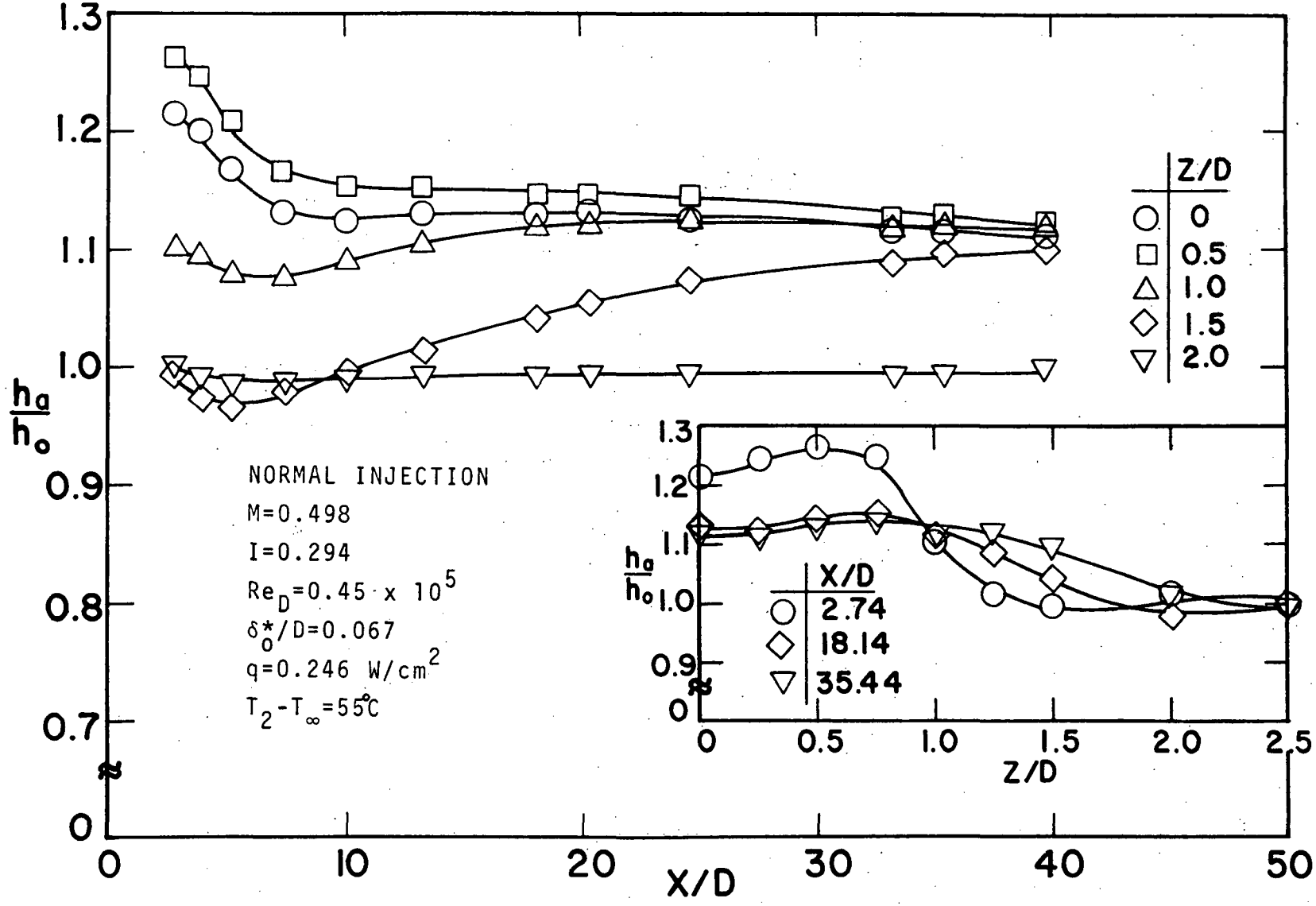

Figure 34 Heat transfer coefficient for heated normal injection through a single hole, M=0.5, Re_D=0.45 x 10^5

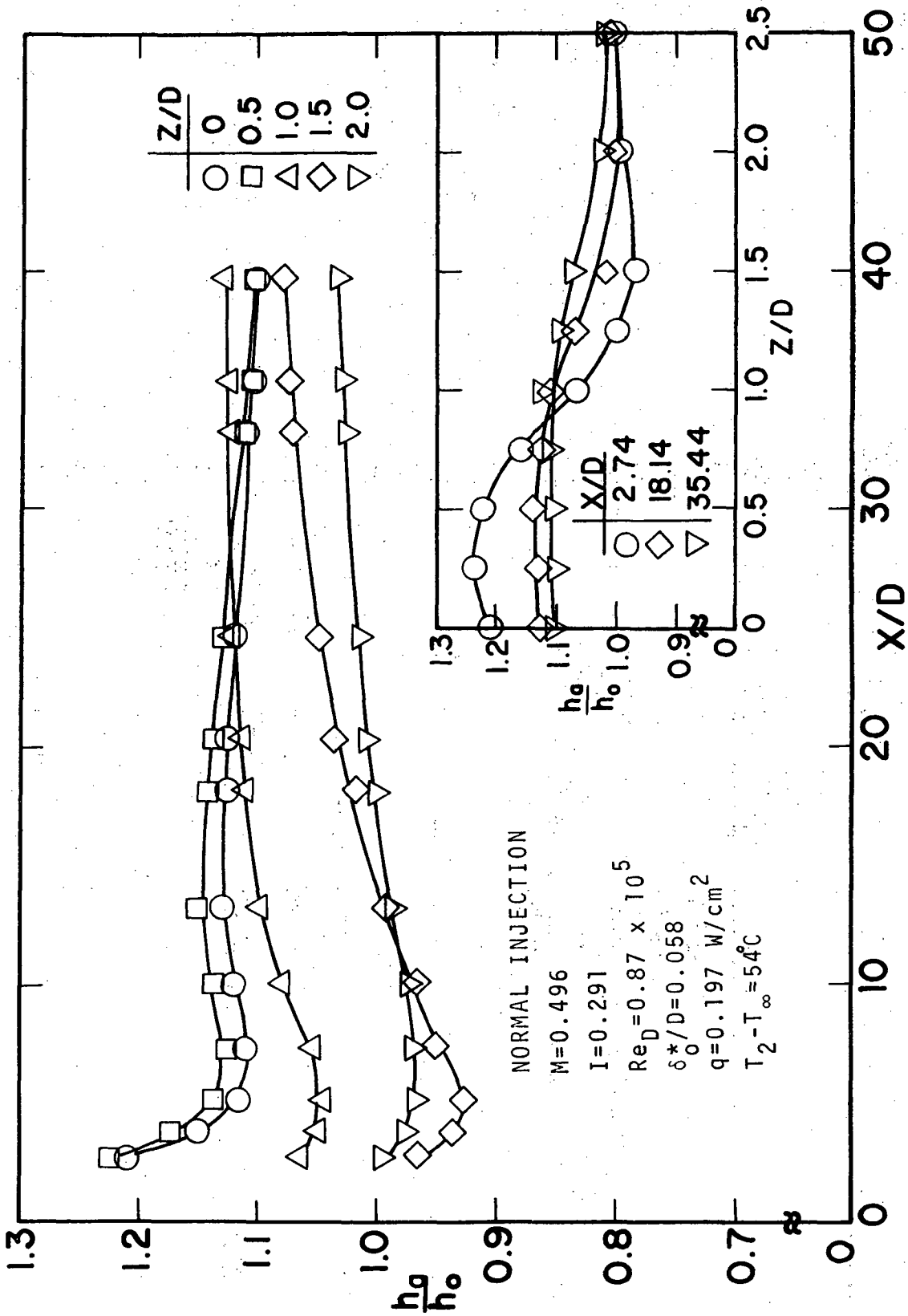

Figure 35 Heat transfer coefficient for heated normal injection through a single hole, M=0.5, Re_D=0.87 x 10^5

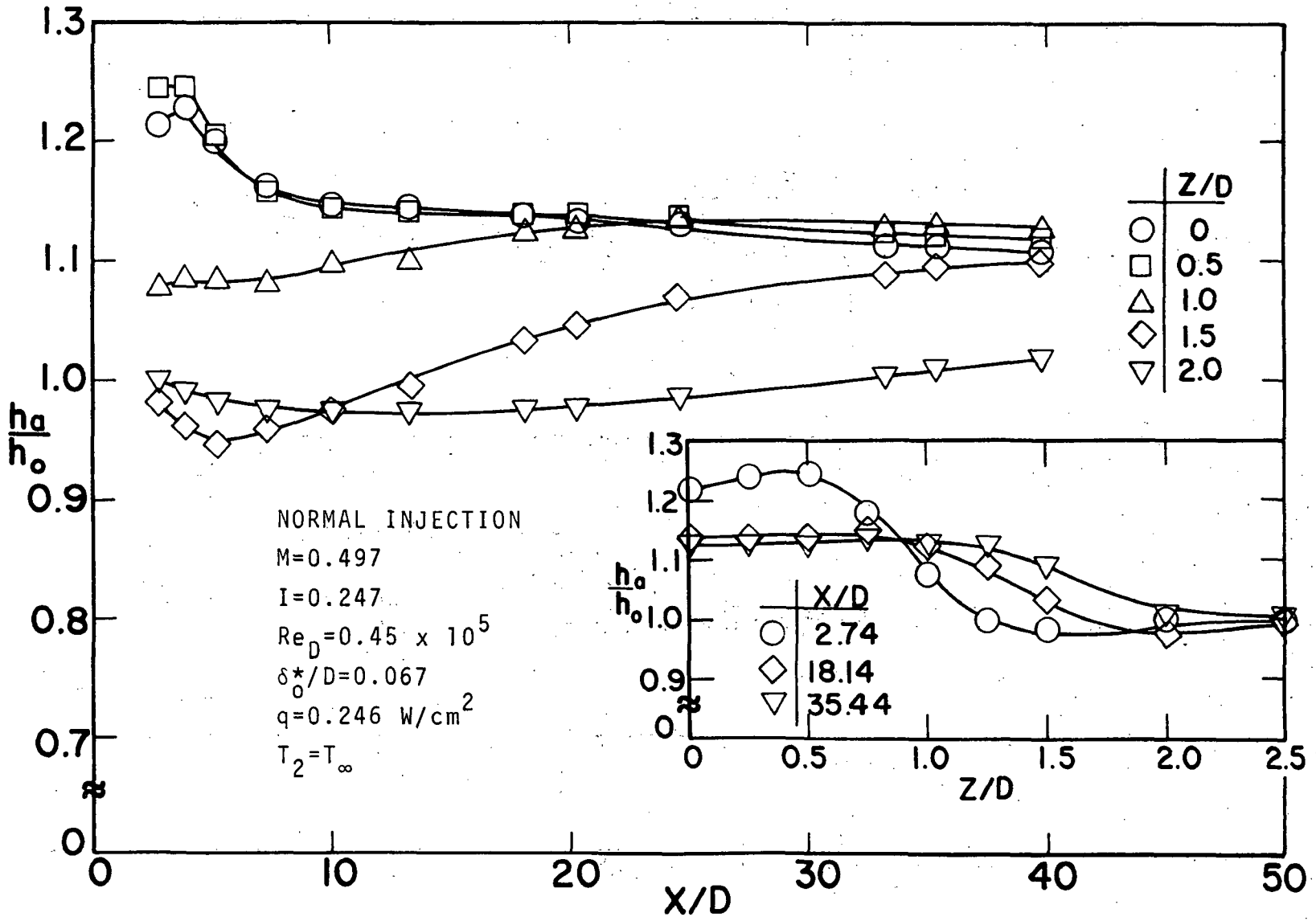

Figure 36 Heat transfer coefficient for unheated normal injection through a single hole, M=0.5, Re_D=0.45 x 10^5

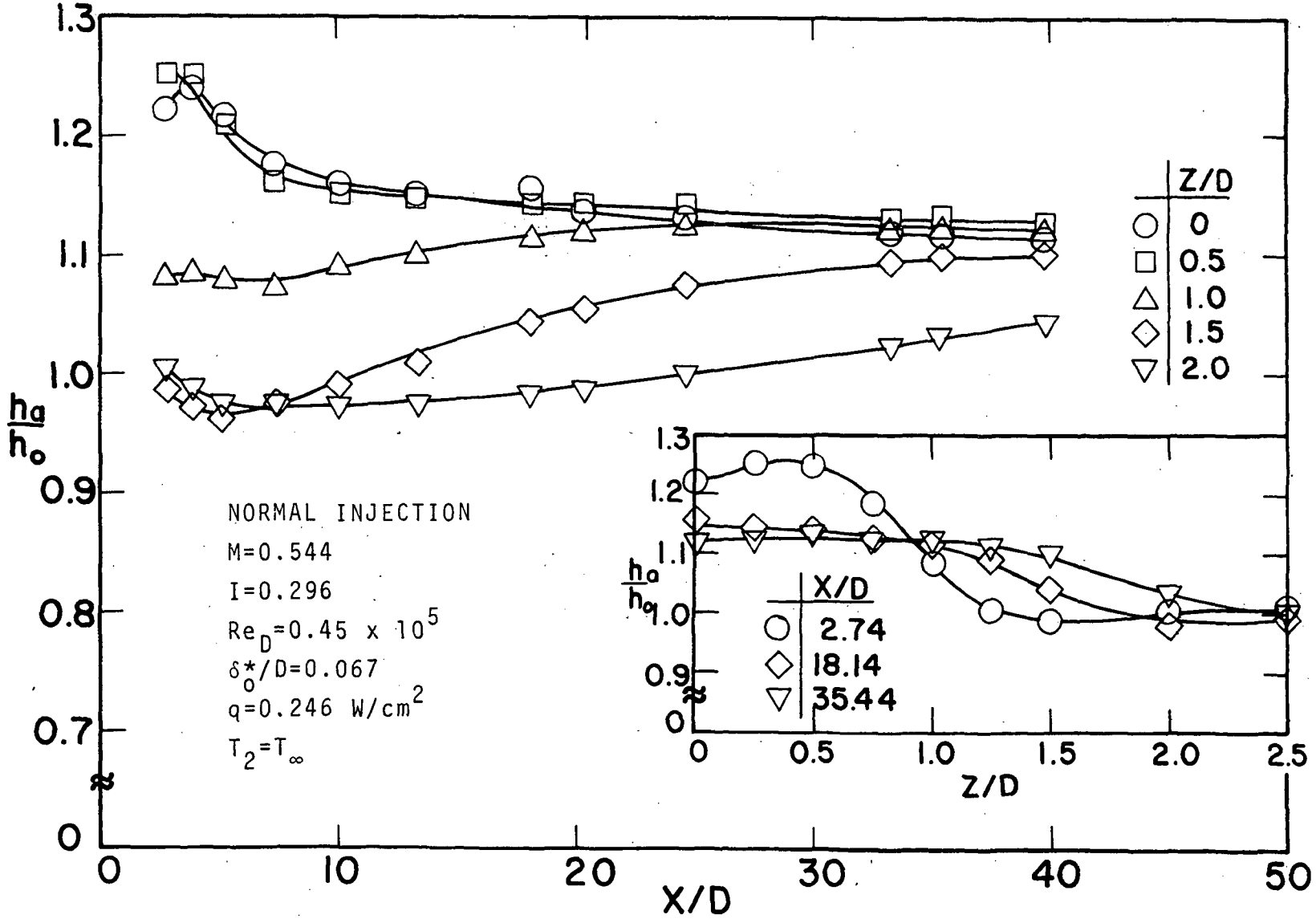

Figure 37 Heat transfer coefficient for unheated normal injection through a single hole, M=0.54, Re_D=0.45 x 10^5

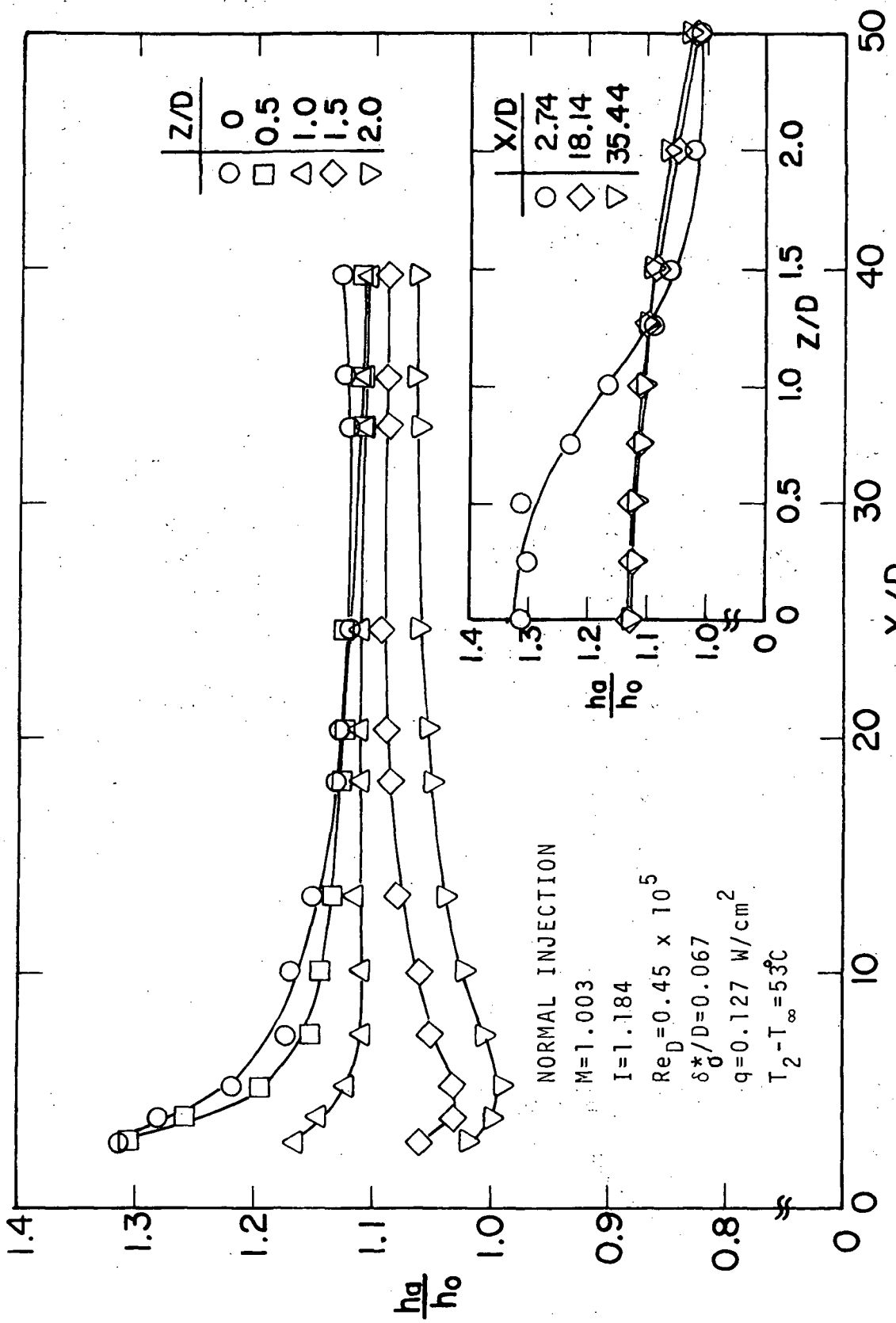

Figure 38 Heat transfer coefficient for heated normal injection through a single hole, M=1.0, Re_D=0.45 x 10^5

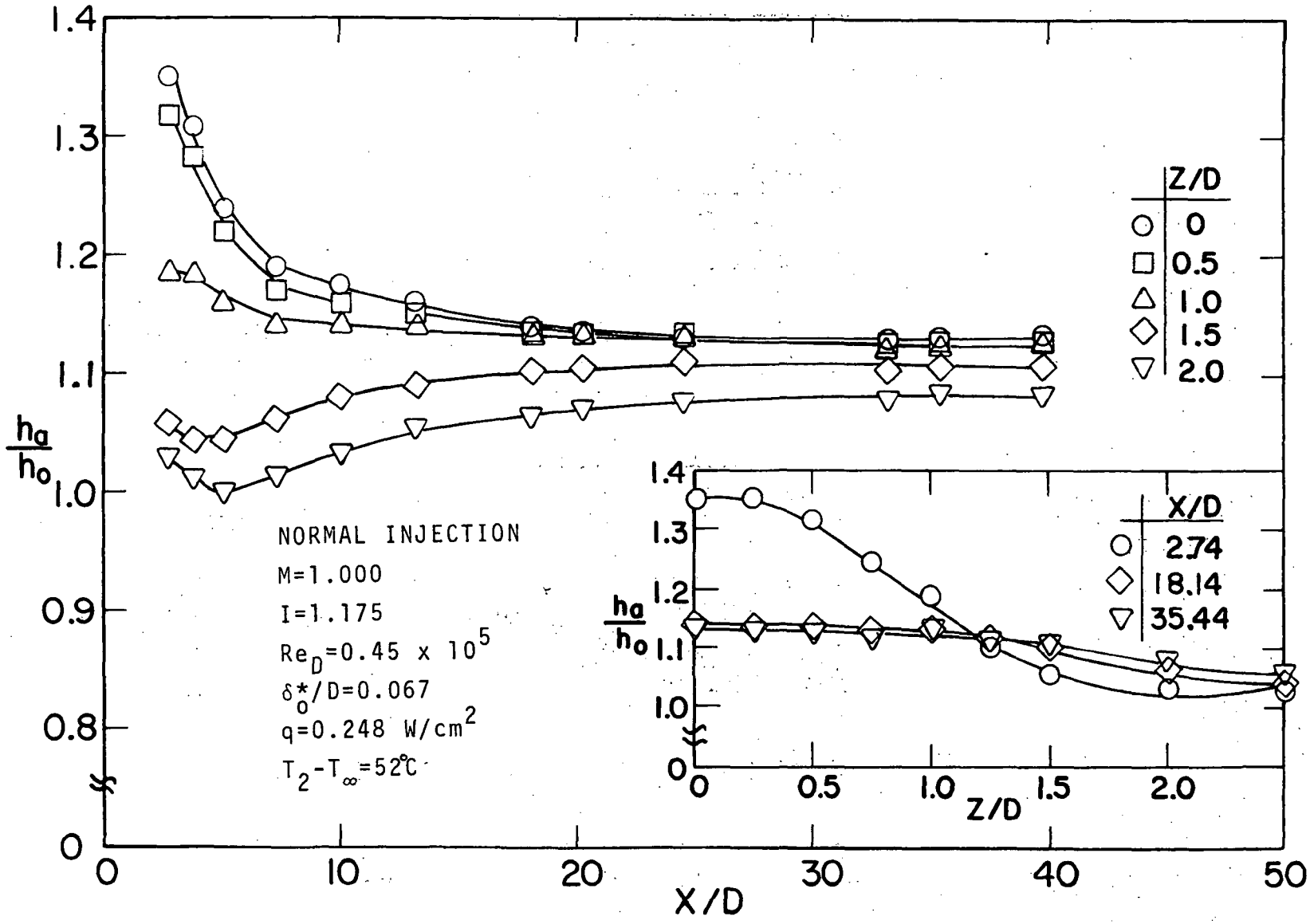

Figure 39 Heat transfer coefficient for heated normal injection through a single hole, M=1.0, $Re_D=0.45 \times 10^5$

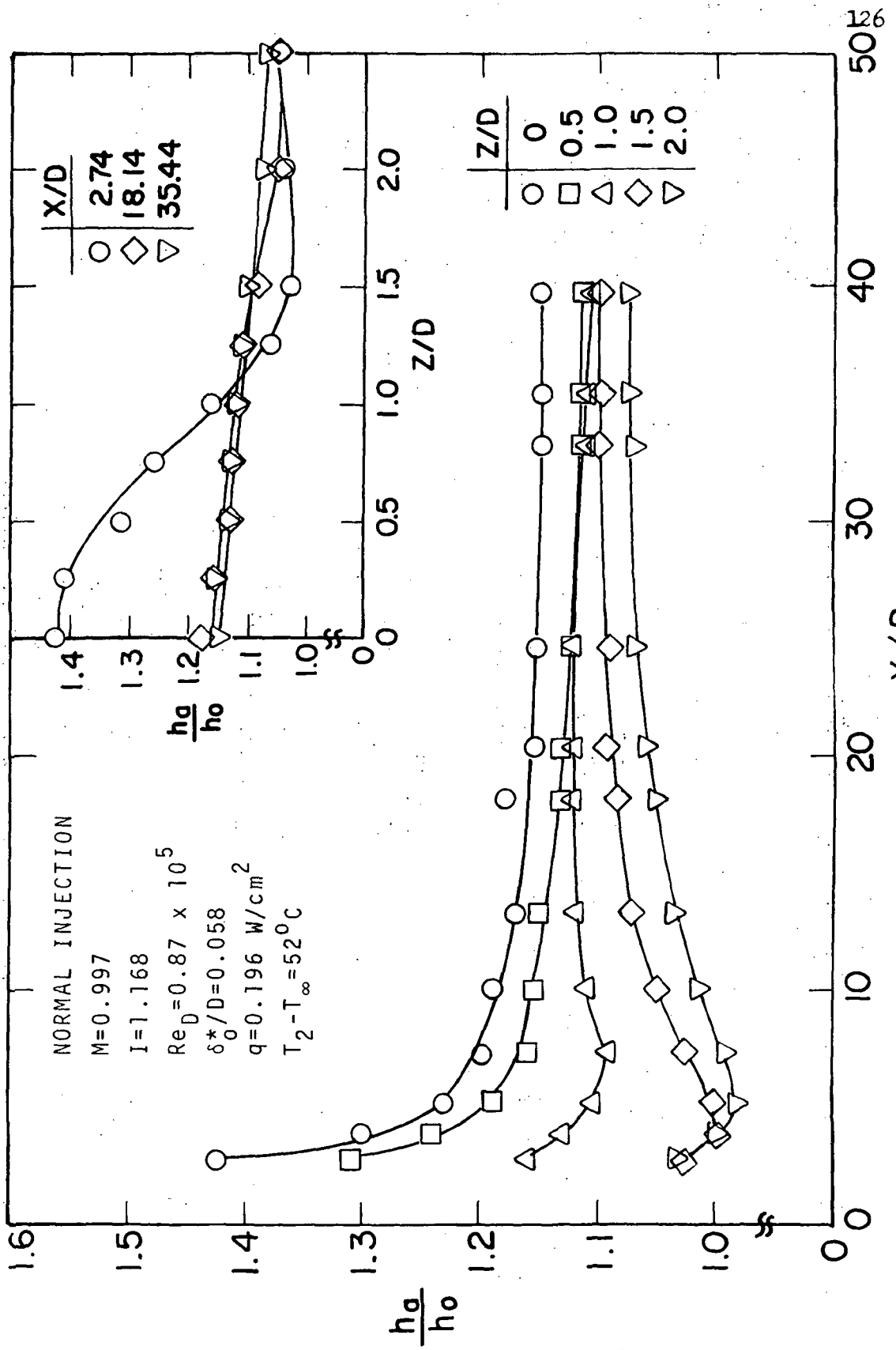

Figure 40 Heat transfer coefficient for heated normal injection through a single hole, M=1.0, Re_D=0.87 x 10^5

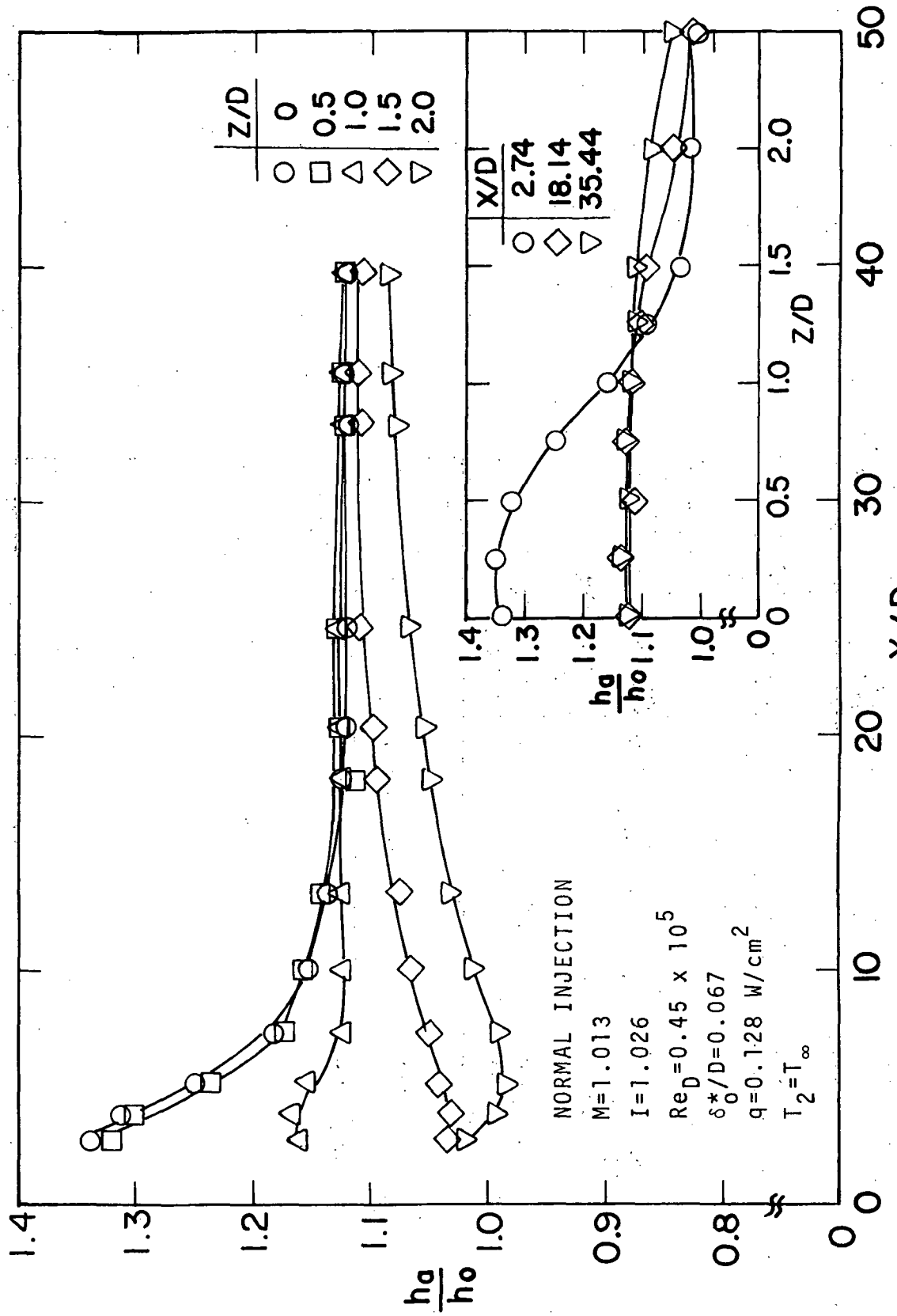

Figure 41 Heat transfer coefficient for unheated normal injection through a single hole, M=1.0, Re_D=0.45 x 10^5

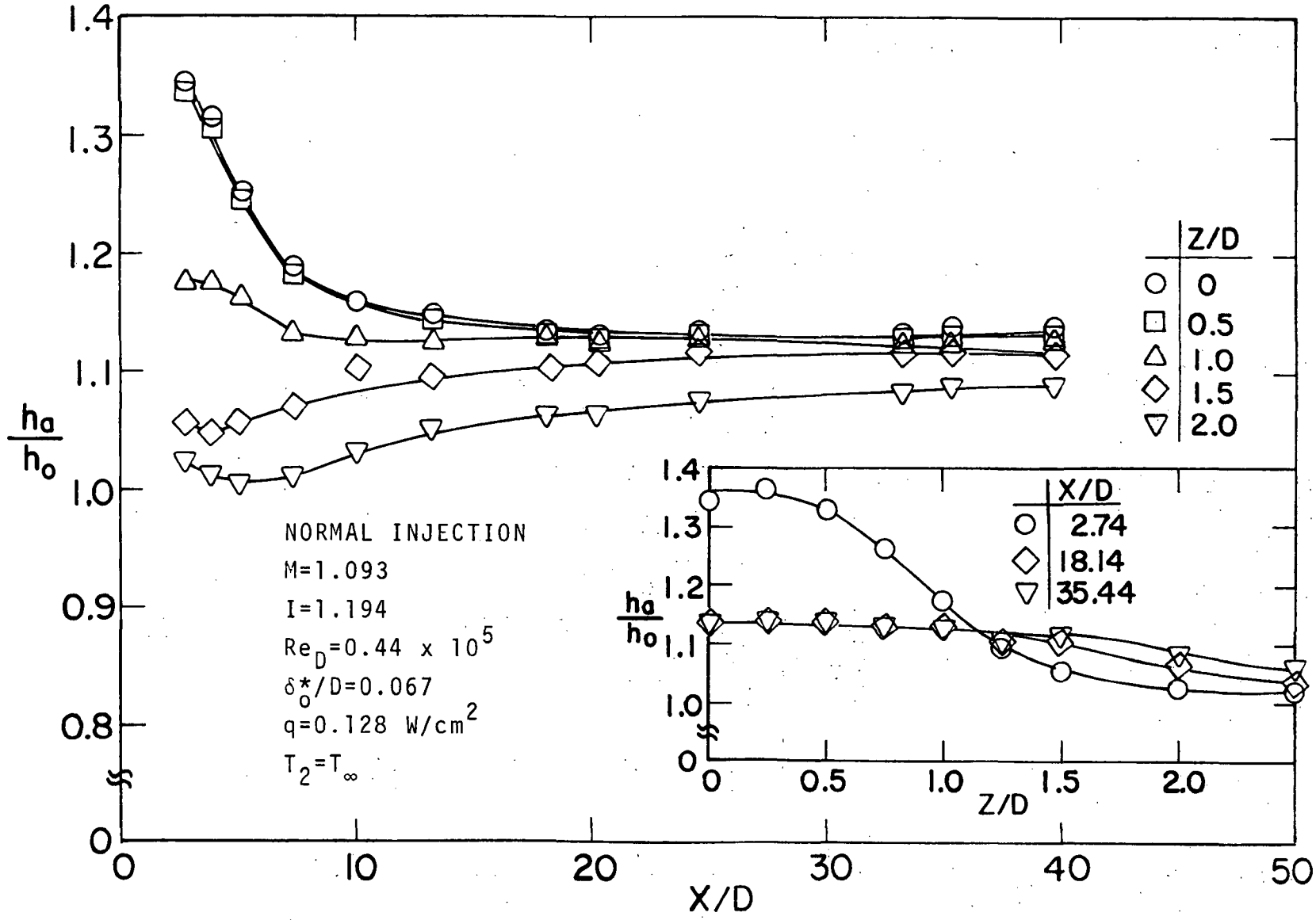

Figure 42 Heat transfer coefficient for unheated normal injection through a single hole, M=1.09, Re_D=0.44 x 10^5

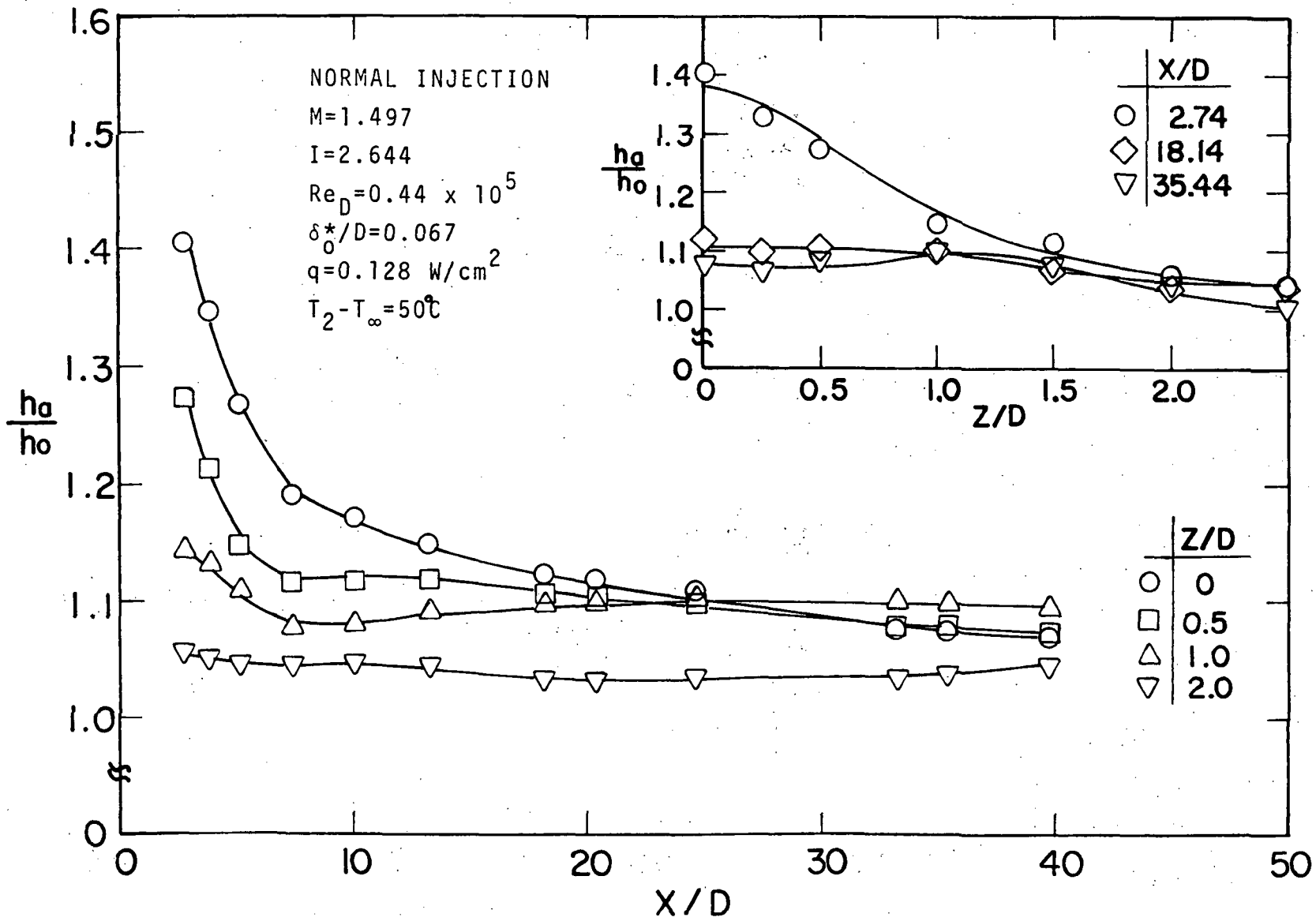

Figure 43 Heat transfer coefficient for heated normal injection through a single hole, M=1.5, Re_D=0.44 x 10^5

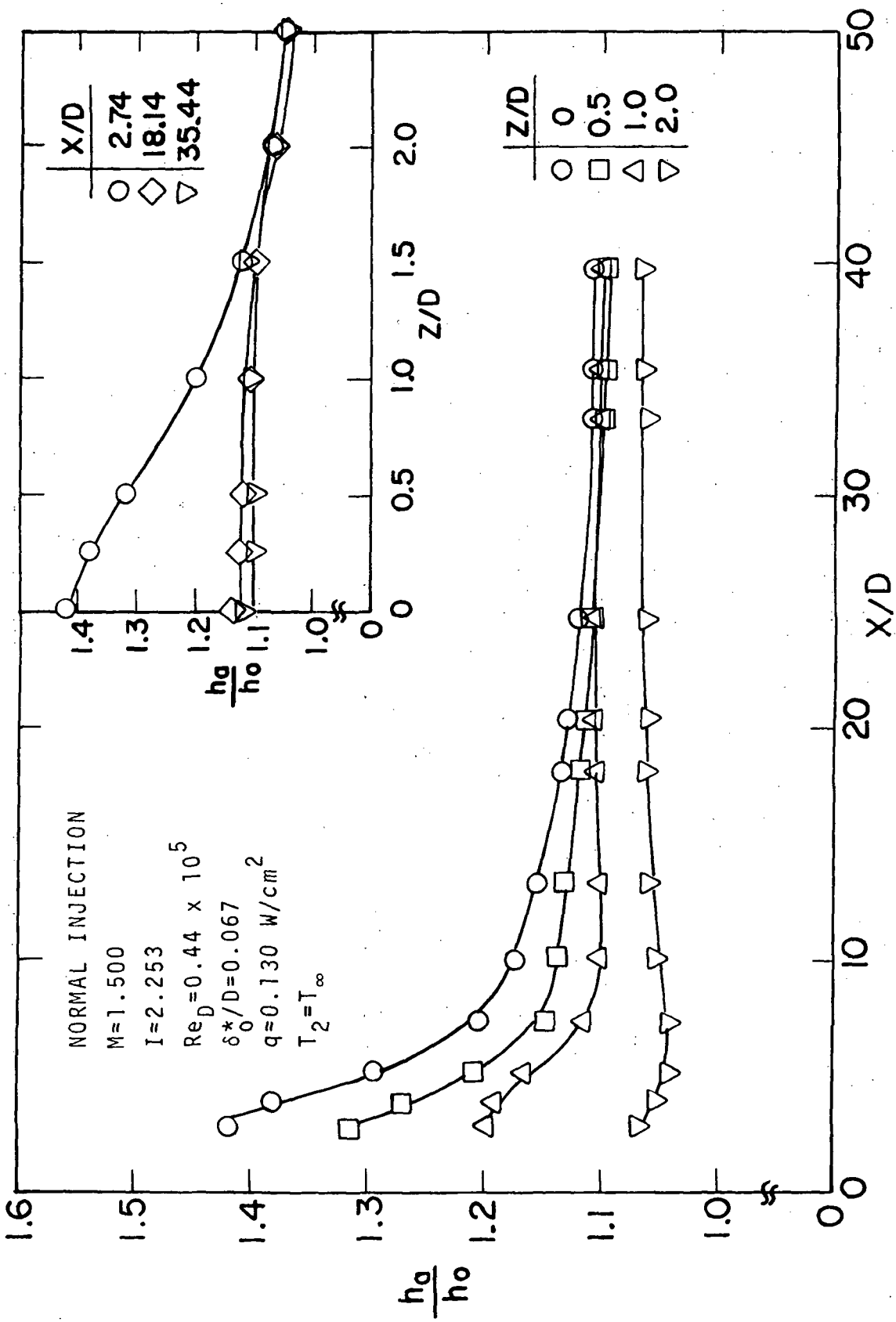

Figure 44 Heat transfer coefficient for unheated normal injection through a single hole, M=1.5, Re_D=0.44 x 10^5

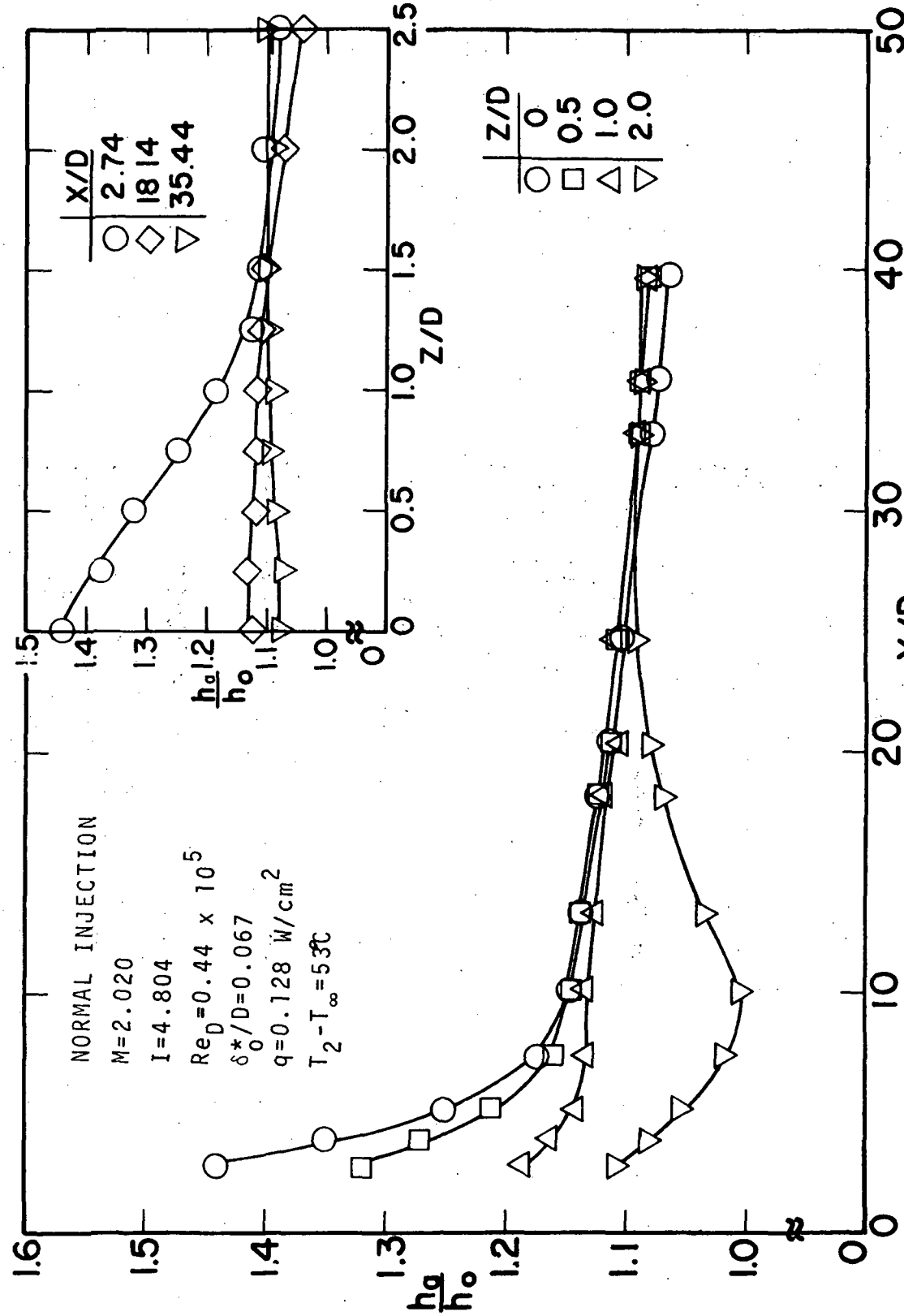

Figure 45 Heat transfer coefficient for heated normal injection through a single hole, M=2.0, Re_D=0.44 x 10^5

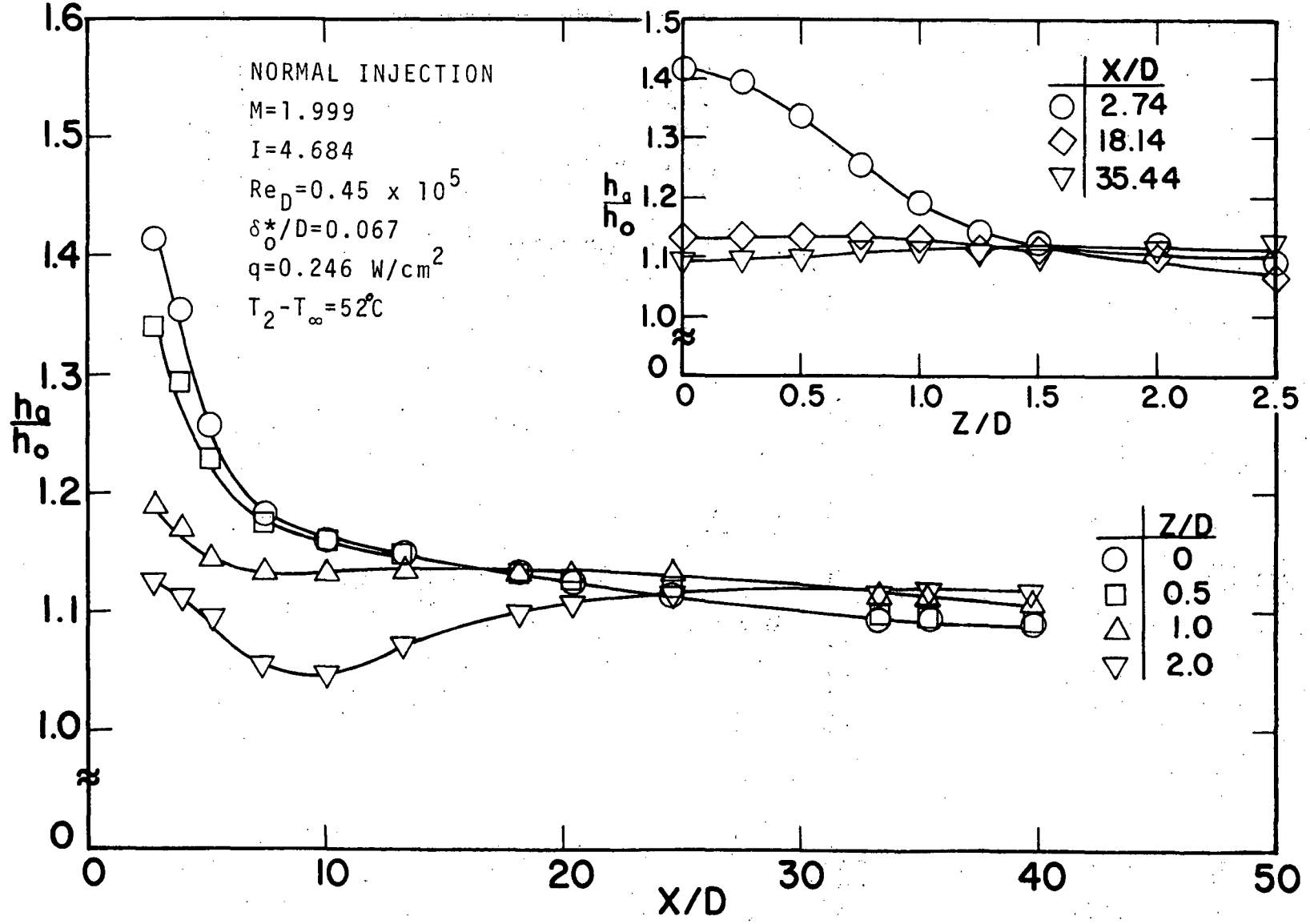

Figure 46 Heat transfer coefficient for heated normal injection through a single hole, M=2.0, Re_D=0.45 x 10^5

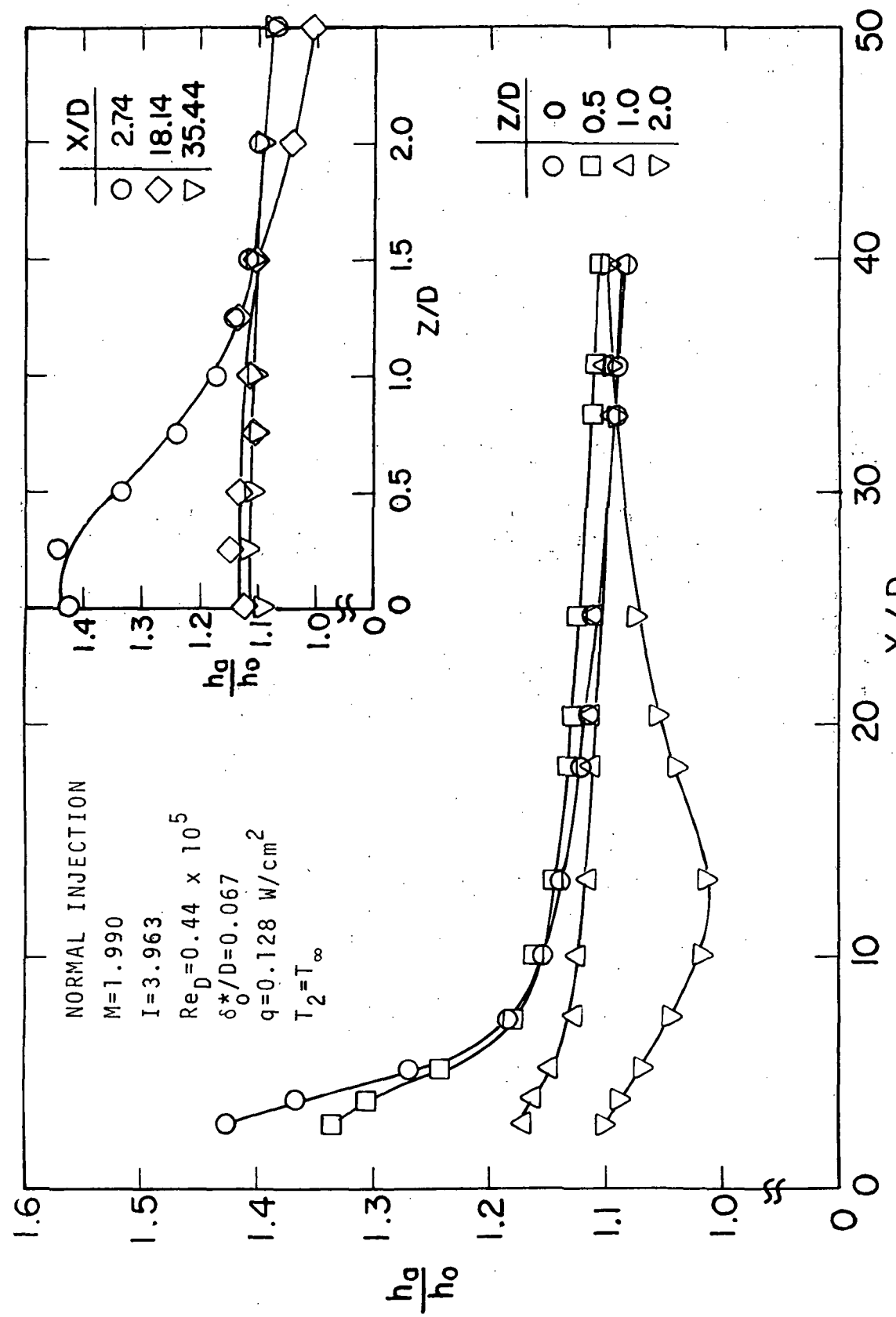

Figure 47 Heat transfer coefficient for unheated normal injection through a single hole, M=2.0, Re_D=0.44 x 10^5

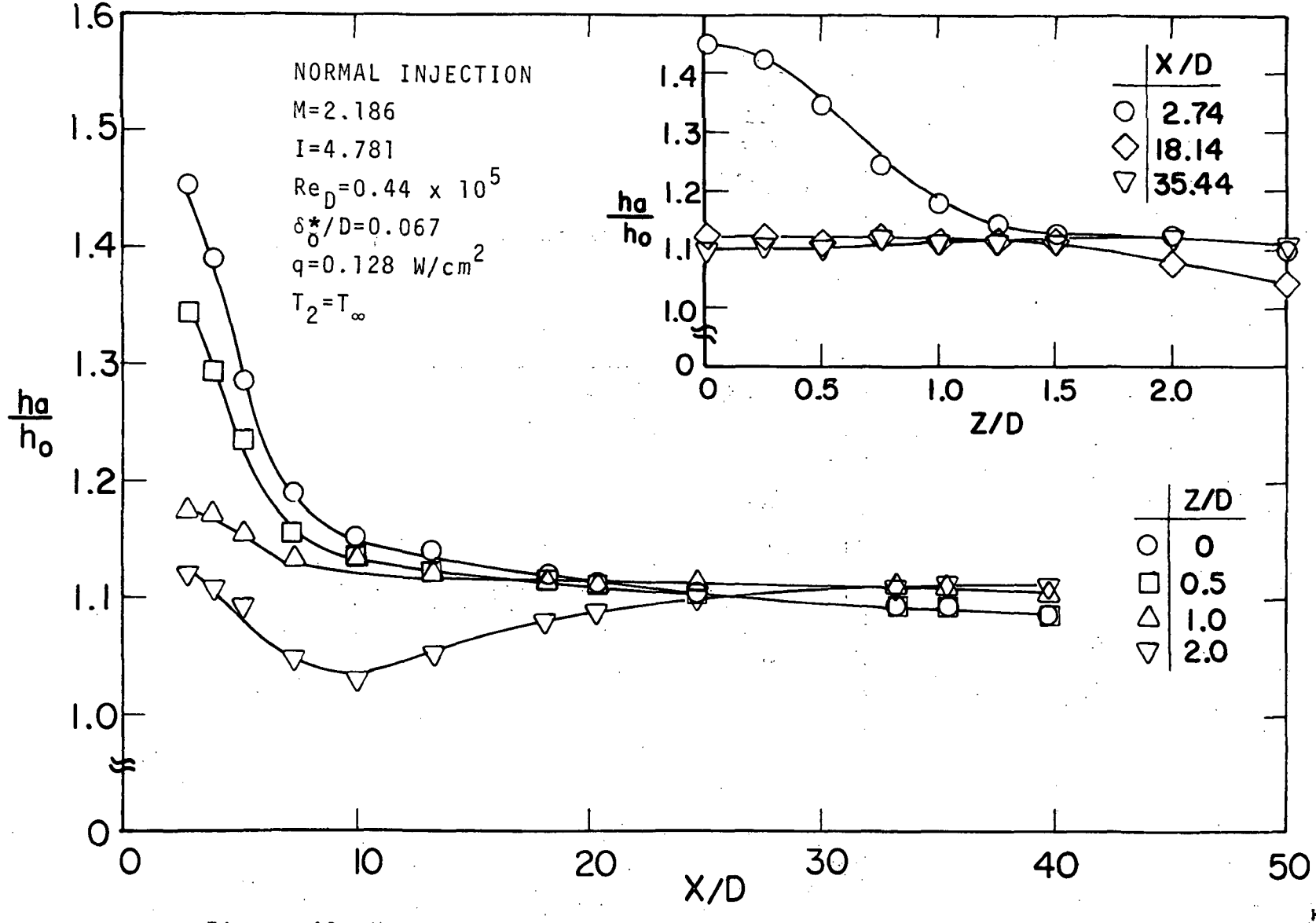

Figure 48 Heat transfer coefficient for unheated normal injection through a single hole, M=2.19, Re_D=0.44 x 10^5

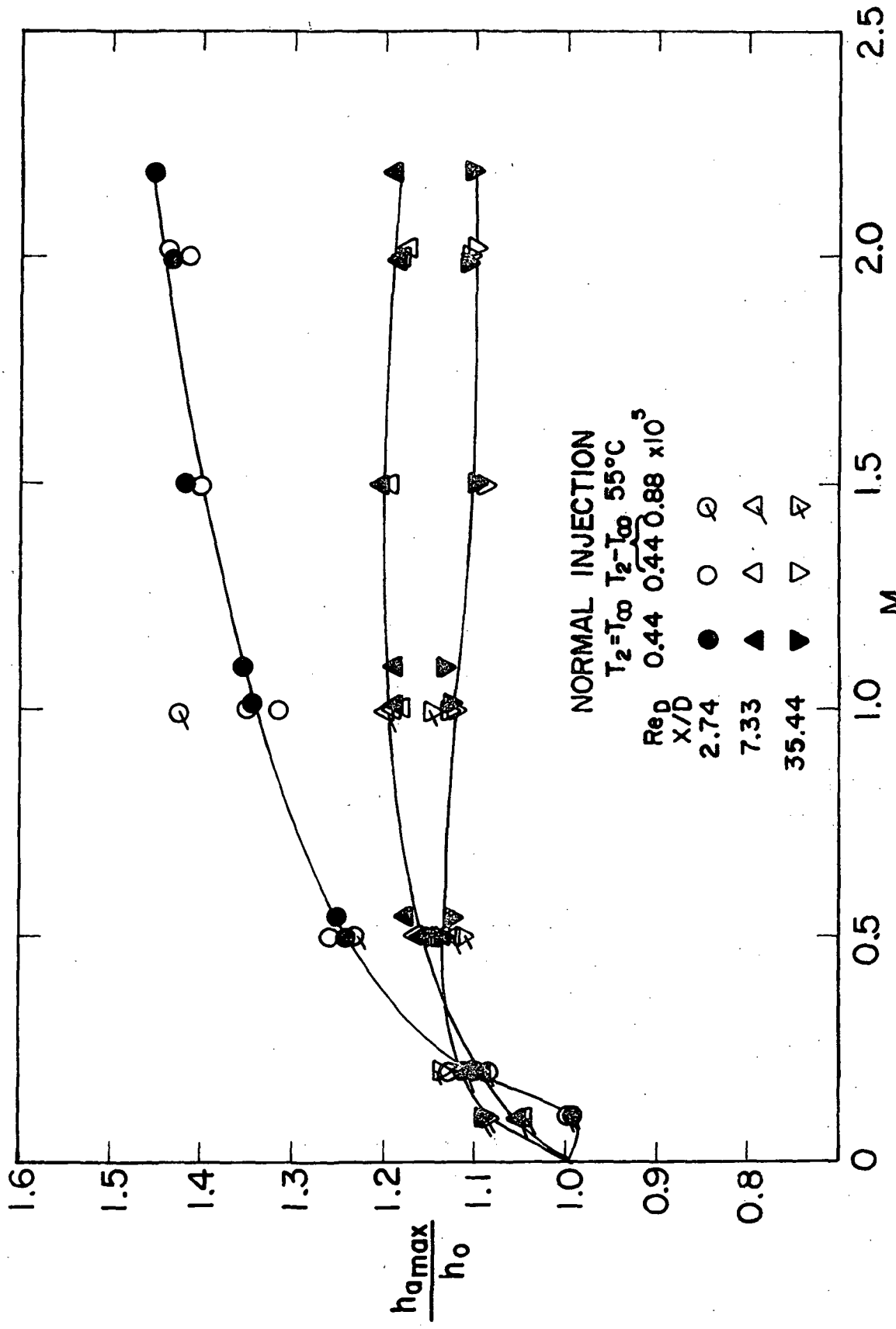

Figure 49 Variation of maximum heat transfer coefficient with blowing rate for normal injection through a single hole

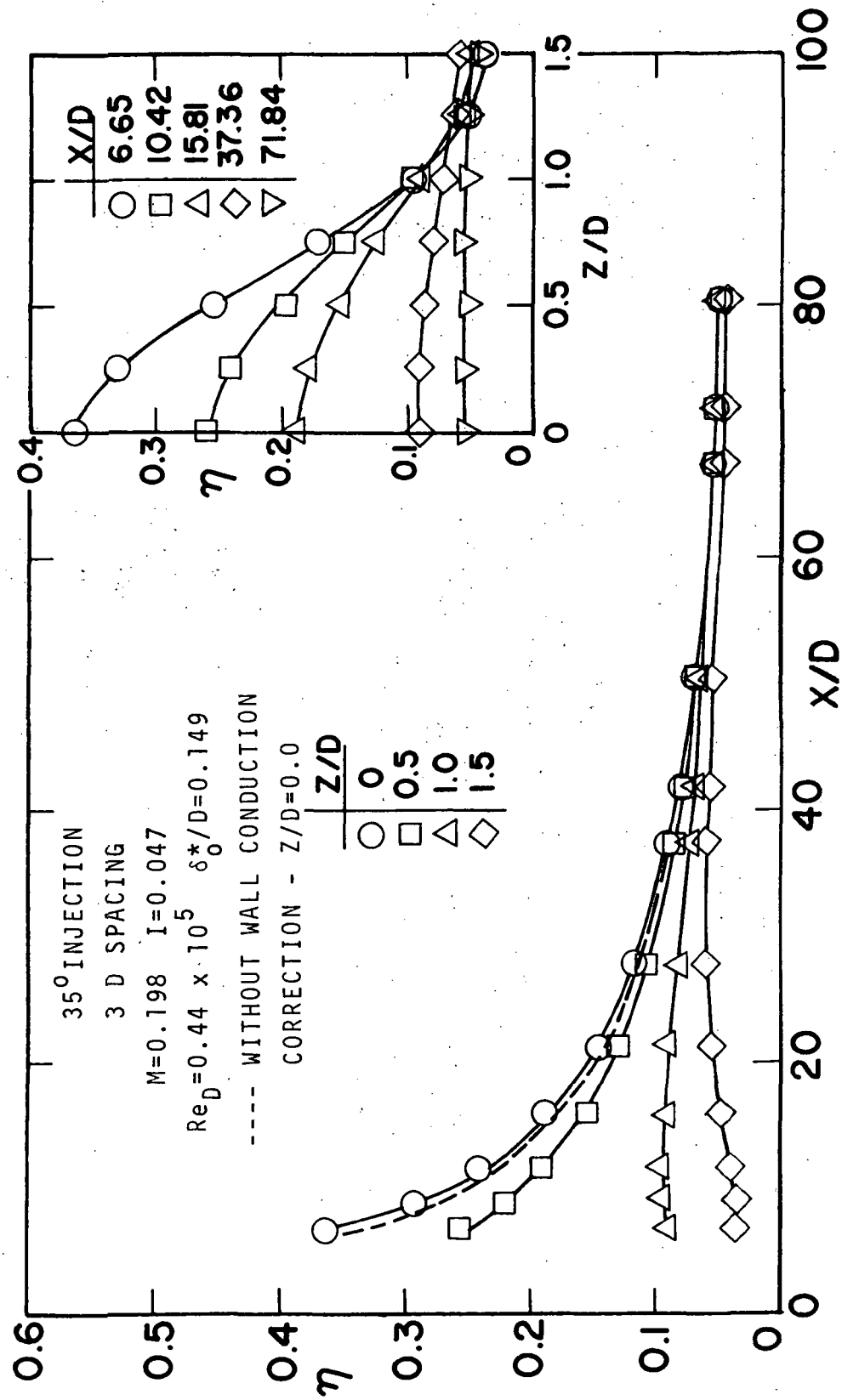

Figure 50 Film cooling effectiveness for 35^{o} injection through a row of holes, M=0.2, $Re_D=0.44 \times 10^5$

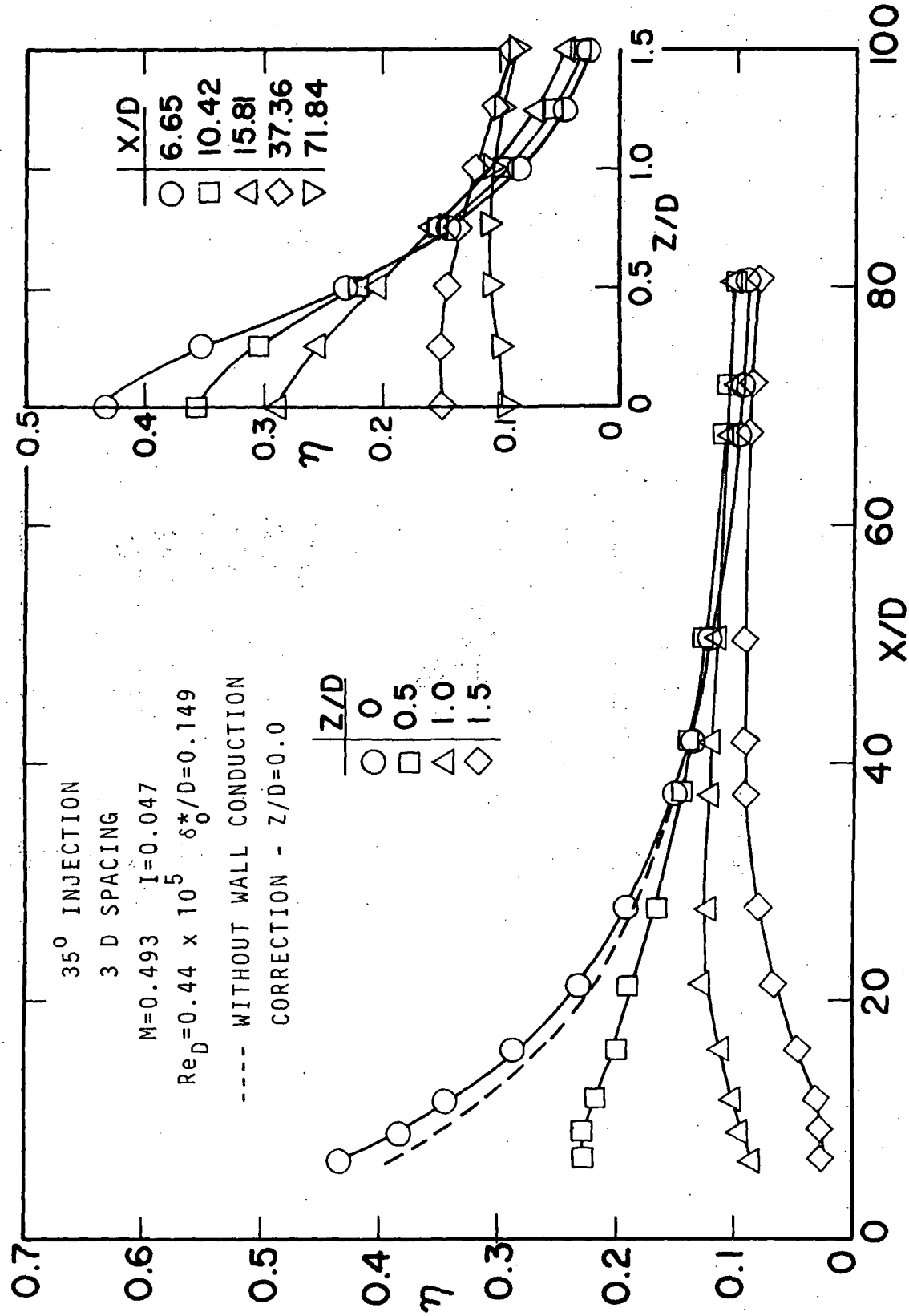

Figure 51 Film cooling effectiveness for 35^0 injection through a row of holes, M=0.5, $Re_D=0.44 \times 10^5$

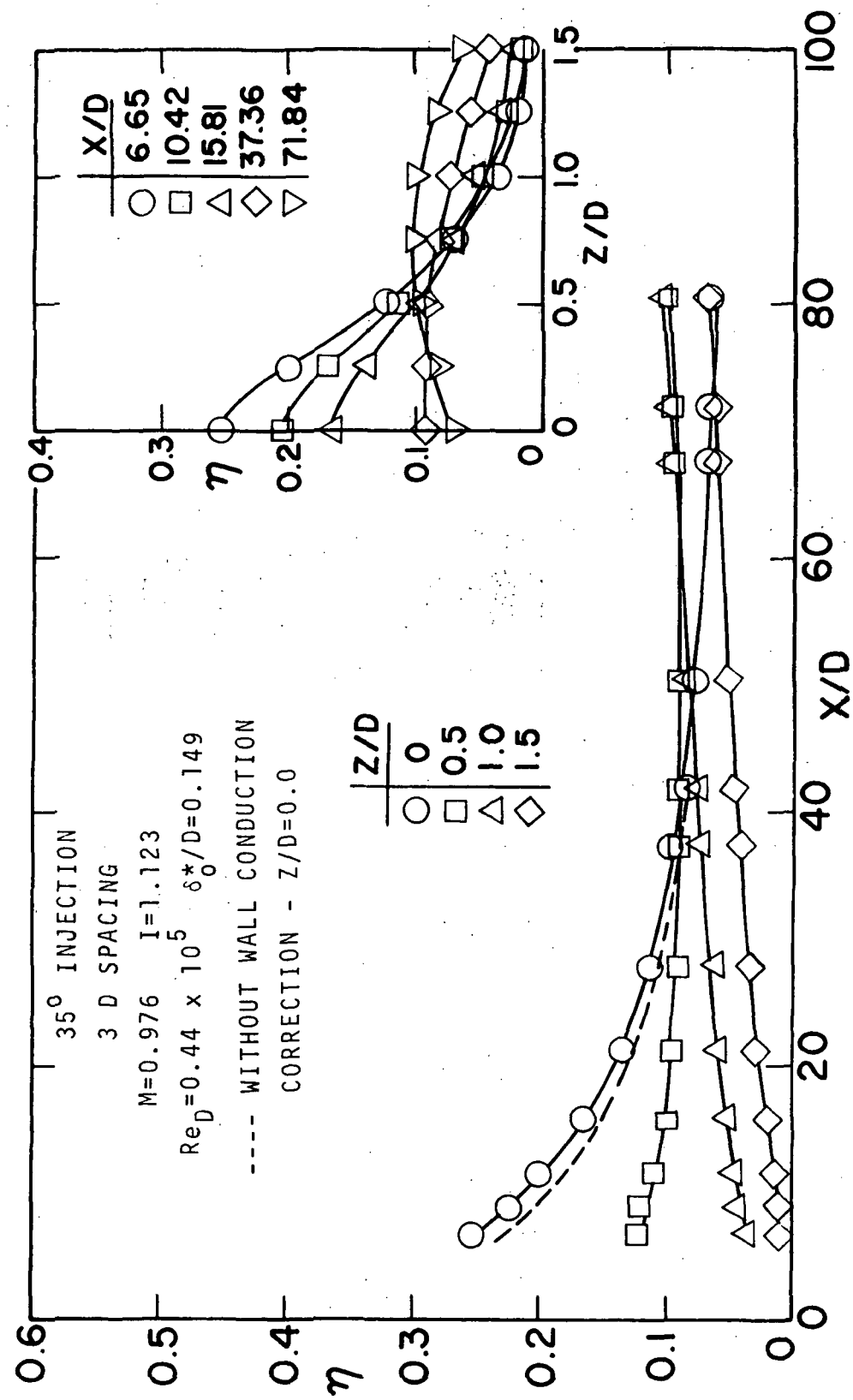

Figure 52 Film cooling effectiveness for 35° injection through a row of holes, M=1.0, Re_D=0.44 x 10^5

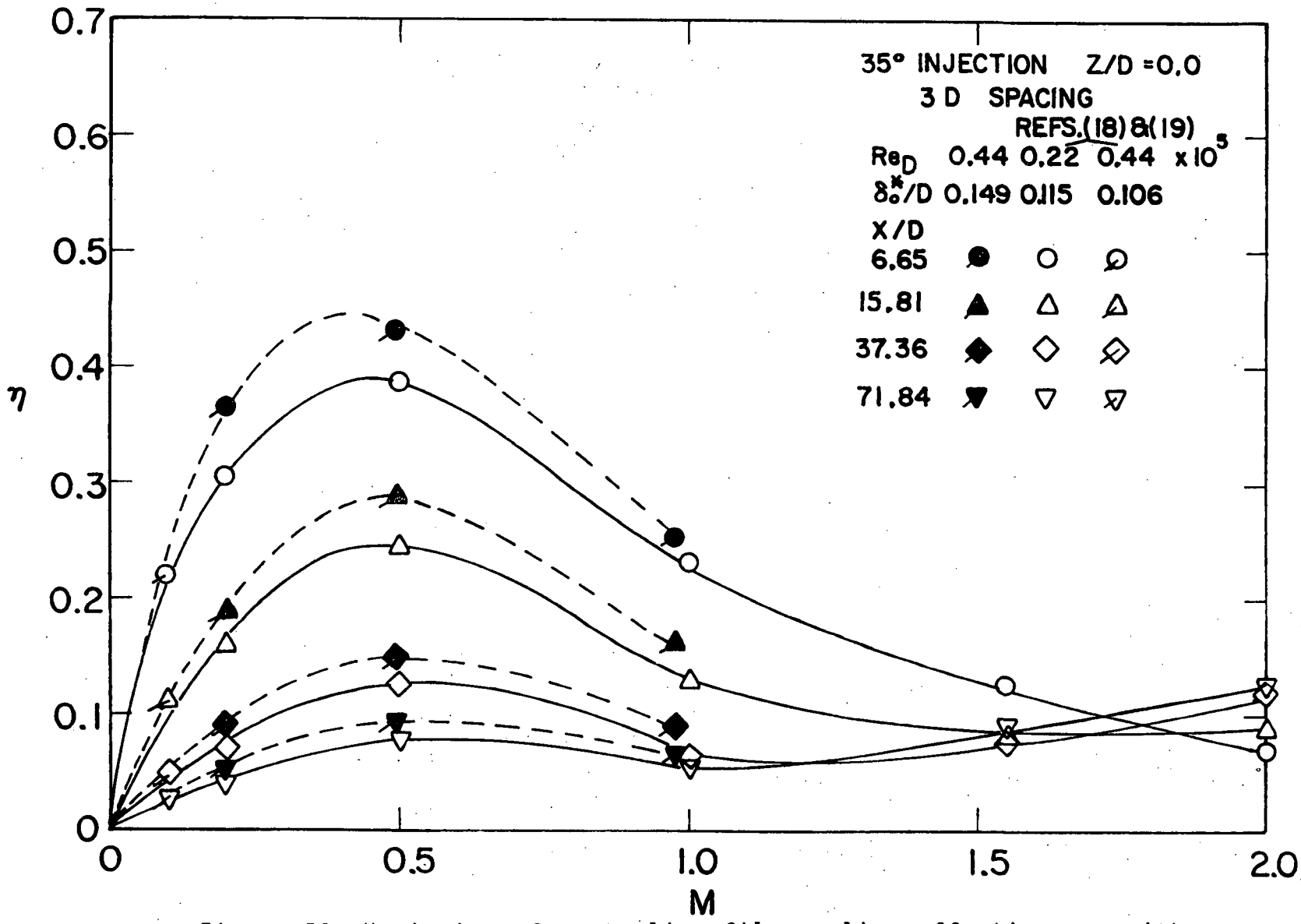

Figure 53 Variation of centerline film cooling effectiveness with blowing rate for 35° injection through a row of holes

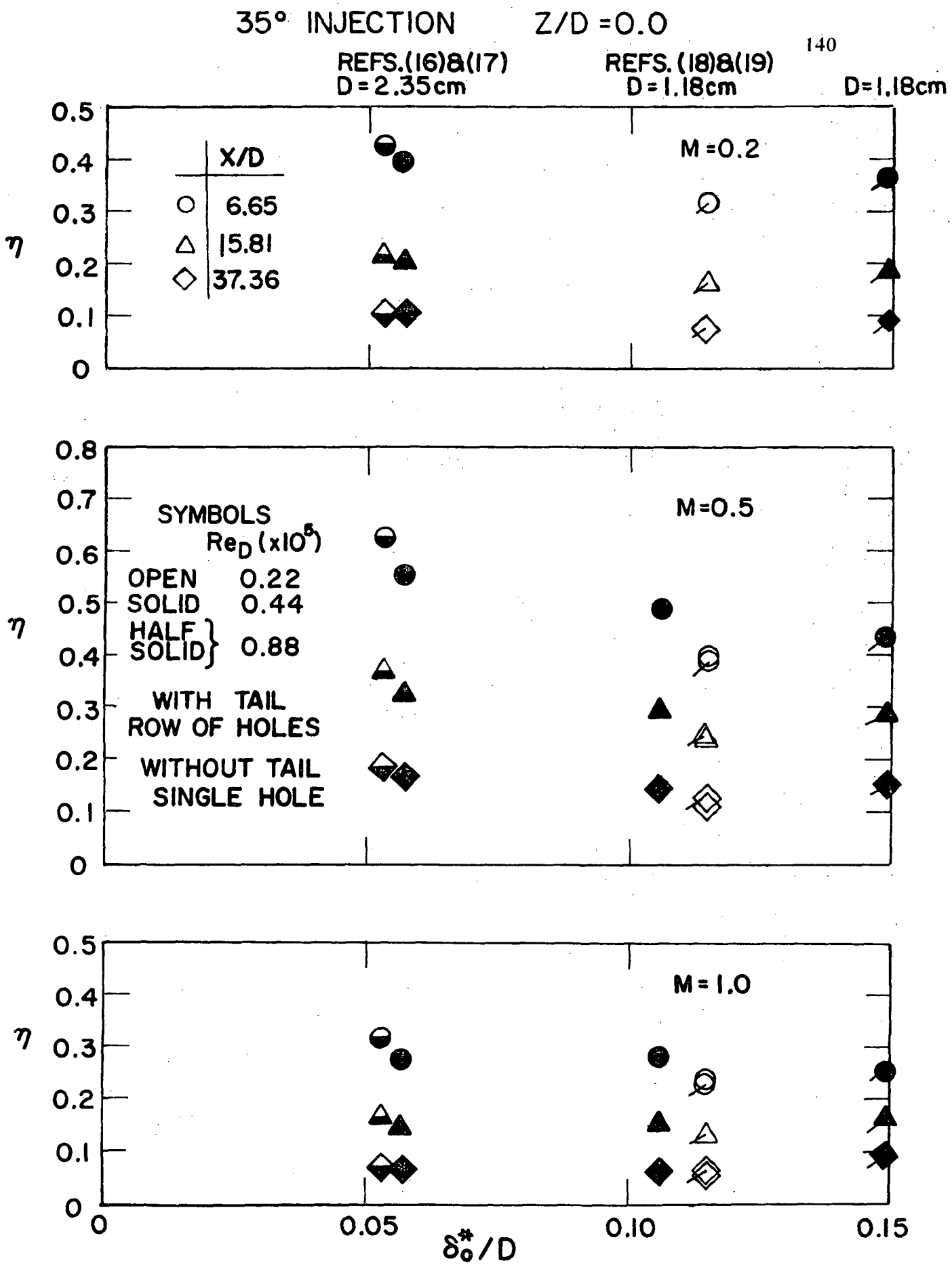

Figure 54 Variation of centerline film cooling effectiveness with displacement boundary layer thickness for 35° injection

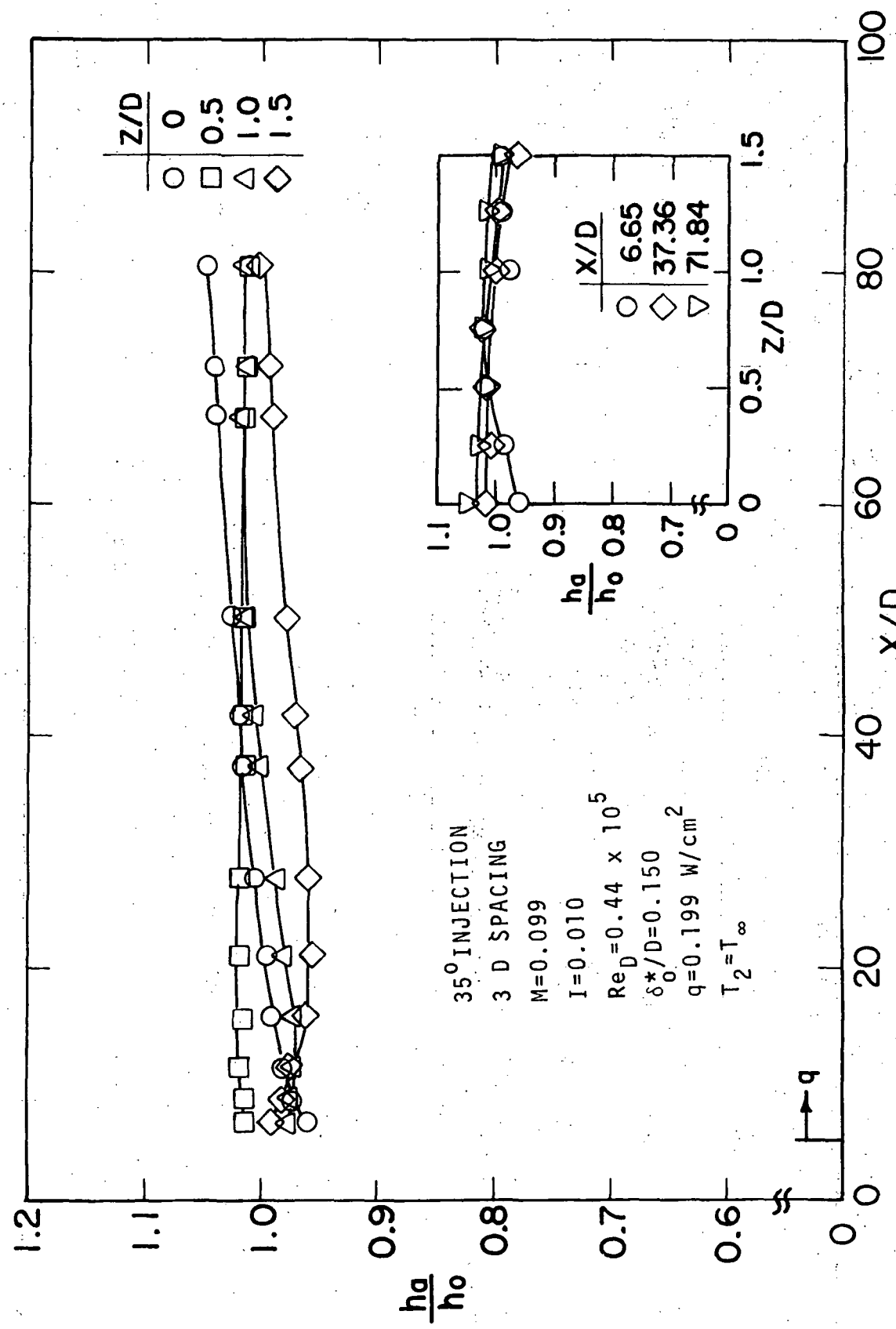

Figure 55 Heat transfer coefficient for unheated 35° injection through a row of holes, M=0.1, Re_D=0.44 x 10^5

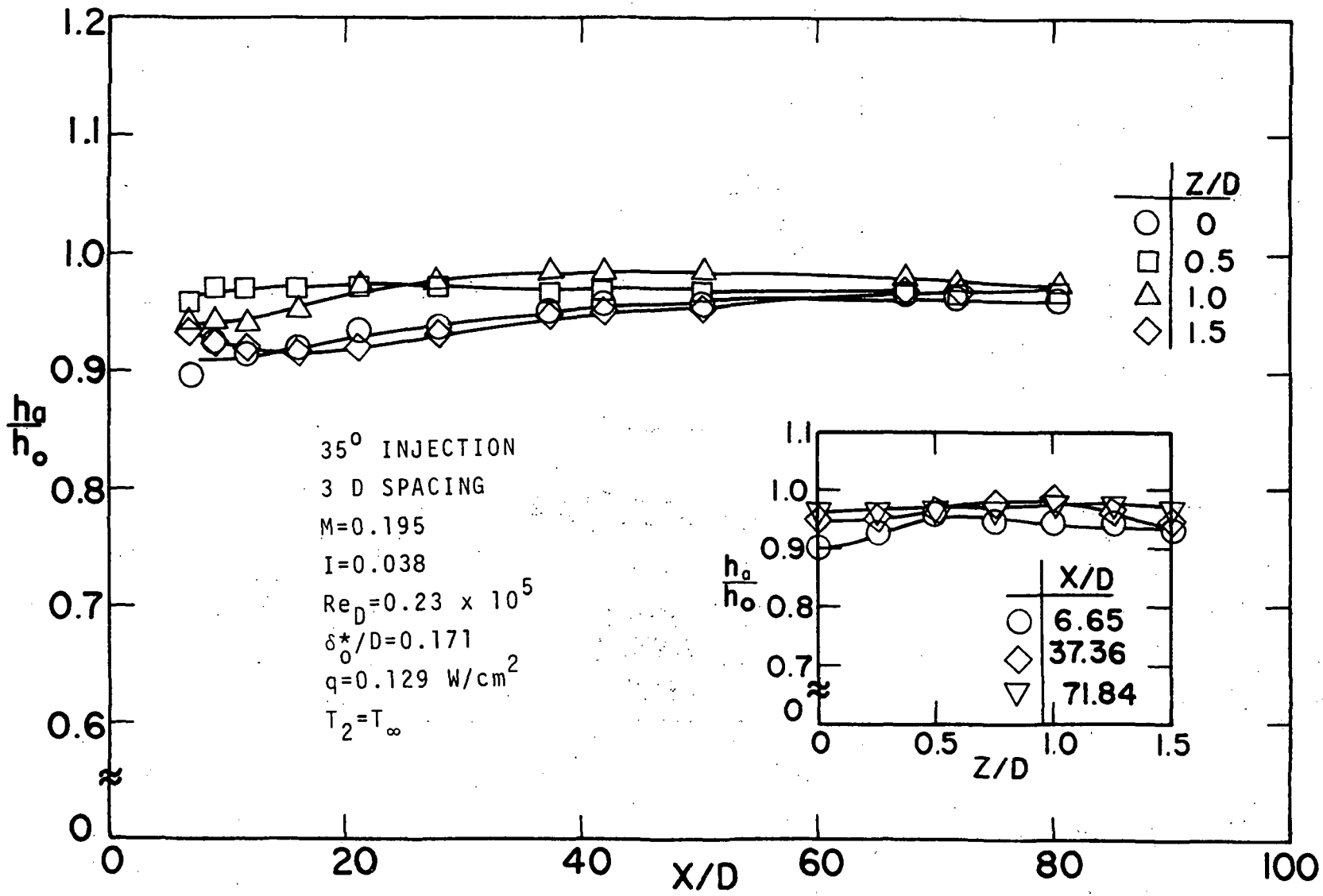

Figure 56 Heat transfer coefficient for unheated 35° injection through a row of holes, M=0.2, Re_D=0.44 x 10^5

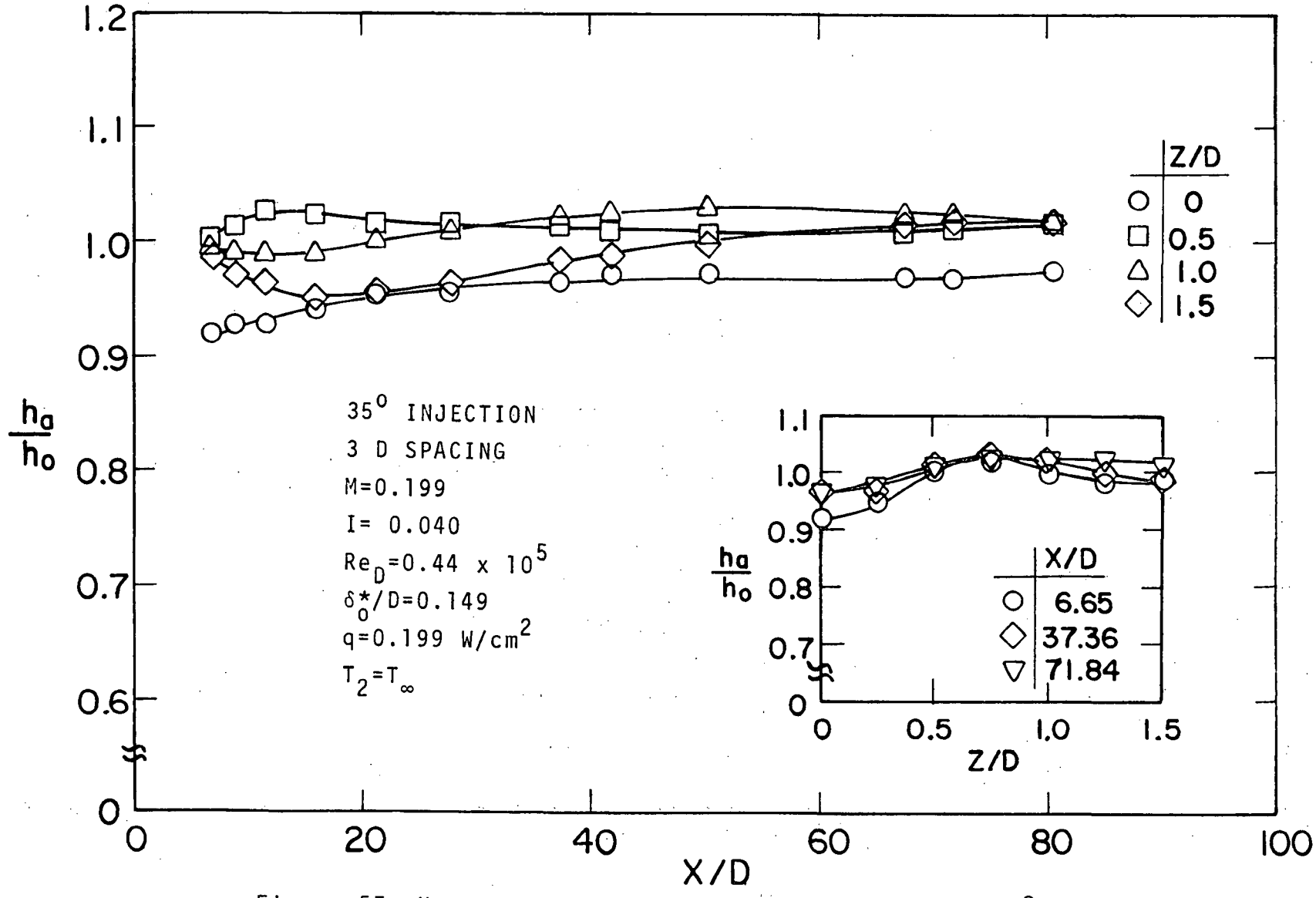

Figure 57 Heat transfer coefficient for unheated 35° injection through a row of holes, M=0.2, Re_D=0.44 x 10^5

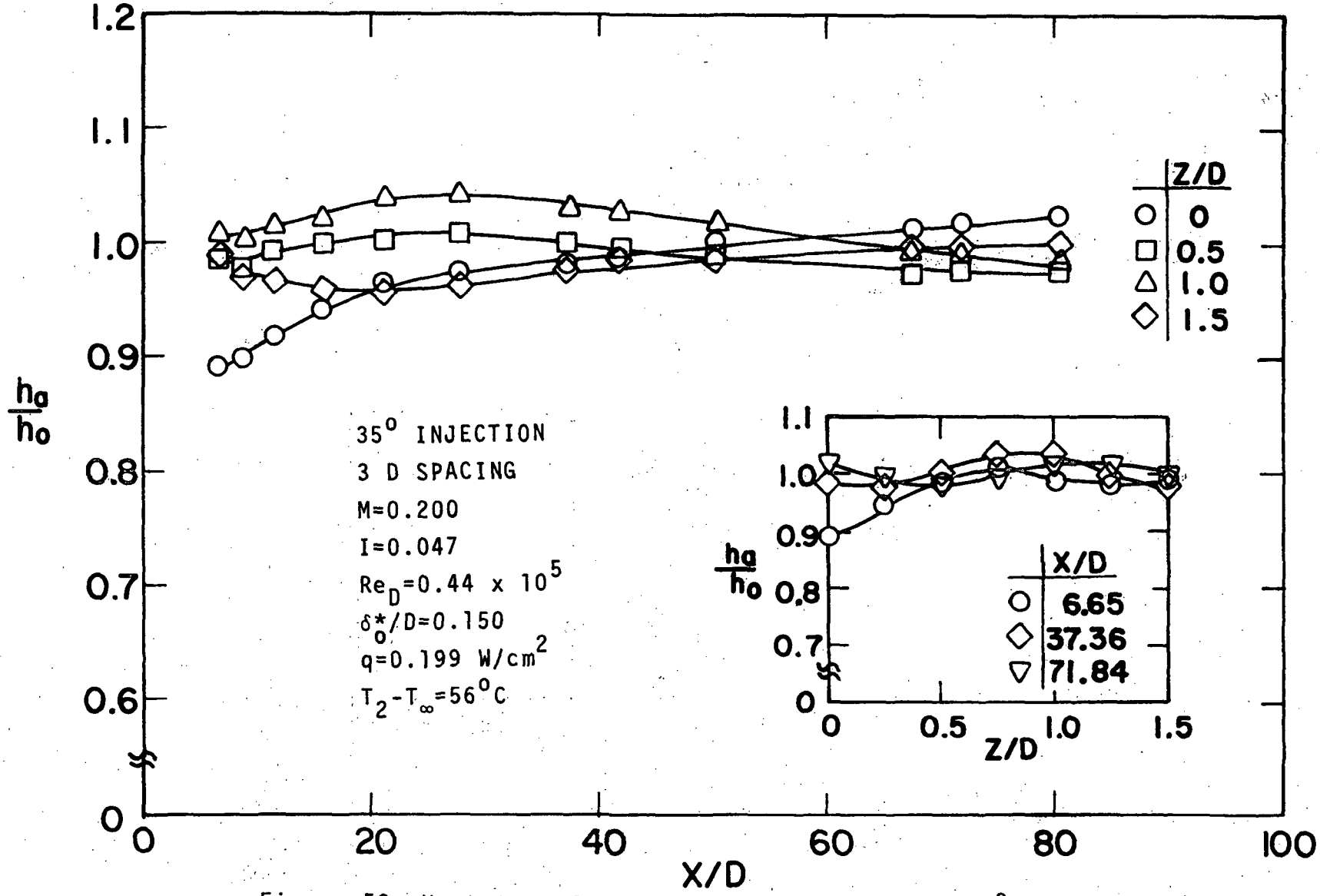

Figure 58 Heat transfer coefficient for heated 35° injection through a row of holes, M=0.2, Re_D=0.44 x 10^5

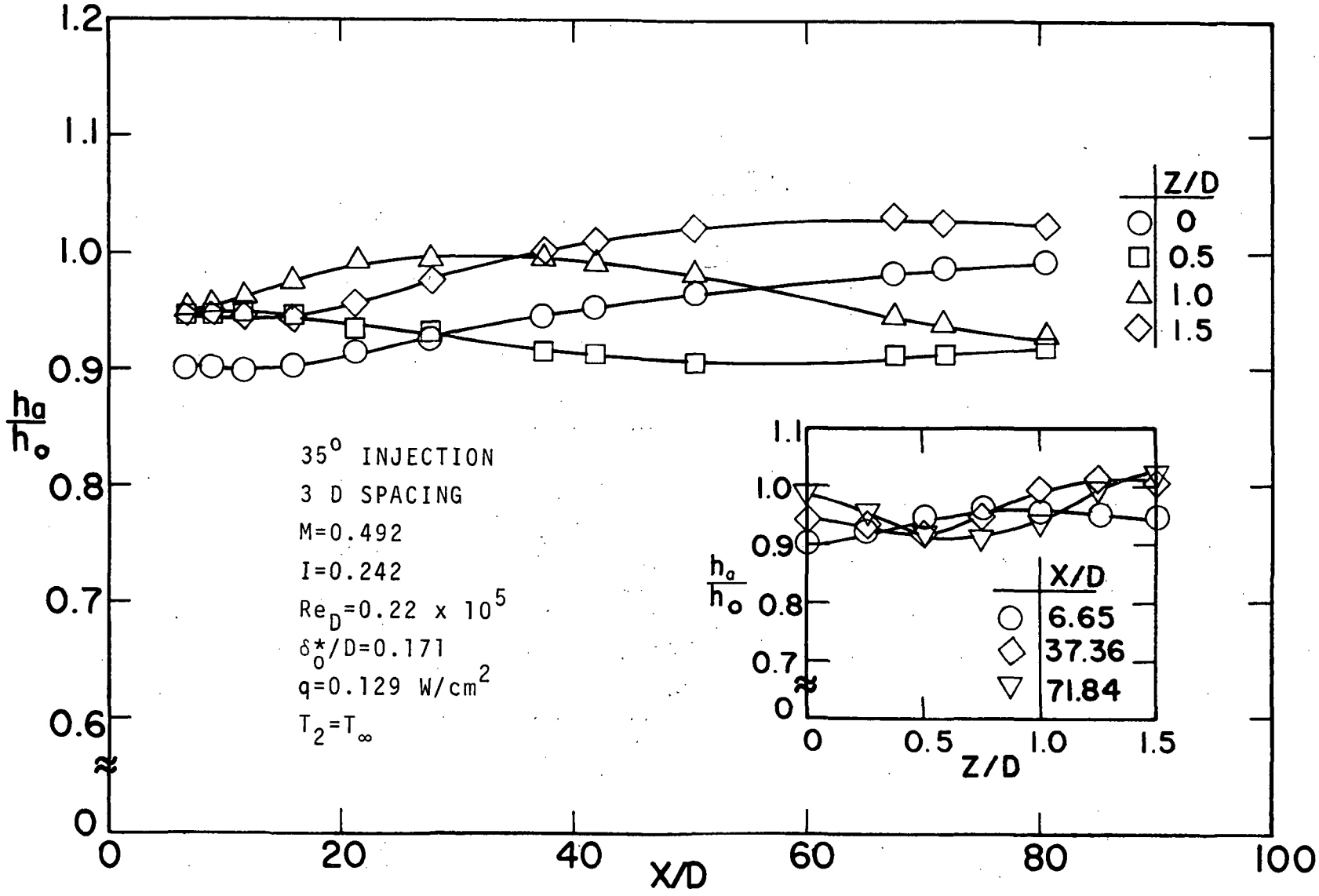

Figure 59 Heat transfer coefficient for unheated 35° injection through a row of holes, M=0.5, Re_D=0.22 x 10^5

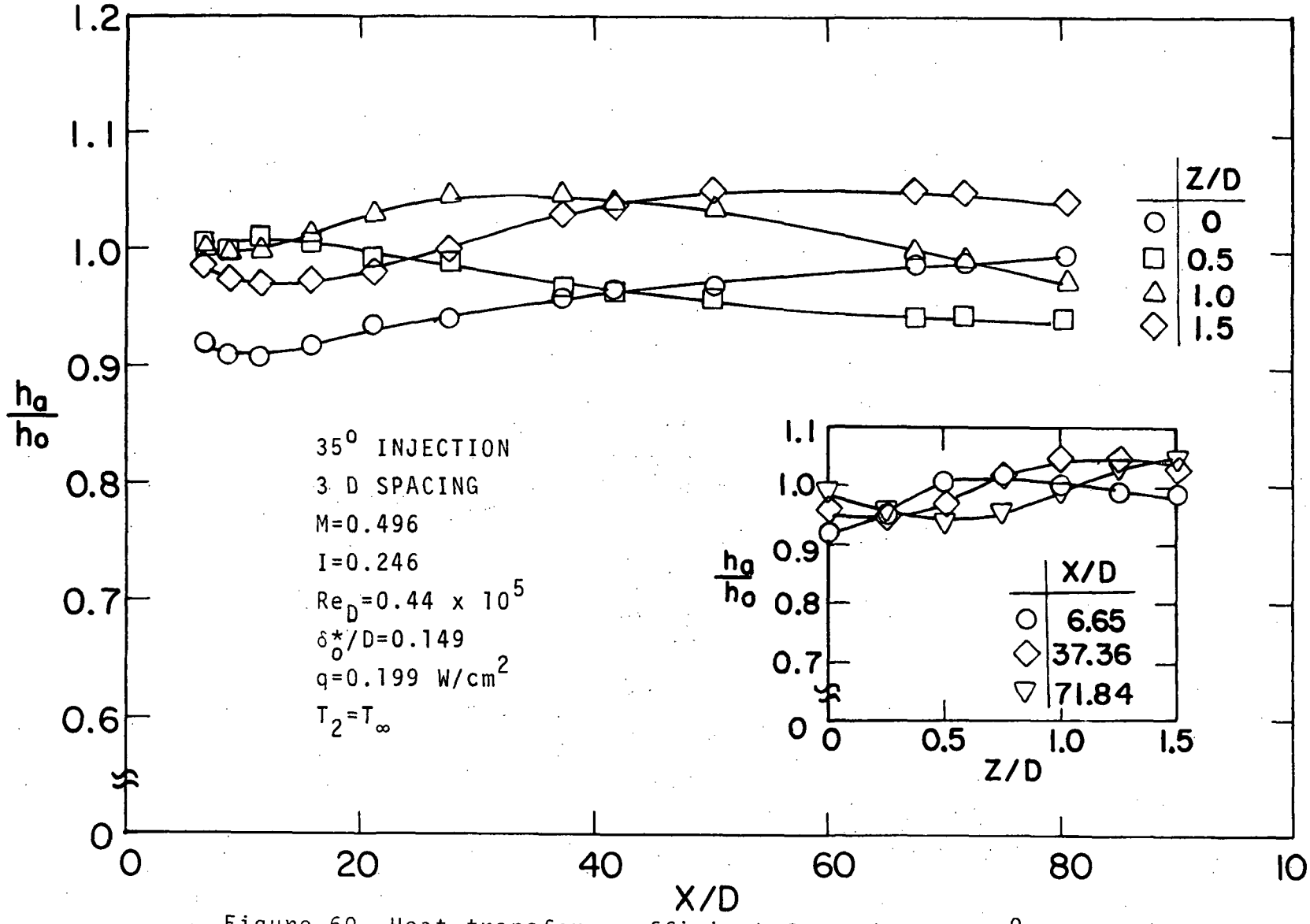

Figure 60 Heat transfer coefficient for unheated 35° injection through a row of holes, M=0.5, Re_D=0.44 x 10^5

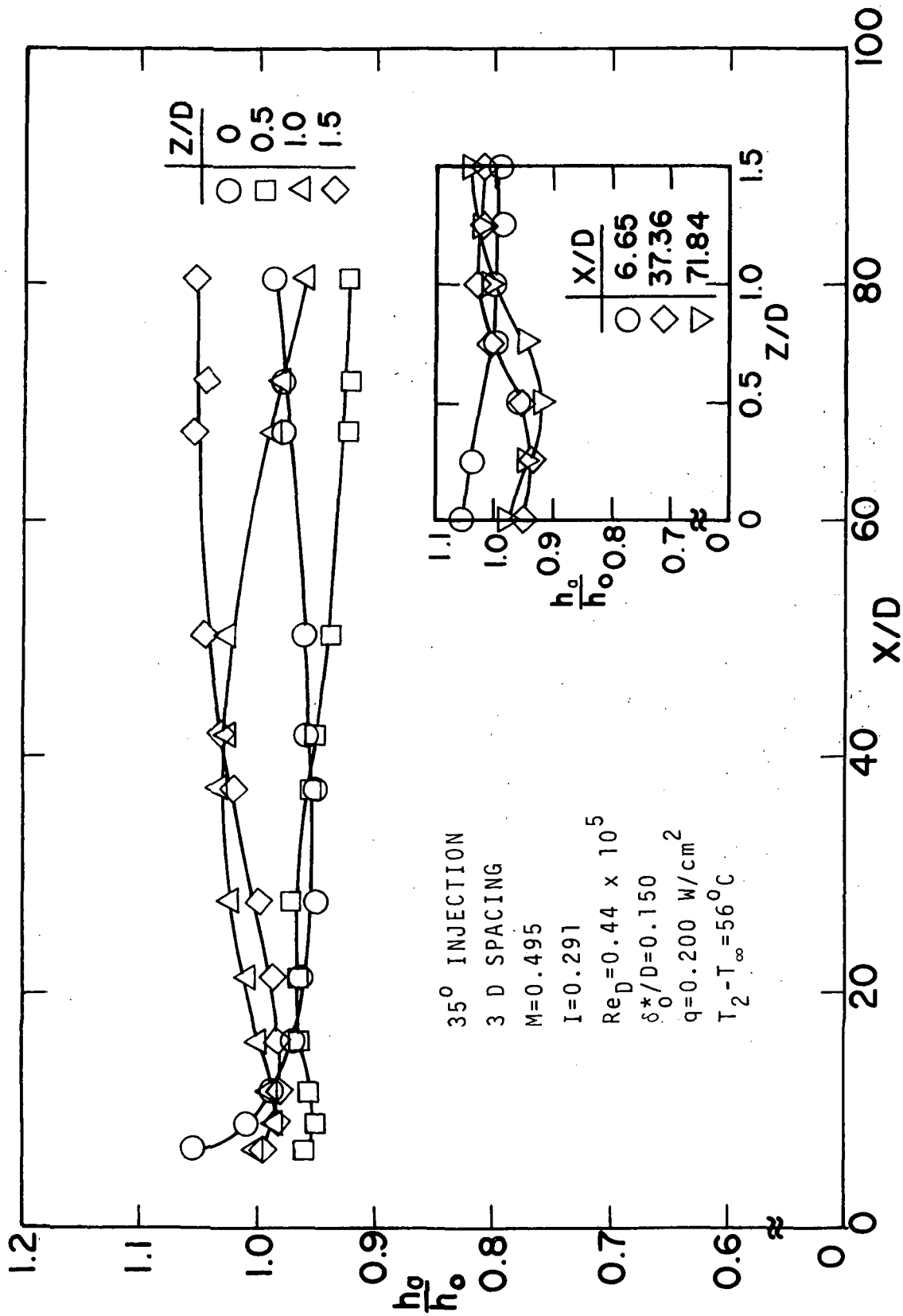

Figure 61 Heat transfer coefficient for heated 35° injection through a row of holes, M=0.5, Re_D=0.44 x 10^5

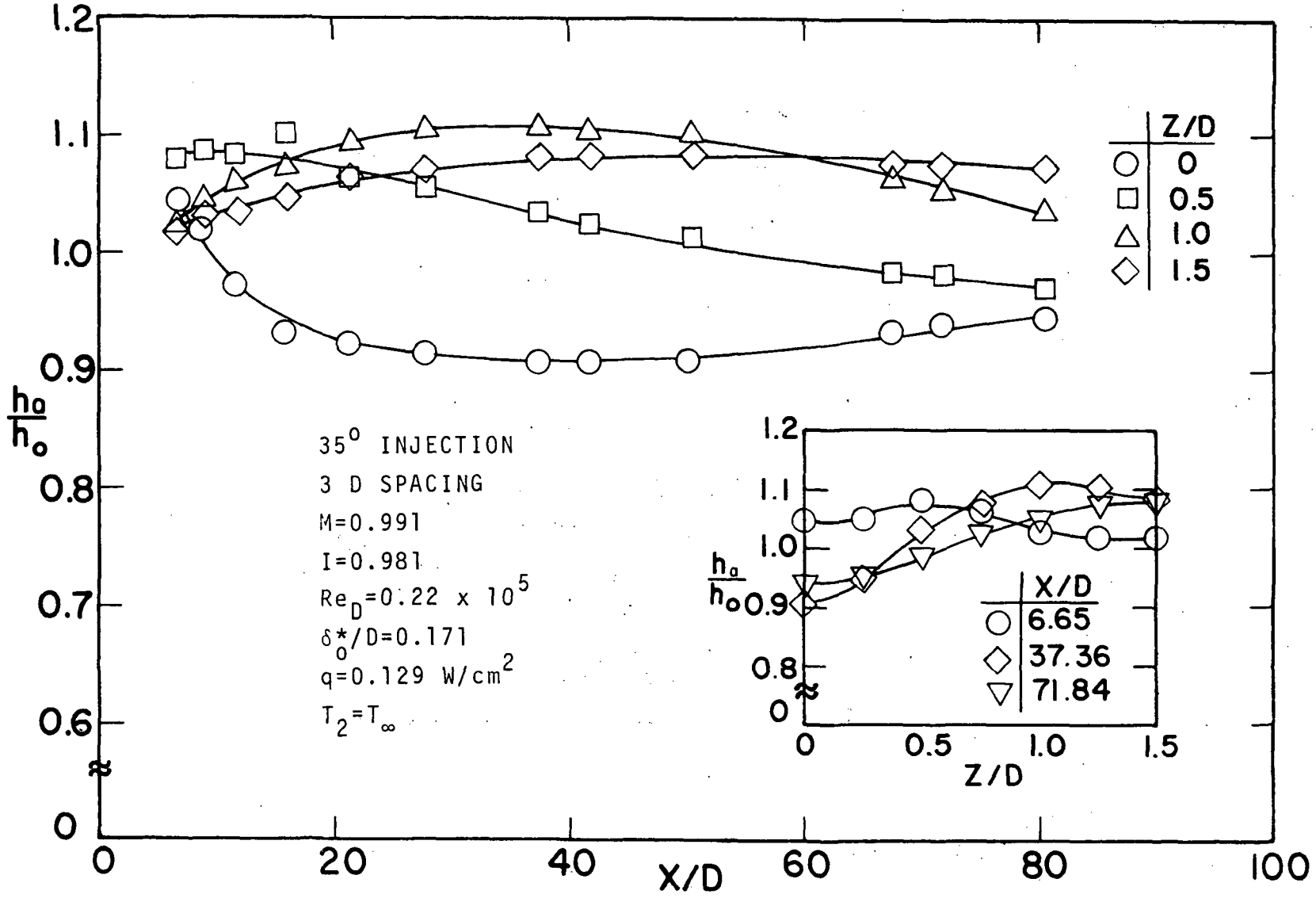

Figure 62 Heat transfer coefficient for unheated 35° injection through a row of holes, M=1.0, Re_D=0.22 x 10^5

SMT

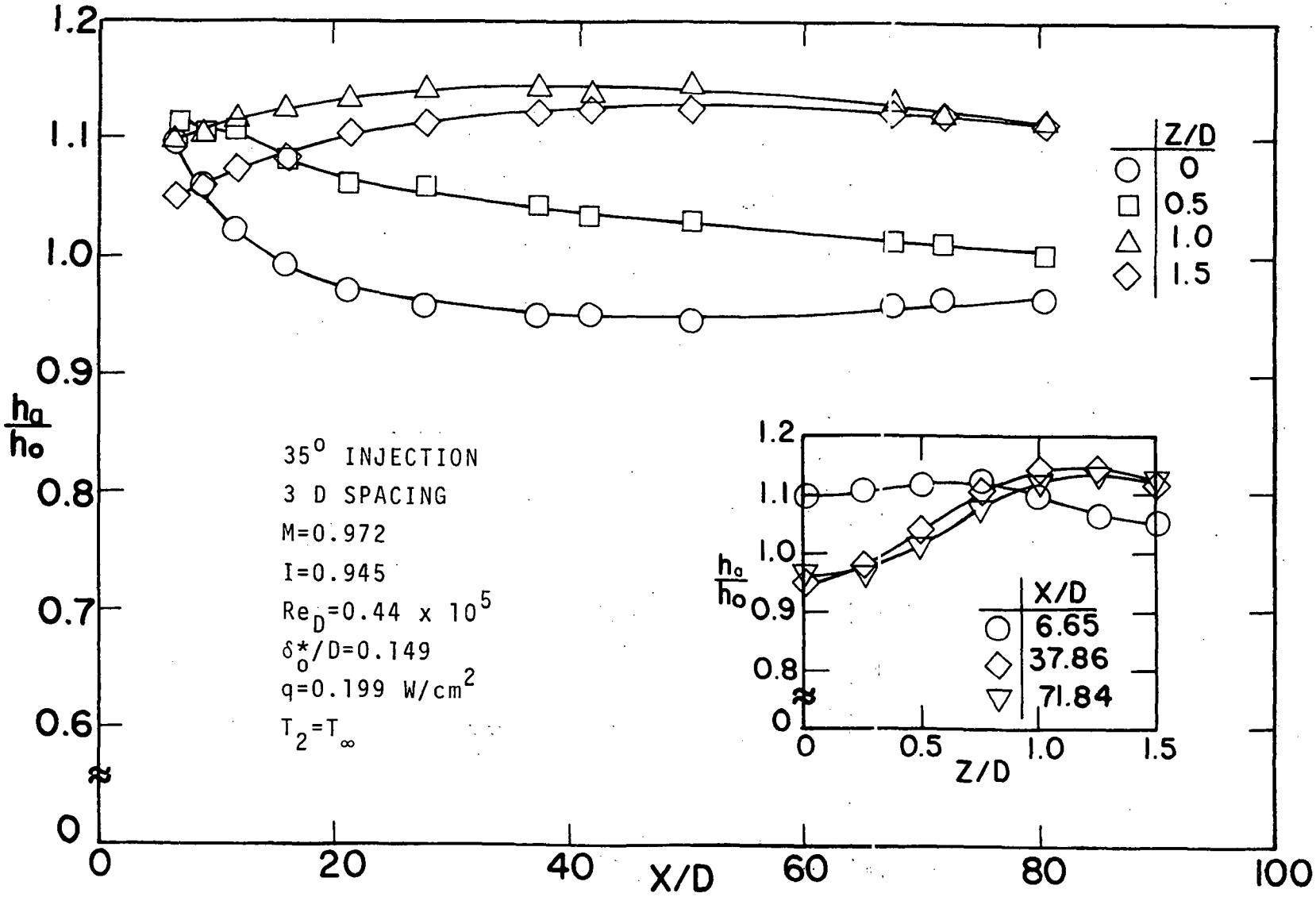

Figure 63 Heat transfer coefficient for unheated 35° injection through a row of holes, M=1.0, Re_D=0.44 x 10^5

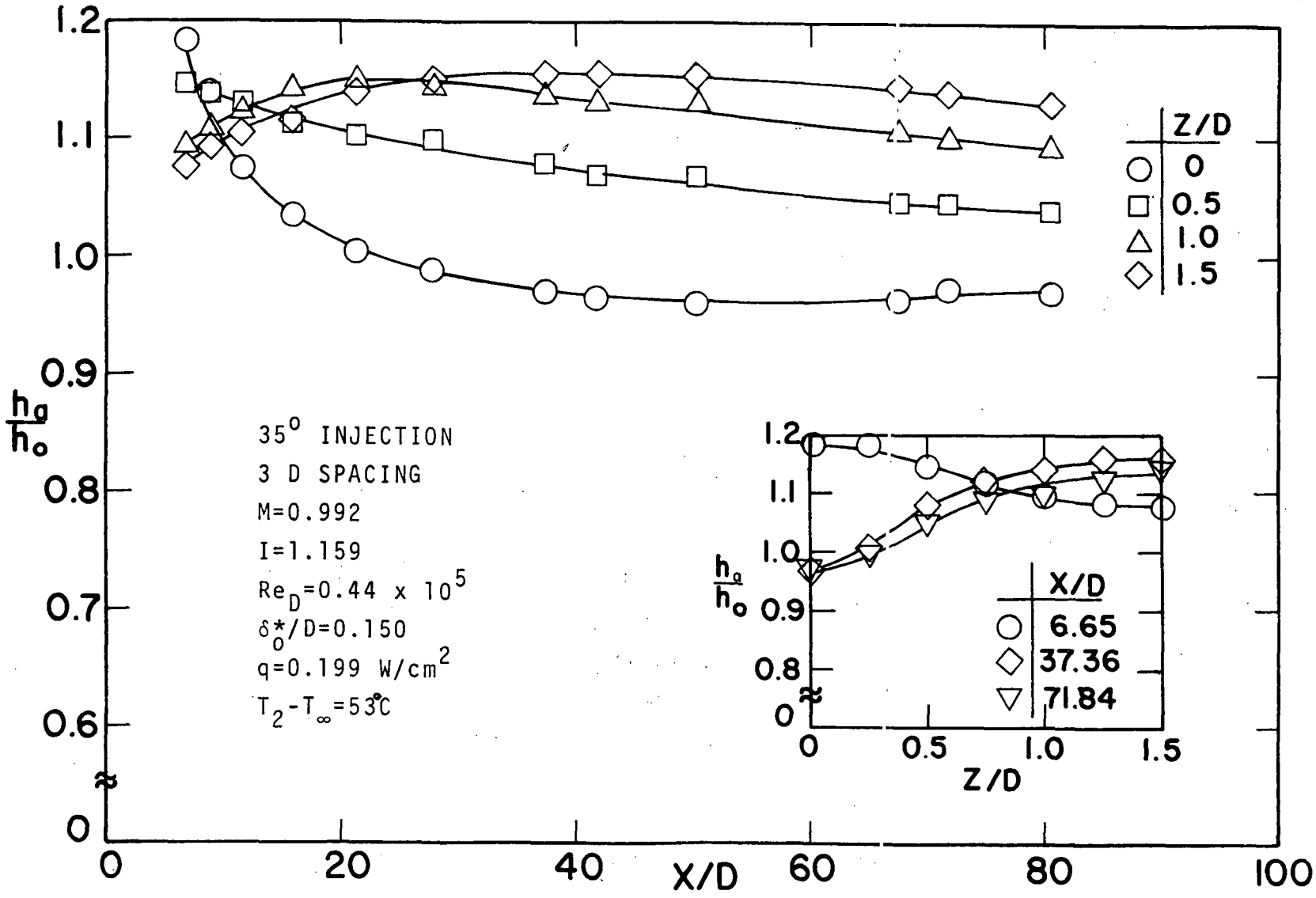

Figure 64 Heat transfer coefficient for heated 35° injection through a row of holes, M=1.0, Re_D=0.44 x 10^5

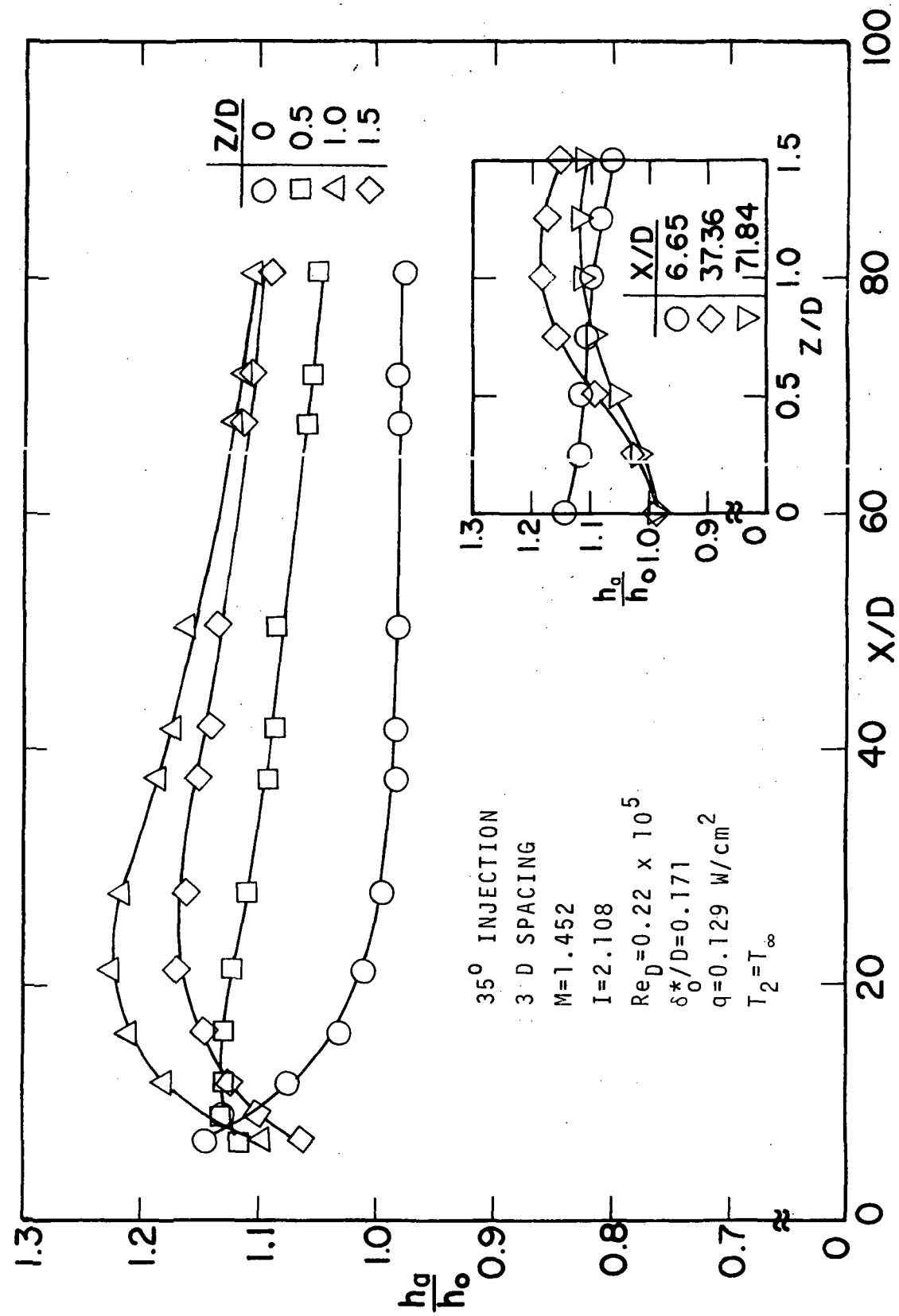

Figure 65 Heat transfer coefficient for unheated 35^0 injection through a row of holes, M=1.45, $Re_D=0.22 \times 10^5$

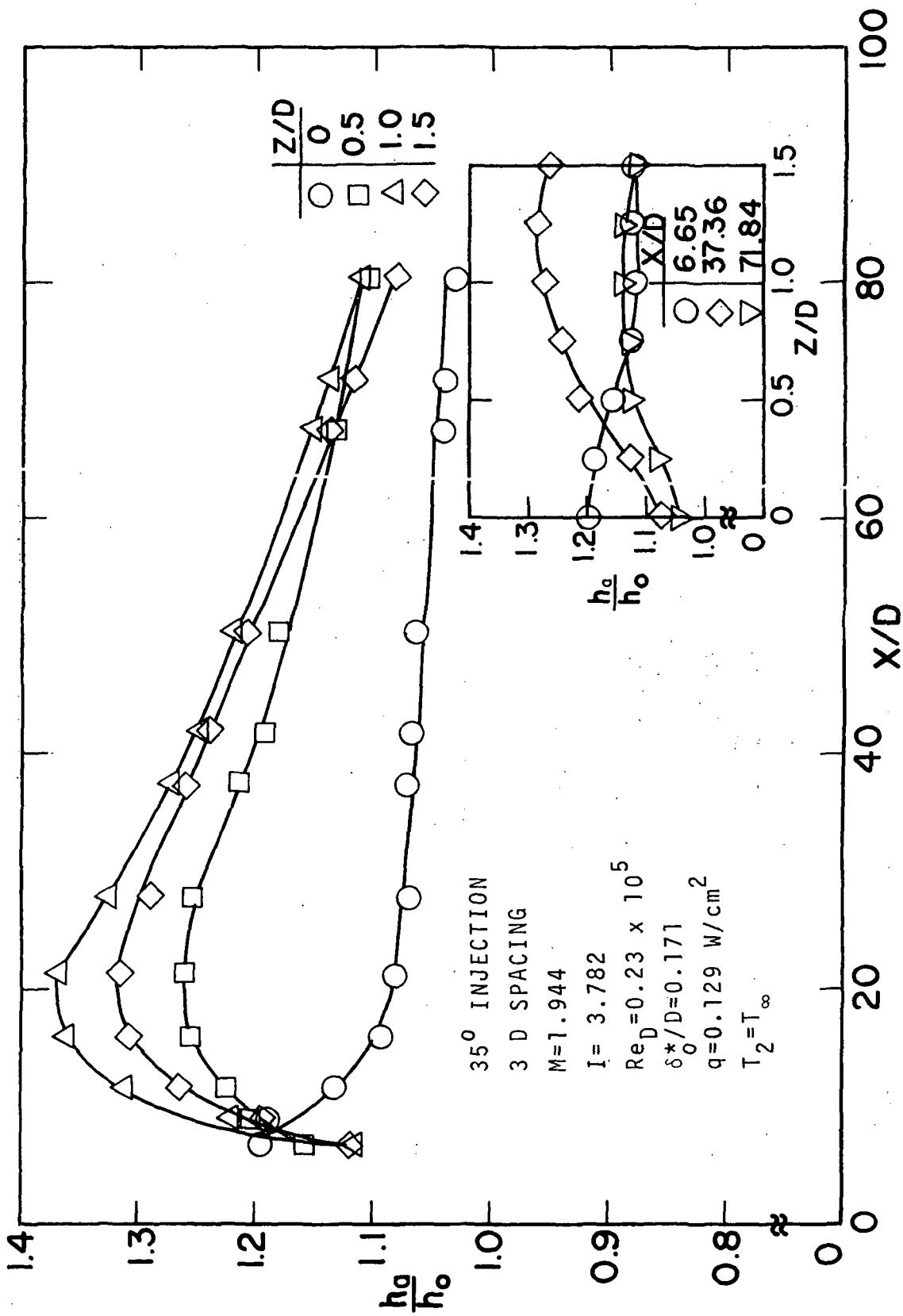

Figure 66 Heat transfer coefficient for unheated 35^0 injection through a row of holes, M=1.94, $Re_D=0.23 \times 10^5$

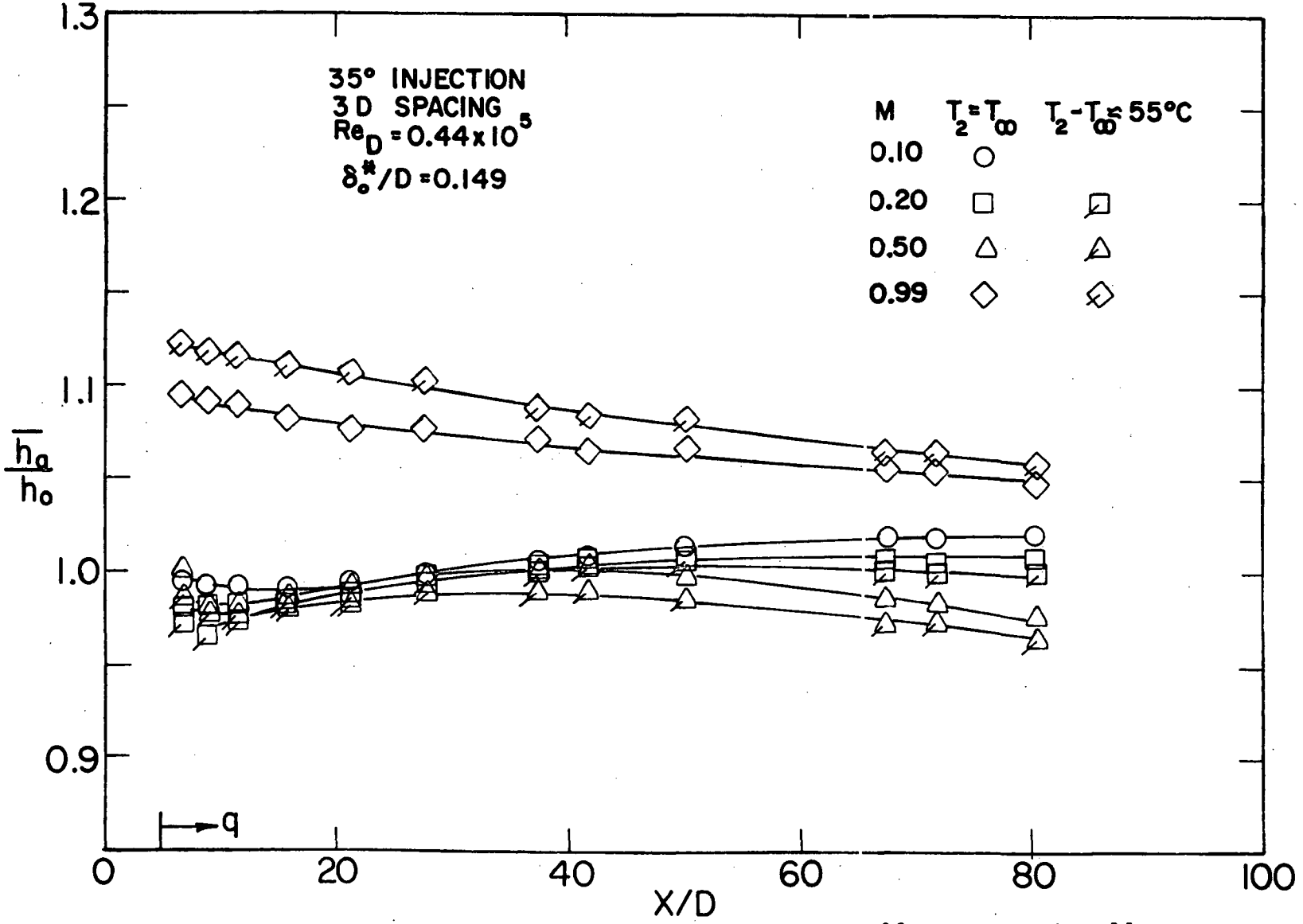

Figure 67 Heat transfer coefficient based on laterally averaged wall temperatures for 35° injection through a row of holes, $Re_D = 0.44 \times 10^5$

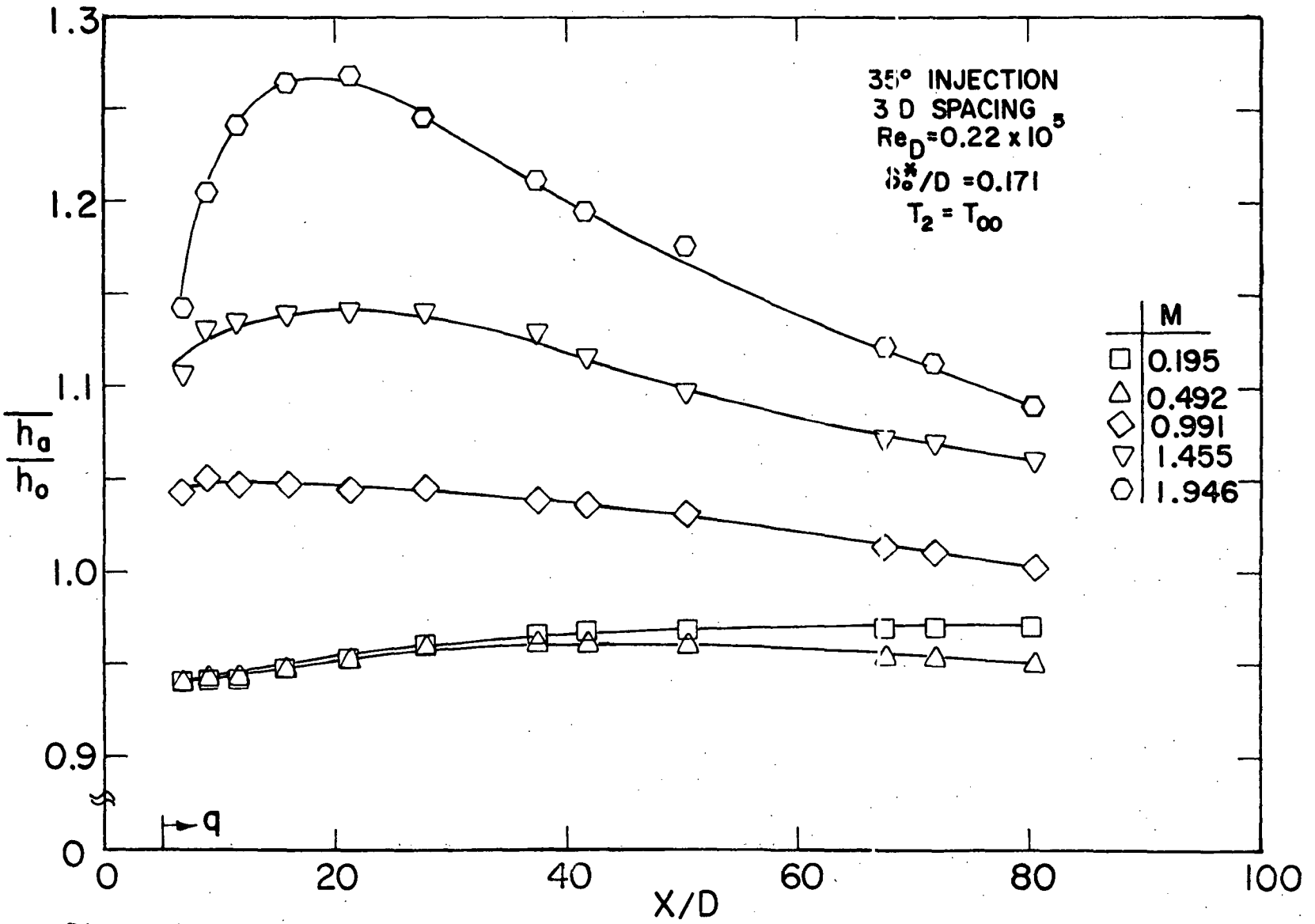

Figure 68 Heat transfer coefficient based on laterally averaged wall temperatures for 35° injection through a row of holes, $Re_D=0.22 \times 10^5$

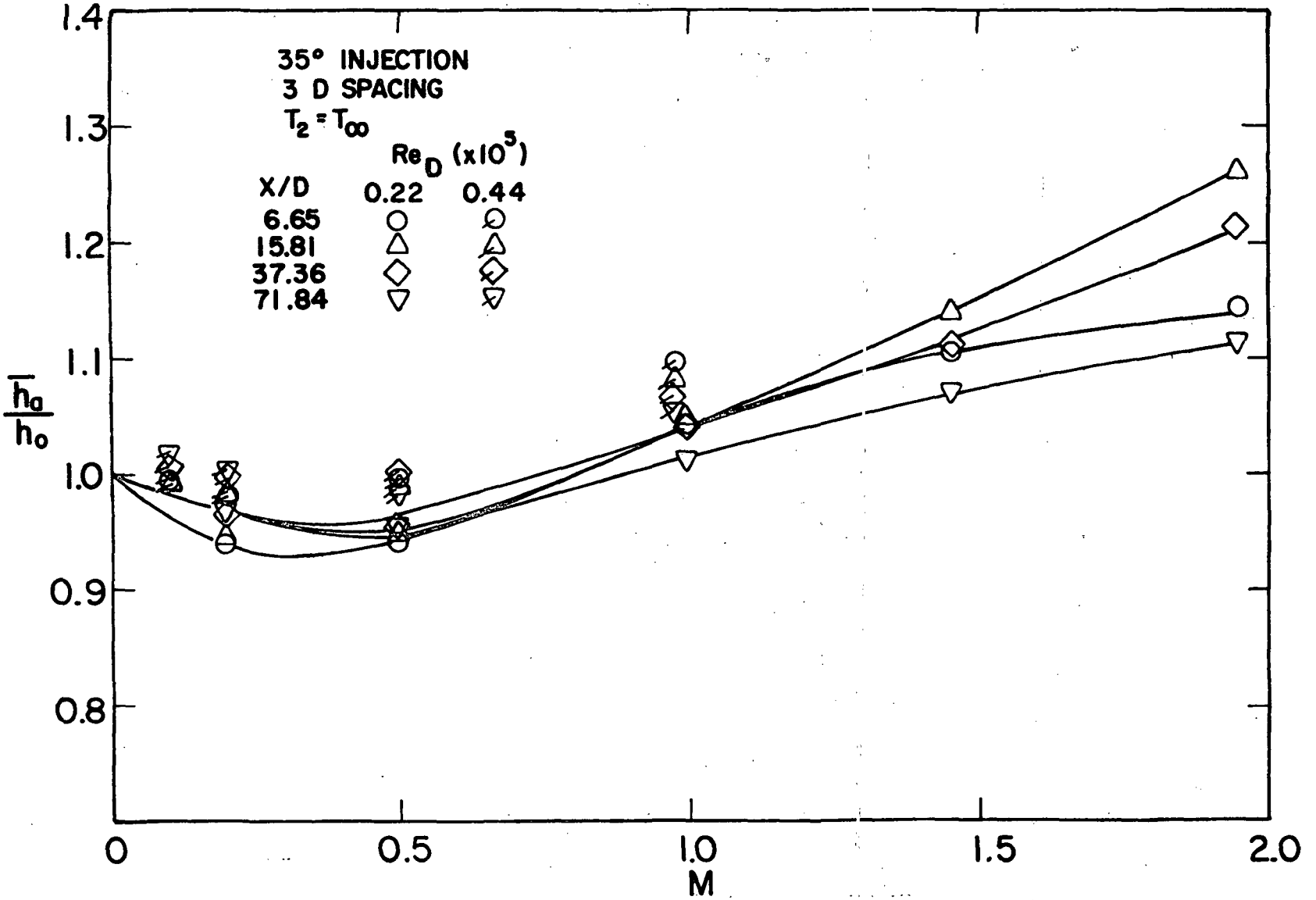

Figure 69 Variation of heat transfer coefficient based on laterally averaged wall temperatures with blowing rate for 35^0 injection through a row of holes

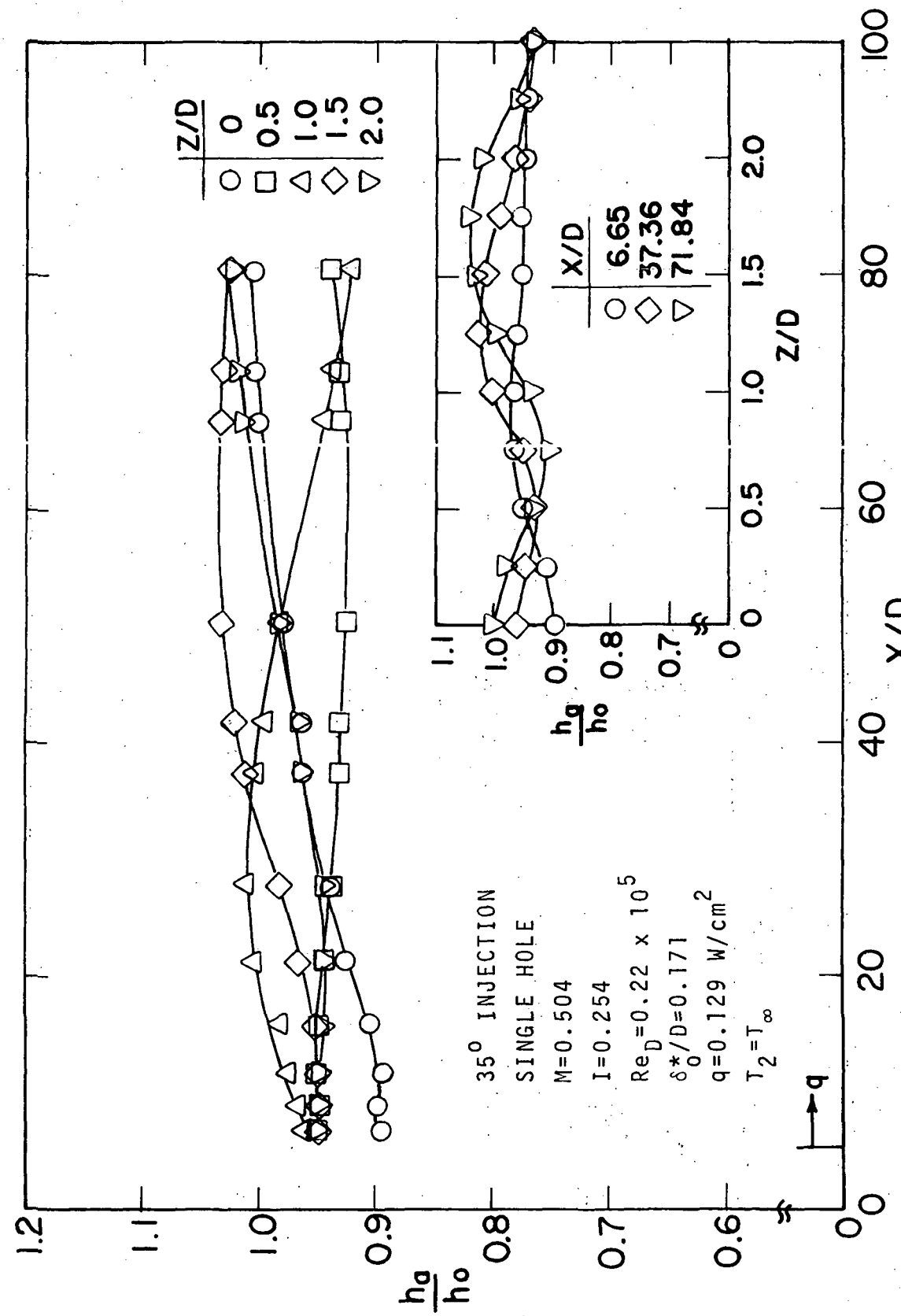

Figure 70 Heat transfer coefficient for unheated 35° injection through a single hole, =0.5, Re_D=0.22 x 10^5

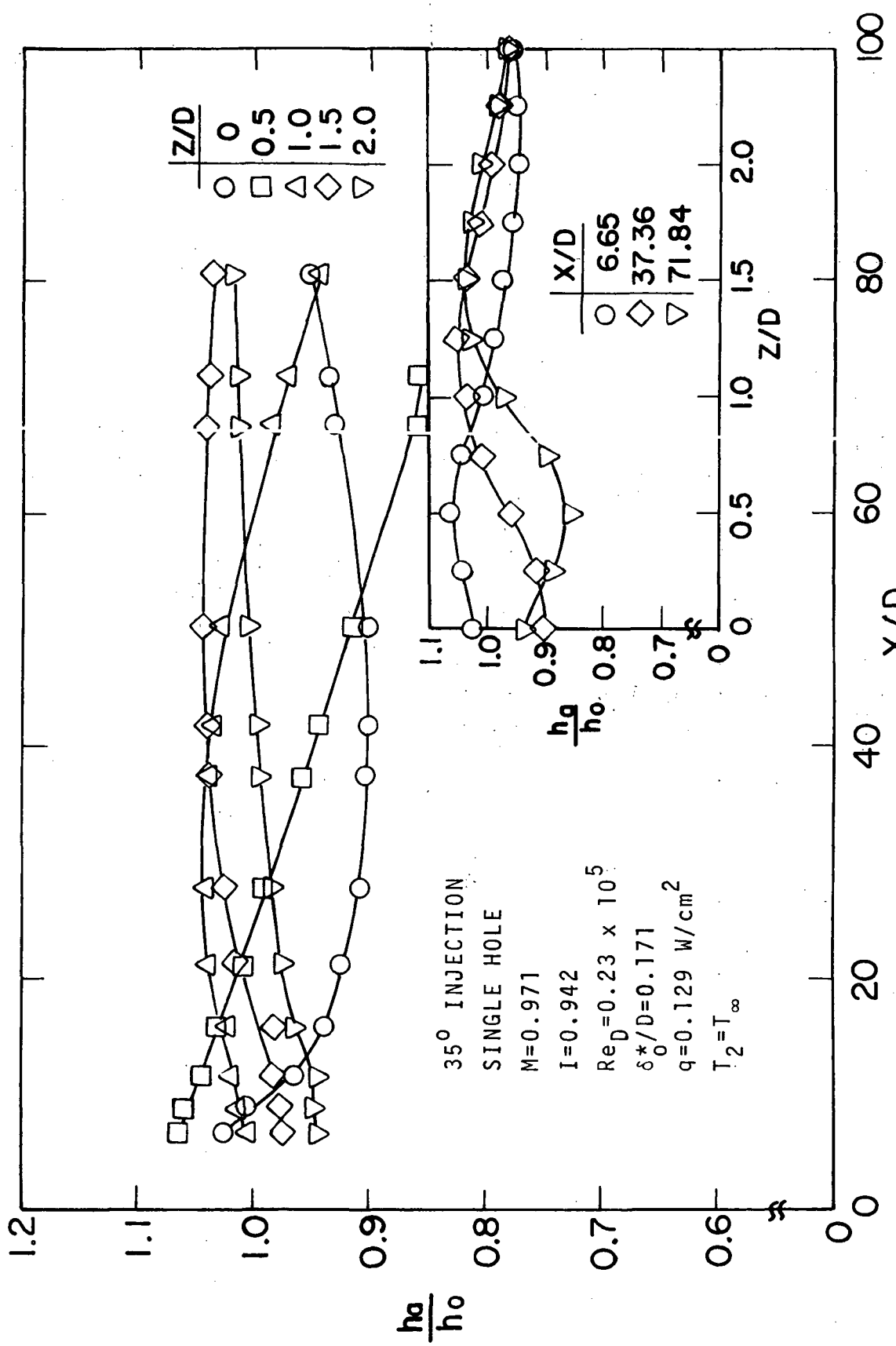

Figure 71 Heat transfer coefficient for unheated 35° injection through a single hole, M=0.97, Re_D=0.23 x 10^5

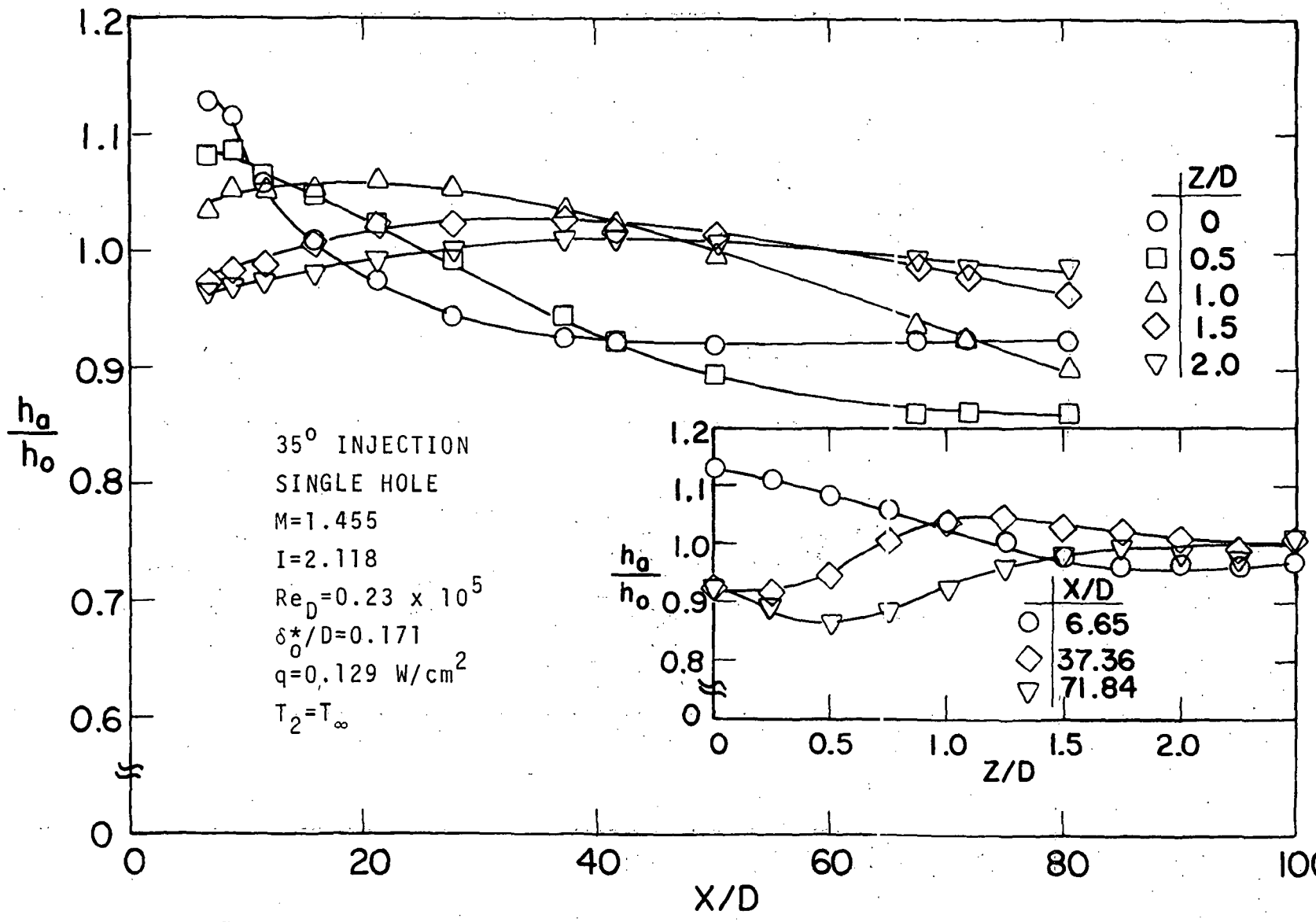

Figure 72 Heat transfer coefficient for unheated 35° injection through a single hole, M=1.46, Re_D=0.23 x 10^5

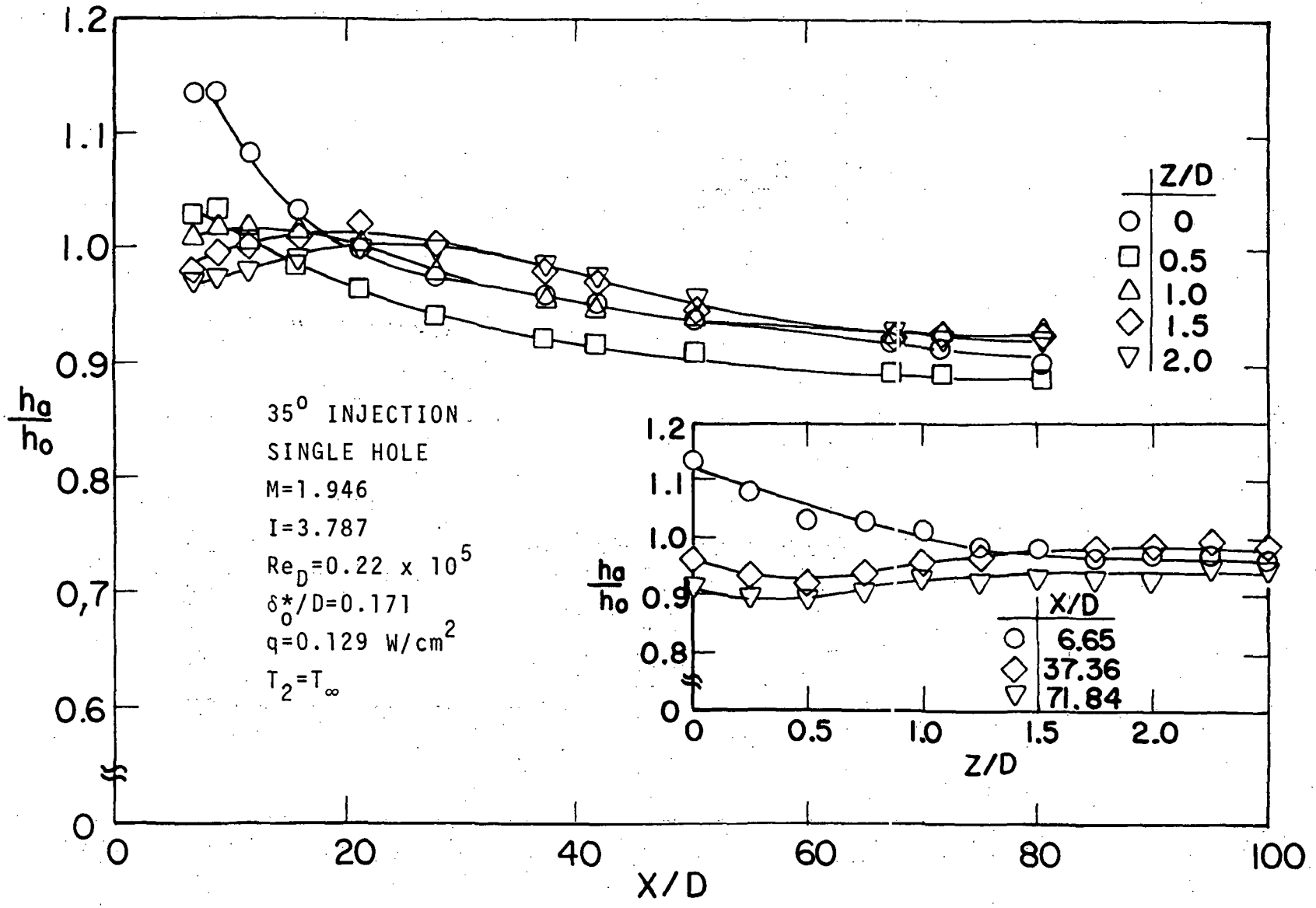

Figure 73 Heat transfer coefficient for unheated 35° injection through a single hole, M=1.95, Re_D=0.22 x 10^5

TABLE II

HEAT TRANSFER COEFFICIENT BASED ON LATERALLY AVERAGED WALL TEMPERATURES, $\bar{h}_a/h_o$

35^o INJECTION -- 3 D SPACING

$Re_D = 0.44 \times 10^5$ $\quad \delta_o^*/D = 0.149$

M	0.099	0.200	0.199	0.495	0.496	0.992	0.972
I	0.010	0.047	0.040	0.291	0.246	1.159	0.945
T_2-T_∞ (^oC)	0	56	0	56	0	53	0
X/D							
6.65	0.993	0.973	0.981	1.001	0.987	1.123	1.095
8.80	0.991	0.965	0.980	0.982	0.978	1.118	1.092
11.50	0.992	0.972	0.983	0.978	0.982	1.117	1.091
15.81	0.991	0.982	0.984	0.981	0.986	1.111	1.082
21.20	0.995	0.991	0.989	0.982	0.993	1.107	1.076
27.66	0.999	0.999	0.993	0.989	1.000	1.103	1.077
37.36	1.006	1.002	1.001	0.989	1.003	1.090	1.072
41.67	1.009	1.004	1.003	0.989	1.001	1.084	1.066
50.29	1.013	1.006	1.005	0.986	0.998	1.083	1.069
67.53	1.020	1.001	1.008	0.973	0.986	1.066	1.057
71.84	1.019	1.000	1.007	0.974	0.983	1.065	1.055
80.46	1.021	1.000	1.008	0.964	0.977	1.058	1.049

TABLE II Continued

HEAT TRANSFER COEFFICIENT BASED ON LATERALLY AVERAGED WALL TEMPERATURES, $\bar{h}_a/h_o$

35^o INJECTION -- 3 D SPACING

$Re_D = 0.44 \times 10^5$ $\quad \delta_o^*/D = 0.171$

M	0.195	0.492	0.991	1.452	1.944
I	0.038	0.242	0.981	2.108	3.782
$T_2 - T_\infty (^oC)$	0	0	0	0	0
X/D					
6.65	0.940	0.941	1.043	1.107	1.143
8.80	0.945	0.941	1.051	1.131	1.206
11.50	0.942	0.943	1.047	1.135	1.242
15.81	0.948	0.948	1.048	1.140	1.264
21.20	0.956	0.954	1.046	1.141	1.268
27.66	0.961	0.959	1.046	1.130	1.247
37.36	0.967	0.961	1.039	1.112	1.213
41.67	0.968	0.961	1.036	1.104	1.195
50.29	0.969	0.960	1.032	1.098	1.176
67.53	0.970	0.954	1.014	1.074	1.122
71.84	0.970	0.953	1.011	1.071	1.113
80.46	0.971	0.950	1.003	1.059	1.090

NAS3-13200
SUMMARY REPORT
DISTRIBUTION LIST

ADDRESSEE	Mail Stop	NUMBER OF COPIES
1. NASA Lewis Research Center 21000 Brookpark Road Cleveland, Ohio 44135		
Attention: Aeronautics Procurement Section	77-3	1
Reports Control Office	5-5	1
Technology Utilization Office	3-19	1
Library	60-3	2
Fluid System Components Div.	5-3	1
B. Lubarsky	3-3	1
J. Howard Childs	60-4	1
J. B. Esgar	60-4	1
F. S. Stepka	60-6	10
R. S. Colladay	60-6	1
H. Ellerbrock	60-4	6
J. Livingood	60-6	1
2. NASA Scientific & Technical Information Facility P.O. Box 33 College Park, Maryland 20740 Attention: NASA Representative RQT-2448		6
3. Dr. W. Kays Stanford University Stanford, California 94305		1
4. NASA Headquarters Washington, D.C. 20546 Attention: N. F. Rekos (RLC)		1
5. Department of the Army U.S. Army Aviation Material Laboratory Fort Eustis, Va. 23604 Attention: John White		1
6. Headquarters Wright-Patterson AFB, Ohio 45433 Attention: Jack Richens (AFAPL/APTC)		2
7. Air Force Office of Scientific Research Propulsion Research Division USAF Washington, D.C. 20025		1

8. Defense Documentation Center (DDC)
Cameron Station
5010 Duke Street
Alexandria, Virginia 22314 — 1

9. NASA-Langley Research Center
Langley Station
Technical Library
Hampton, Virginia 23365
Attention: Mark R. Nichols — 1
John V. Becker — 1

10. United Aircraft Corporation
Pratt & Whitney Aircraft Division
Florida Research & Development Center
P.O. Box 2691
West Palm Beach, Florida 33402
Attention: R. A. Schmidtke — 1

11. United Aircraft Corporation
Pratt & Whitney Aircraft Division
400 Main Street
East Hartford, Connecticut 06108
Attention: C. Andreini — 2
Library — 1
M. Suo — 1

12. United Aircraft Research
East Hartford, Connecticut
Attention: Library — 1

13. Allison Division of GMC
Department 8894, Plant 8
P.O. Box 894
Indianapolis, Indiana 46206
Attention: J. N. Barney — 1
C. E. Holbrook — 1
Library — 1

14. Northern Research & Engineering Corporation
219 Vassar Street
Cambridge, Massachusetts
Attention: K. Ginwala — 1

15. General Electric Company
Flight Propulsion Division
Cincinnati, Ohio 45125
Attention: J. W. McBride — N-44 — 1
F. Burggraf — H-32 — 1
S. N. Suciu — H-32 — 1
Technical Information Center — N-32 — 1

16. General Electric Company
1000 Western Avenue
West Lynn, Massachusetts 01905
Attention: Dr. C. W. Smith--Library Bldg. 2-40M 1

17. Curtiss-Wright Corporation
Wright Aeronautical Division
Wood-Ridge, New Jersey 07075
Attention: S. Lombardo 1

18. Air Research Manufacturing Company
402 South 36th Street
Phoenix, Arizona 85034
Attention: Robert O. Bullock 1

19. Air Research Manufacturing Company
9851 Sepulveda Boulevard
Los Angeles, California 90009
Attention: Fred Faulkner 1

20. AVCO Corporation
Lycoming Division
350 South Main Street
Stratford, Connecticut 06497
Attention: Claus W. Bolton 1
Charles Kuintzle 1

21. Continental Aviation & Engineering Corporation
12700 Kercheval
Detroit, Michigan 48215
Attention: Eli H. Benstein 1
Howard C. Walch 1

22. International Harvester Company
Solar Division - 2200 Pacific Highway
San Diego, California 92112
Attention: P. A. Pitt 1
Mrs. L. Walper 1

23. George Derderian AIR 53662B
Department of Navy
Bureau of Navy
Washington, D.C. 20360 1

24. The Boeing Company
Commercial Airplane Division
P.O. Box 3991
Seattle, Washington 98124
Attention: C. J. Schott 80-66 1

25. Aerojet-General Corporation
Sacramento, California 95809
Attention: M. S. Nylin 1
Library 1
William Heath 1

26. Newark College of Engineering
323 High Street
Newark, New Jersey 07102
Attention: Dr. Peter Hrycak 1

27. Department of Mechanical Engineering
Arizona State University
Tempe, Arizona
Attention: Dr. D. E. Metzger 1